

**Ninevah University**  
**College of Electronics Engineering**  
**Electronic Department**



**Root-MUSIC Technique for Direction of Arrival  
Estimation in Ultrasonic Applications**

**Mohammed Rafea Shukri**

**A Thesis in**

**Electronic Engineering**

**Supervised By**

**Assist. Prof.**

**Dr Mujahid Fahmy Al-Azzo**

**1445 AH**

**2024 AD**

**Root-MUSIC Technique for Direction of Arrival  
Estimation in Ultrasonic Applications**

**A Thesis Submitted by**

**Mohammed Rafea Shukri**

To

**The Council of the College of Electronics Engineering**

**Ninevah University**

**as a Partial Fulfillment of the Requirements**

**For the Degree of Master of Science**

In

**Electronics Engineering**

**Supervised by**

**Assist. Prof.**

**Dr Mujahid Fahmy Al-Azzo**

**1445 AH**

**2024 AD**

### *Supervisor's Certification*

We certify that the dissertation entitled (**Root-MUSIC Technique for Direction of Arrival Estimation in Ultrasonic Applications**) was prepared by **Mohammed Rafea Shukri** under my supervision at the Department of Electronic Engineering, Ninevah University, as a partial requirement for the Master of Science Degree in Electronic Engineering.

**Signature:**

**Name:**

**Date:** / 3 /2024

### **Report of Linguistic Reviewer**

I certify that the linguistic reviewing of this dissertation was carried out by me and it is accepted linguistically and in expression.

**Signature:**

**Name:**

**Date:** / 3 /2024

### **Report of the Head of Department**

I certify that this dissertation was carried out in the Department of Electronic Engineering. I nominate it to be forwarded to discussion.

**Signature:**

**Name:**

**Date:** / 3 /2024

### **Report of the Head of Postgraduate Studies Committee**

According to the recommendations presented by the supervisor of this dissertation and the linguistic reviewer, I nominate this dissertation to be forwarded to discussion.

**Signature:**

**Name:**

**Date:** / 3 /2024

### *Committee Certification*

We the examining committee, certify that we have read this dissertation entitled (**Root-MUSIC Technique for Direction of Arrival Estimation in Ultrasonic Applications**) and have examined the postgraduate student (**Mohammed Rafea Shukri** ) in its contents and that in our opinion; it meets the standards of a dissertation for the degree of Master of Science in Electronic Engineering.

**Signature:**

**Name:**

Head of committee

**Date:** / 3 /2024

**Signature:**

**Name:**

Member

**Date:** / 3 /2024

**Signature:**

**Name:**

Member

**Date:** / 3 /2024

**Signature:**

**Name:**

Member and Supervisor

**Date:** / 3 /2024

The college council, in its ..... meeting on / / , has decided to award the degree of Master of Science in Electronic Engineering to the candidate.

**Signature:**

**Name:** Prof. Khaled Khalil Muhammad

Dean of the College

**Date:** / 3 /2024

**Signature:**

**Name:** Assist. Prof. Dr. Bilal A.Jebur

Council registrar

**Date:** / 3 /2024

## **Acknowledgments**

Thanks to God the Almighty for providing me with the blessings and energy to carry out this research work.

Thanks to Dr. Mujahid Fahmy Al-Azzo, my supervisor. He is a good source of inspiration, encouragement, and useful advice. Without his aid and instruction, this dissertation would be so difficult to be achieved.

As a result, I would like to extend my gratitude to the department's head as well as all of the faculty and students who have contributed in some way to the completion of this research, in particular, engineer Tarek Hussein for his help in preparing the experimental set in a laboratory.

I would like to express my gratitude to my parents, brothers, and sisters and their unwavering support and encouragement during the duration of my studies.

**Mohammed.R. Shukri**

## **Abstract**

In this work we discuss the challenge of distinguishing between close frequencies and angles of sources in spectral analysis, emphasizing the limitations of conventional methods like the Fourier transform, which requires a large amount of data and often results in poor resolution due to side lobes. It introduces the Direction of Arrival (DOA) estimation as a critical area for improvement and presents the Root Multiple Signal Classification (Root-MUSIC) method as a high-resolution alternative to traditional approaches like the Fast Fourier Transform (FFT). The study compares Root-MUSIC and FFT using various parameters, including the number of samples, spatial sampling interval, and wavelength, with both single and dual emitting sources. The findings highlight Root-MUSIC's superior accuracy and efficiency with fewer data requirements. The efficacy of high-resolution methods over the Fourier technique in accurately separating source angles is further supported by experiments conducted with ultrasonic transducers at different source angles, demonstrating the high-resolution approaches' advantage over traditional methods. Implementing the DOA estimation experiments have been performed through ultrasonic transducers. Each experiment involves different angles of sources. The experimental results have demonstrated that the high-resolution approaches outperformed the traditional approaches.

From the simulated and practical results, we conclude that the maximum error is as high as possible in the practical results and less than it in the noisy simulation results data, the least of which is

noiseless simulation results data, for the FFT method and the Root-MUSIC method. This means that the best results are in noiseless results data, then in the results of noisy results data, and the worst results are the practical results in the results of one source and two emitting sources for all results.

## TABLE OF CONTENTS

Subject		Page
Acknowledgments		I
Abstract		II
Table of contents		IV
List of Figures		VI
List of Abbreviation		XIV
List of Symbols		XV
<b>Chapter One: Introduction and Literature Review</b>		<b>1</b>
1.1	Overview	1
1.2	Literature Review	4
1.3	Research Objectives	8
1.4	Study Organization	9
<b>Chapter Two: Theoretical Background</b>		<b>10</b>
2.1	Overview	10
2.2	Frequency Estimation	10
2.2.1	Classical (Non-Parametric) Methods	13
2.2.2	Autoregressive (AR) Model and power spectrum	15
2.2.3	Subspace Methods (High-Resolution Techniques)	16
2.2.3.1	Matrices	18
2.2.3.2	Autocorrelation Matrices	19
2.2.3.3	Eigenvectors and Eigenvalues	20
2.2.3.4	Eigendecomposition of autocorrelation Matrices	21
2.2.3.5	Pisarenko Harmonic Decomposition Algorithm (PHD)	26
2.2.3.6	Multiple Signal Classification (MUSIC) Algorithm	29
2.2.3.7	Root-MUSIC Algorithm	30
2.3	Direction of Arrival (DOA) Estimation	32
2.3.1	Model of the Data	33
2.3.2	Antenna Array	34
2.3.3	DOA Problem Formulation	37
<b>Chapter Three: Simulation Results</b>		<b>40</b>
3.1	Introduction	40

3.2	Simulation Results with Noiseless Data	41
3.2.1	Single Source for DOA Estimation	41
3.2.2	Double (two) emitting Sources for DOA Estimation	46
3.3	Simulation Results with Noise Data	68
3.3.1	Single Source for DOA Estimation	68
3.3.2	Double (two) emitting Sources for DOA Estimation	73
<b>Chapter Four: Experimental Results</b>		<b>86</b>
4.1	Introduction	86
4.2	Ultrasonic Transducer	86
4.3	The DOA Estimation System Using Ultrasound	87
4.4	Practical Experimental Results	88
4.5	Experimental with Single Source	89
4.5.1	Single-Source with Negative Angle	90
4.5.2	Single-Source with Positive Angle	94
4.6	Experimental with Two Source	96
<b>Chapter Five: Conclusions and Suggestions for Future Work</b>		<b>103</b>
5.1	Conclusions	103
5.2	Suggestions for Future Work	104
<b>References</b>		<b>105</b>

## LIST OF FIGURES

Figure	Title	Page
Figure (2.1)	An antenna of 3 elements	35
Figure (2.2)	DOA estimation data model on N elements	37
Figure (3.1)	Magnitude (power(dB)) versus angle (degree) for a single-source angle $\theta = 20^\circ$ using the FFT method (N=12)	41
Figure (3.2)	Magnitude (power(dB)) versus angle (degree) for a single-source angle $\theta = 37^\circ$ using the FFT method (N=11)	42
Figure (3.3)	Magnitude (power(dB)) versus angle (degree) for a single-source angle $\theta = -50^\circ$ using the FFT method (N=10)	43
Figure (3.4)	Magnitude (power(dB)) versus angle (degree) for a single-source angle $\theta = 6^\circ$ using the FFT method (N=12)	43
Figure (3.5)	Magnitude (power(dB)) versus angle (degree) for a single-source angle $\theta = -10^\circ$ using the FFT method (N=10)	44
Figure (3.6)	Magnitude (power(dB)) versus angle (degree) for a single-source angle $\theta = -11^\circ$ using the FFT method (N=8)	45
Figure (3.7)	Percentage error of versus N and angles (Theta) for a single source DOA Estimation for (FFT) algorithm method.	46
Figure (3.8)	Magnitude (power(dB)) versus angle (degree) for a double (two)-source angle ( $\theta_1 = 17^\circ$ , $\theta_2 = 37^\circ$ ) using the FFT method (N=8)	47
Figure (3.9)	Magnitude (power(dB)) versus angle (degree) for a double (two)-source angle	48

	( $\theta_1=17^\circ$ , $\theta_2=37^\circ$ ) using the FFT method (N=12)	
Figure (3.10)	Percentage error of angle versus N for double (two) sources ( $\theta_1=17^\circ$ , $\theta_2=37^\circ$ ) for DOA Estimation	49
Figure (3.11)	Magnitude (power(dB)) versus angle (degree) for a double (two)-source angle ( $\theta_1=20^\circ$ , $\theta_2=35^\circ$ ) using the FFT method (N=11)	50
Figure (3.12)	Magnitude (power(dB)) versus angle (degree) for a double (two)-source angle ( $\theta_1=20^\circ$ , $\theta_2=35^\circ$ ) using the FFT method (N=15)	50
Figure (3.13)	Percentage error of angle versus N for double (two) sources ( $\theta_1=20^\circ$ , $\theta_2=35^\circ$ ) for DOA Estimation	51
Figure (3.14)	Magnitude (power(dB)) versus angle (degree) for a double (two)-source angle ( $\theta_1=-25^\circ$ , $\theta_2=-35^\circ$ ) using the FFT method (N=16)	52
Figure (3.15)	Magnitude (power(dB)) versus angle (degree) for a double (two)-source angle ( $\theta_1=-25^\circ$ , $\theta_2=-35^\circ$ ) using the FFT method (N=22)	53
Figure (3.16)	Percentage error of angle versus N for double (two) sources ( $\theta_1=-25^\circ$ , $\theta_2=-35^\circ$ ) for DOA Estimation	54
Figure (3.17)	Magnitude (power(dB)) versus angle (degree) for a double (two)-source angle ( $\theta_1=-15^\circ$ , $\theta_2=-40^\circ$ ) using the FFT method (N=8)	55
Figure (3.18)	Magnitude (power(dB)) versus angle (degree) for a double (two)-source angle	55

	( $\theta_1=-15^\circ$ , $\theta_2=-40^\circ$ ) using the FFT method (N=17)	
Figure (3.19)	Percentage error of angle versus N for double (two) sources ( $\theta_1=-15^\circ$ , $\theta_2=-40^\circ$ ) for DOA Estimation	56
Figure (3.20)	Magnitude (power(dB)) versus angle (degree) for a double (two)-source angle ( $\theta_1=-17^\circ$ , $\theta_2=13^\circ$ ) using the FFT method (N=5)	57
Figure (3.21)	Magnitude (power(dB)) versus angle (degree) for a double (two)-source angle ( $\theta_1=-17^\circ$ , $\theta_2=13^\circ$ ) using the FFT method (N=14)	58
Figure (3.22)	Percentage error of angle versus N for double (two) sources ( $\theta_1=-17^\circ$ , $\theta_2=13^\circ$ ) for DOA Estimation	59
Figure (3.23)	Magnitude (power(dB)) versus angle (degree) for a double (two)-source angle ( $\theta_1=-10^\circ$ , $\theta_2=15^\circ$ ) using the FFT method (N=6)	60
Figure (3.24)	Magnitude (power(dB)) versus angle (degree) for a double (two)-source angle ( $\theta_1=-10^\circ$ , $\theta_2=15^\circ$ ) using the FFT method (N=17)	60
Figure (3.25)	Percentage error of angle versus N for double (two) sources ( $\theta_1=-10^\circ$ , $\theta_2=15^\circ$ ) for DOA Estimation	61
Figure (3.26)	Magnitude (power(dB)) versus angle (degree) for a double (two)-source angle ( $\theta_1=-29^\circ$ , $\theta_2=26^\circ$ ) using the FFT method (N=5)	62
Figure (3.27)	Magnitude (power(dB)) versus angle (degree) for a double (two)-source angle	63

	$(\theta_1=-29^\circ, \theta_2=26^\circ)$ using the FFT method (N=14)	
Figure (3.28)	percentage error of angle versus N for double (two) sources $(\theta_1=-29^\circ, \theta_2=26^\circ)$ for DOA Estimation	64
Figure (3.29)	Magnitude (power(dB)) versus angle (degree) for a double (two)-source angle $(\theta_1=-10^\circ, \theta_2=14^\circ)$ using the FFT method (N=8)	65
Figure (3.30)	Magnitude (power(dB)) versus angle (degree) for a double (two)-source angle $(\theta_1=-10^\circ, \theta_2=14^\circ)$ using the FFT method (N=20)	65
Figure (3.31)	percentage error of angle versus N for double (two) sources $(\theta_1=-10^\circ, \theta_2=14^\circ)$ for DOA Estimation	66
Figure (3.32)	Relationship between Difference Angle and minimum number of samples $N_{min}$ for noiseless double (two) sources	67
Figure (3.33)	Percentage error of angle versus N for single angle source with $\theta=20^\circ$ , SNR=10dB, $d=0.6\text{cm}$ , $\Psi=2\text{cm}$ using DOA Estimation	68
Figure (3.34)	Percentage error of angle versus N for single angle source with $\theta=20^\circ$ , SNR=5dB, $d=0.6\text{cm}$ , $\Psi=2\text{cm}$ using DOA Estimation	69
Figure (3.35)	Percentage error of angle versus N for single angle source with $\theta=37^\circ$ , SNR=10dB, $d=0.6\text{cm}$ , $\Psi=2\text{cm}$ using DOA Estimation	70
Figure (3.36)	Percentage error of angle versus N for single angle source with $\theta=37^\circ$ ,	71

	SNR=5dB, d=0.6cm, $\Psi=2$ cm using DOA Estimation	
Figure (3.37)	Percentage error of angle versus N for single angle source with $\theta = -50^0$ , SNR=10dB, d=0.6cm, $\Psi=2$ cm using DOA Estimation	72
Figure (3.38)	Percentage error of angle versus N for single angle source with $\theta = -50^0$ , SNR=5dB, d=0.6cm, $\Psi=2$ cm using DOA Estimation	73
Figure (3.39)	Percentage error of angle versus N for double (two) sources ( $\theta_1 = 17^0$ , $\theta_2 = 37^0$ ) for the first actual angle ( $\theta_1 = 17^0$ ), SNR=10dB for DOA Estimation	74
Figure (3.40)	Percentage error of angle versus N for double (two) sources ( $\theta_1 = 17^0$ , $\theta_2 = 37^0$ ) for the second actual angle ( $\theta_2 = 37^0$ ), SNR=10dB for DOA Estimation	75
Figure (3.41)	Percentage error of angle versus N for double (two) sources ( $\theta_1 = 17^0$ , $\theta_2 = 37^0$ ) for the first actual angle ( $\theta_1 = 17^0$ ), SNR=5dB for DOA Estimation	76
Figure (3.42)	Percentage error of angle versus N for double (two) sources ( $\theta_1 = 17^0$ , $\theta_2 = 37^0$ ) for the second actual angle ( $\theta_2 = 37^0$ ), SNR=5dB for DOA Estimation	77
Figure (3.43)	Percentage error of angle versus N for double (two) sources ( $\theta_1 = -15^0$ , $\theta_2 = -40^0$ ) for the first actual angle ( $\theta_1 = -15^0$ ), SNR=10dB for DOA Estimation	78
Figure (3.44)	Percentage error of angle versus N for double (two) sources ( $\theta_1 = -15^0$ , $\theta_2 = -40^0$ )	79

	for the second actual angle ( $\theta_2=-40^\circ$ ), SNR=10dB for DOA Estimation	
Figure (3.45)	Percentage error of angle versus N for double (two) sources ( $\theta_1=-15^\circ, \theta_2=-40^\circ$ ) for the first actual angle ( $\theta_1=-15^\circ$ ), SNR=5dB for DOA Estimation	80
Figure (3.46)	Percentage error of angle versus N for double (two) sources ( $\theta_1=-15^\circ, \theta_2=-40^\circ$ ) for the second actual angle ( $\theta_2=-40^\circ$ ), SNR=5dB for DOA Estimation	81
Figure (3.47)	Percentage error of angle versus N for double (two) sources ( $\theta_1=-10^\circ, \theta_2=15^\circ$ ) for the first actual angle ( $\theta_1=-10^\circ$ ), SNR=10dB for DOA Estimation	82
Figure (3.48)	Percentage error of angle versus N for double (two) sources ( $\theta_1=-10^\circ, \theta_2=15^\circ$ ) for the second actual angle ( $\theta_2=15^\circ$ ), SNR=10dB for DOA Estimation	83
Figure (3.49)	Percentage error of angle versus N for double (two) sources ( $\theta_1=-10^\circ, \theta_2=15^\circ$ ) for the first actual angle ( $\theta_1=-10^\circ$ ), SNR=5dB for DOA Estimation	84
Figure (3.50)	percentage error of angle versus N for double (two) sources ( $\theta_1=-10^\circ, \theta_2=15^\circ$ ) for the second actual angle ( $\theta_2=15^\circ$ ), SNR=5dB for DOA Estimation	85
Figure (4.1)	Ultrasonic Ceramic Transducer	87
Figure (4.2)	Experimental Setup System Parts	89
Figure (4.3)	Magnitude (power (dB)) versus angle (degree) for a single-source ( $\theta = -10^\circ$ ) using the FFT approach (N=11)	90
Figure (4.4)	Percentage error of angle versus N for single source with $\theta = -10^\circ$ for DOA Estimation	91

Figure (4.5)	Magnitude (power (dB)) versus angle (degree) for a single-source ( $\theta = -11^\circ$ ) using the FFT approach (N=18)	92
Figure (4.6)	Percentage error of angle versus N for single source with $\theta=-11^\circ$ for DOA Estimation	93
Figure (4.7)	Magnitude (power (dB)) versus angle (degree) for a single-source ( $\theta = 6^\circ$ ) using the FFT approach (N=13)	94
Figure (4.8)	Percentage error of angle versus N for a single source with $\theta = 6^\circ$ for DOA Estimation	95
Figure (4.9)	Magnitude (power (dB)) versus angle for a double (two) sources ( $\theta_1=-29^\circ$ , $\theta_2=26^\circ$ ) for DOA estimation using the FFT approach (N=17)	96
Figure (4.10)	Percentage error of angle versus N for double (two) sources ( $\theta_1= -29^\circ$ , $\theta_2= 26^\circ$ ) with the first actual angle ( $\theta_1=-29^\circ$ ) for DOA Estimation	98
Figure (4.11)	Percentage error of angle versus N for double (two) sources ( $\theta_1= -29^\circ$ , $\theta_2= 26^\circ$ ) with the second actual angle ( $\theta_2= 26^\circ$ ) for DOA Estimation	99
Figure (4.12)	Magnitude (power (dB)) versus angle for a double (two) sources ( $\theta_1= -10^\circ$ , $\theta_2= 14^\circ$ ) for DOA estimation using the FFT approach (N=25)	100
Figure (4.13)	percentage error of angle versus N for double (two) sources ( $\theta_1= -10^\circ$ , $\theta_2= 14^\circ$ ) with the first actual angle ( $\theta_1= -10^\circ$ ) for DOA Estimation	101
Figure (4.14)	percentage error of angle versus N for double (two) sources ( $\theta_1= -10^\circ$ , $\theta_2=$	102

	14°) with the second actual angle ( $\theta_2 = 14^\circ$ ) for DOA Estimation	
--	---	--

## LIST OF ABBREVIATIONS

Abbreviation	Name
AOA	Angle of Arrival
AR	Autoregressive
AWGN	Additive White Gaussian Noise
BA	Burg Algorithm
BW	Band Width
DFT	Discrete Fourier Transform
DOA	Direction of Arrival
DSP	Digital Signal Processing
DTFT	Discrete-Time Fourier Transform
EV	EigenVector
FDOA	Frequency Difference of Arrival
FFT	Fast Fourier Transform
H	Herimitan (Complex Conjugate Transpose)
KHZ	Kilo Hertz
ME	Maximum Entropy
ML	Maximum Likelihood
MUSIC	Multiple Signal Classification
PHD	Pisarenko Harmonic Decomposition
SNR	Signal to Noise Ratio
T	Matrix Transpose
TDOA	Time Difference of Arrival
ULA	Uniform Linear Array
WSS	Wide Sense Stationary

## LIST OF SYMBOLS

Symbol	NAME
D	Dimension of antenna
d	Distance between elements (Sampling interval)
E	Statistical expectation
f	Frequency
$f_c$	Carrier frequency
<b>I</b>	Identity matrix
M	Number of sources
N	Total number of samples
$\hat{P}_{MU}$	The estimation of the power spectrum using MUSIC method
$\hat{P}_{PHD}$	The estimation of the power spectrum using Pisarenko method
$r$	Narrow band signal
$r_{ss}$	Autocorrelation function
$u_i$	Eigenvector
$V_q$	Noise autocorrelation Matrix
$V_s$	Signal autocorrelation Matrix
$\sigma_q$	White noise variance
$\lambda_i$	Eigenvalues
$\theta$	Angle of signal
$\omega$	Radian frequency
$\Psi$	wavelength
$\beta$	Phase shift

# Chapter One

## Introduction

### 1.1 Overview

In the current era, the fields of communication and signal processing are crucial, serving as the foundation of our digital existence by playing key roles in various sectors such as business, economy, education, and health[1]. Signal processing involves analyzing, modifying, and controlling different types of signals (like electromagnetic, images, and sound) through operations like storage, reconstruction, compression, and feature extraction[2]. These operations, which aim to enhance storage and transmission efficiency while preserving signal quality, rely on mathematical, and statistical methods, and hardware devices. Their effectiveness is assessed using various metrics tailored to the specific goals and operation types[3]. Additionally, array signal processing, a subset of signal processing that uses sensor or antenna arrays to gather signal source data, is highlighted for its widespread application in different fields such as medicine, astronomy, radar systems, sonar systems, positioning systems, etc[4][5].

Spectrum analysis focuses on identifying a signal's spectral components, a practice dating back to early studies by Pythagoreans, Newton, Bernoulli, and Prony on planetary motion, with Gauss' work hinting at principles of the Fast Fourier Transformation based on Fourier's 1807 work[6]. It's used in various applications, particularly for analyzing stationary stochastic data through autoregressive

processes[7]. Spectral analysis plays a key role in processing signals received from various objects like airplanes, medical imaging devices, and missiles, aiming to determine parameters such as signal direction, magnitude, speed, and range[8][9][10]. Signals, considered to be emitted by point sources, are categorized into narrowband and wideband based on their bandwidth[11]. Spectral estimation techniques, which aim to estimate a signal's spectral density from time samples, are crucial and vary as parametric, non-parametric, or semi-parametric, depending on the application's nature and requirements[2].

Direction of Arrival (DOA) estimation, also known as Direction Finding, is a significant application in array signal processing used to determine the direction from which a signal arrives, using forms like acoustic or electromagnetic waves through antenna arrays or sensors[12]. This technique is crucial for tracking and locating signal sources in both military and civilian contexts, such as rescue operations, exploration, emergency response, and monitoring applications[13]. DOA estimation involves analyzing the sensor array's spatial spectrum with specific mathematical models, where its performance can be affected by data model errors and noise[14]. The literature highlights DOA's effectiveness in addressing various engineering challenges, including:

- Locating the direction relative to the array of a source.
- Identifying multiple signal sources around a specific point of interest.
- Employing in radio telescopes to pinpoint locations in the sky.

- Enhancing beamforming in wireless communications to lower data rate complexities.
- Addressing direction of arrival issues alongside other technologies like Time Difference of Arrival (TDOA), Angle of Arrival (AoA), and Frequency Difference of Arrival (FDOA).
- Improving accuracy in digital signal processing[12][15][16].

DOA estimation utilizes various algorithms, broadly classified into classical, parametric, and subspace categories, with subspace algorithms like Pisarenko Harmonic Decomposition (PHD), Eigen Vector (EV), Multiple Signal Classification (MUSIC), and Root-MUSIC being preferred for their high-resolution capabilities. Classical algorithms, though available, lack the efficiency of these modern approaches. This study aims to offer a detailed analysis and benchmarking to evaluate these algorithms, preparing to present the latest research in the subsequent section.

The PHD algorithm, introduced in 1973 by Pisarenko, represents a high-resolution method based on eigenanalysis of the data model's autocorrelation matrix, designed to surpass classical method limitations[17]. However, PHD has its own weaknesses, prompting the development of the MUSIC algorithm by Schmidt to address these issues, noted for its super-resolution capabilities[18]. Additionally, Barabell suggested another variant of MUSIC, utilizing the polynomial's root in the MUSIC spectrum for Angle of Arrival (AOA) estimation. Unlike MUSIC, which typically presents results in visual plots, Root-MUSIC outputs numerical results[19].

## 1.2 Literature Review

The Direction of Arrival (DOA) techniques have been used since four decades ago for addressing different kinds of issues such as estimating the DOA of signals, reducing the power transmitted, etc. One of the earliest studies was performed by Mahapatra [20] in 1980. He suggested an approach that was based on a mobile direction finder for the passive location of the radio emitter. A vehicle was used to carry the direction finder.. A year after, Klose and Skudera [21] proposed a technique that accurately measured the information obtained from frequency and angle of arrival. The technique, then, has been utilized in high-density environments for identifying parameters emitters. Nine years later, using a basic Bayesian approach, Farrier. and D.R [22] developed a useful direction-of-arrival (DOA) estimator in 1990. However, the threshold for this estimator is substantially lower than that of MUSIC, making it nearly identical to this approach. Two years after, Wong [23] estimated the DOA of signals considering its noise with an unknown covariance matrix. The author tested data projection on the noise subspace. The strength of the approach is that there is no need to have the noise covariance matrix known.

In 2000, Larsson and Stoica [24] investigated the case when having sensors failure before the completion of the measurement process. The authors have found the direction of arrival DOA estimation with both covariance matching and MUSIC algorithm. The authors showed that the covariance matching technique can use the information on the array covariance matrix estimation accuracy.

The findings of the experiments on their method reflected efficient performance gain.

When a large number of sources ( $M$ ) are used in the estimation of the direction of arrival (DOA), the number of sensors ( $N$ ) that can be used to determine the DOA can be exceeded, as was the case in the paper by Araki, et al. [25] (2006). Two uniform linear arrays (ULAs) were used to solve the challenge of associating multiple targets' estimated arrival angles (DOAs) with each other in a study published in (2008), by Bai et al. [26]. Rejfeek et al. [27] offered a comparison of parametric power spectrum density approaches for application in meteorological radar, and used pulses of the pulse radar in it for frequency modulation in their article in (2015). Auto regression (AR) and Eigen Vector (EV) have both been used in this study.

Another study performed by Yuan [28] proposed an accurate and fast DOA estimation for multi target in “Additive White Gaussian Noise”. The proposed method used two highest magnitudes (DFT) coefficients of the input and two of their “associated neighboring bins”. The authors also analyzed the mean square errors. The results showed the high efficient of the proposed approach under several DOA estimators. Zhang et. [29] suggested a fast DOA estimation for single channel antenna array. The suggested approach used spatial FFT that considers the switching time into operation aiming to construct a new transformation function. This function was used to directly operate spatial Fast Fourier Transformation (FFT) to

the single-channel antenna array sampled data. The proposed method was proved to be highly efficient.

Researchers and developers from worldwide institutions and companies have significantly contributed to this field. The study of Shaghghi and Vorobyov [30] proposed a high-resolution DOA estimation approach that was based on using root MUSIC algorithm. The aim of the algorithm was to improve the quality of DOA estimation when having small sample size. The main idea behind the approach was identifying undesirable phenomenon in the sample covariance matrix that causes perturbations. The metrics used in evaluating the proposed approach were MSE and detection rate. The simulation results showed the efficient performance of the proposed approach. Another study performed by Vasylyshyn [31] used root-MUSIC approach for DOA estimation. The approach involved resampling procedure by adding some noise “pseudo noise”. The root-MUSIC algorithm polynomial was used as alternative of eliminating of the entire estimator. Yan et al. [32] developed a low-computational cost approach using root-MUSIC for DOA estimation. The developed approach aimed to reduce the computational cost consumed in the estimation process. The approach utilized eigenvalue decomposition for extracting real noise subspace. The approach showed high performance in terms of the mean squared error.

Furthermore, other DOA estimation algorithms such as “Pisarenko Harmonic Decomposition (PHD)” were examined in the literature. For instance, the work of Kamil et al. [33] (2021) achieved

a comprehensive and evaluative study on PHD, MUSIC, and other DOA estimation algorithms. The results reflected the high efficiency of the MUSIC algorithm compared to PHD and other estimation algorithms. This was because MUSIC requires fewer number of antennas than Pisarenko and other algorithms to address the “Angle of Arrival” of the received signals.

In 2021, Fathtabar et al. [34] proposed an Eigen-Structure approach for DOA estimation. The strength of their proposed approach is that it does not require prior-knowledge about the source angle estimation. Their approach transformed the covariance matrix to reference frequency. Then, they formed a “Hankel Matrix” for each “Signal Subspace Eigenvector”. Many experiments were performed and the results under different conditions reflected an efficient performance compared to other approaches in the literature under a variety of conditions. Vesa [35] used root-MUSIC algorithm for DOA estimation. The author showed that root-MUSIC was able to improve the performance of the estimation. The study also showed that root-MUSIC can be efficiently used with smart antennas since it adds the possibility of user separation.

The literature includes a lot of works that are able to deal with different kinds of problems. For example, the problem of time-varying DOA in “Uniform Linear Array ULA” was investigated by one of the most recent studies performed by Zhao e al. [36] in 2021.

### 1.3 Research Objectives

This study is dedicated to the exploration of advanced Direction of Arrival (DOA) estimation methodologies, with a particular emphasis on the Root-MUSIC algorithm. These methodologies are distinguished by their high-resolution characteristics and their foundation in eigenanalysis. A comparative analysis is conducted to evaluate the performance of these contemporary techniques against conventional methods, notably the Fast Fourier Transform (FFT).

The investigation encompasses several critical areas:

- Analyzing auto-covariance and auto-correlation processes to elucidate the procedures for extracting Eigenvalues and Eigenvectors from the auto-correlation matrix.
- An extensive examination of the Root-MUSIC method as a contemporary approach to DOA estimation.
- The application of these methodologies across various scenarios to assess their efficacy and validate the findings.
- Benchmarking the results obtained to formulate recommendations regarding the application efficacy of the explored methodologies.
- Verification of the applicability of these findings through experiments involving ultrasonic waves.

The research aims to offer a comprehensive evaluation framework and actionable insights for the implementation of DOA

estimation techniques, thereby enhancing their applicability and accuracy in practical scenarios.

## **1.4 Study Organization**

Chapter one (Introduction with Literature Review): tries to explain most of the different algorithm methods for the Direction of Arrival (DOA) Estimation.

Chapter two (Principles of Direction of Arrival (DOA) Estimation): covers the required background on the topics considered in this study.

Chapter three (DOA Methods): presents the research method followed in this study including simulation with and without noise data.

Chapter four (Experimental Results): contains the results of the experiments of the implemented approaches.

Chapter five (Conclusions): contains some concluding the study has come up with in terms of the approaches considered providing general recommendations. The chapter also states the future works that can be done by other researchers and the area of development.

## Chapter Two

### Theoretical Background

#### 2.1 Overview

In this chapter the required theoretical background about the topics considered in this study is presented. Descriptions of the non-parametric and high-resolution methods as well as an explanation about autocorrelation matrices, eigenvectors, and other algorithms required in this study are also presented. Also, estimation approaches will be elaborated in detail such as the modern (parametric) Autoregressive (AR) method, EV (Eigenvectors), PHD (Pisarenko Harmonic Decomposition), MUSIC (Multiple Signal Classification Algorithm), and Root-MUSIC.

#### 2.2 Frequency Estimation

Power spectral estimation is considered an important area in Digital Signal Processing (DSP). A spectrum reflects the relationship between the frequency and the magnitude, which can be graphically represented as a plot. It has many different applications, for instance, in speech recognition, it can be utilized in reducing the bandwidth of a speech [37]. Moreover, it is widely used in modern radar systems for tracking and monitoring static and mobile objects [38]. Signals are categorized into periodic and random; the former can be predicted since its behavior is almost known, while it is difficult to predict the behavior of the second type “the random”. Random signals are also called random processes  $s(n)$  and have two types; *stationary*, the

variance and mean of a stationary random process are both constant, meaning they don't change with time when its order is  $O$  such that  $s(n)$  and  $s(n+k)$  have the same “ $O^{\text{th}}$ -order joint density functions”, while if  $O > 0$  it is considered a *non-stationary* in “*Strict Sense*”, the means, variances, and covariances of data points are frequently non-stationary or fluctuate with time [39]. A random process may be also termed “*Ergodic*” when the statistical averages are able to be defined using a single sample function [40]. Furthermore, there is another form of stationery that is called “*Wide Sense Stationary (WSS)*”, if both the mean function and the correlation function of a random process remain unchanged when time shifts the process is referred to as weak-sense stationary, or wide-sense stationary (WSS), when process means is constant ( $\mu_R(n) = \mu_R$ ) and process variance are finite ( $\sigma_R(0) < \infty$ ).

The Fourier transform of the signal  $s(n)$  is [63]:

$$S(\omega) = \sum_{n=-\infty}^{\infty} s(n) e^{-j\omega n} \quad (2.1)$$

or, equivalently:

$$S(f) = \sum_{n=-\infty}^{\infty} s(n) e^{-j2\pi f n} \quad (2.2)$$

The WSS autocorrelation sequence of a discrete signal  $s(n)$  can provide a “*time-domain description*” of the 2<sup>nd</sup> order moment of the signal (process). The autocorrelation of the signal  $s(n)$  is given as follows [41]:

$$r_{ss}(k) = \sum_{n=-\infty}^{\infty} s^*(n) s(n+k) \quad (2.3)$$

It has a Fourier transform:

$$P_{SS}(\omega) = \sum_{k=-\infty}^{\infty} r_{SS}(k) e^{-jk\omega} \quad (2.4)$$

The formula above is called “*Power Spectrum*” or “*Power Spectral Density*” of the process. The autocorrelation sequence is determined by the inverse DT-FT [41]:

$$r_{SS}(k) = \frac{1}{2\pi} \int_{-\pi}^{\pi} P_{SS}(e^{j\omega}) e^{jk\omega} d\omega \quad (2.5)$$

Also  $P_{SS}(\omega)$  can be written as:

$$P_{SS}(\omega) = |S(\omega)|^2 \quad (2.6)$$

$$P_{SS}(\omega) = \left| \sum_{n=-\infty}^{\infty} s(n) e^{-jn\omega} \right|^2 \quad (2.7)$$

The power spectrum estimation in the frequency domain is equivalent to the autocorrelation estimation in the time domain. The ergodic process autocorrelation is formalized as follows [41]:

$$r_{SS}(k) = \lim_{N \rightarrow \infty} \left\{ \frac{1}{2N+1} \sum_{n=-N}^N s(n+k) s^*(n) \right\} \quad (2.8)$$

The power spectrum estimation is directly obtained when the  $s(n)$  is known for all  $n$ . However, the problem in the above formulas lies on two main issues, as follows:

- The data cannot be unlimited.
- Noisy or corrupted signals may exist, which lead to have incorrect data.

Therefore, the estimation of the spectrum is performed on a limited (finite) number of noisy measurements  $s(n)$ . It should be mentioned that spectrum estimation aims to, using a finite dataset, illustrate the distribution of power over signal frequency, to

characterize the power encoded in the signal's distribution across frequencies, spectral estimation is utilized. A signal's power spectrum becomes more condensed the more correlated or predictable it is [42]. The spectrum estimation can be performed using two kinds of approaches; classical (non-parametric) and modern (parametric) and subspace is as described in the following sections.

### 2.2.1 Classical (Non-Parametric) Methods

This kind does not need assumptions on the data generation approach. Using a given data, the first step starts with estimating the “*autocorrelation sequence*” of the random process. The estimation is performed using the FT of the previous step. As mentioned, the autocorrelation ergodic process  $s(n)$  is evaluated by a limited (finite) interval. The estimation can be performed using the following formula [43]:

$$\hat{r}_{ss}(k) = \frac{1}{N} \sum_{n=0}^{N-1} s(n+k)s^*(n) \quad (2.9)$$

The non-parametric estimation is considered a periodogram that is simple to calculate and the power spectrum resolution is limited to low-scale data. In this context, a resolution is crucial when it comes to performance analysis of spectral estimation and reflects the ability in distinguishing spectral features [44]. The literature includes a lot of approaches that have modified the periodogram aiming to enhancing its statistical features (e.g., Welch, Bartlett, and Blackman-Tukey methods).

According to the previous description and equations, the values outside the interval  $[0, N-1]$  of  $s(n)$  are excluded from Equation 2.9 and can be re-formalized as follows:

$$\hat{r}_{ss}(k) = \frac{1}{N} \sum_{n=0}^{N-1-k} s(n+k)s^*(n) \quad (2.10)$$

Where  $k=0$  to  $N-1$  and by taking the DT-FT of  $\hat{r}_{ss}(k)$ , the power spectrum estimate is called “Periodogram” as follows:

$$\hat{P}_{per}(e^{j\omega}) = \sum_{k=-N+1}^{N-1} \hat{r}_{ss}(k)e^{-jk\omega} \quad (2.11)$$

The above formula can be directly obtained in terms of  $s(n)$  as follows:

$$\hat{P}_{per}(e^{j\omega}) = \frac{1}{N} \left| \sum_{n=0}^{N-1} s(n) e^{-j\omega n} \right|^2 = \frac{1}{N} |S(\omega)|^2 \quad (2.12)$$

$$\hat{P}_{per}(e^{j\omega}) = \frac{1}{N} S(\omega) S^*(\omega) = \frac{1}{N} |S(\omega)|^2 \quad (2.13)$$

where  $S(\omega)$  is the DT-FT of data sequence  $s(n)$  with  $N$  points.

Regardless of its simplicity, the periodogram needs large-scale data for obtaining good “*Frequency Resolution*” [45][46]. However, this method struggles with what has been called in the literature “*Spectral Leakage*”, spectrum leaking is the term used to describe this blending of data. When doing transforms over data that contains a noninteger period signal, you can minimize spectral leakage by using a technique known as windowing. By using windowing, a signal is multiplied by a vector that depicts a smooth curve with

boundary values close to or equal to zero, which is due to the windowing technique involved [47][48].

### **2.2.2 Autoregressive (AR) model and power spectrum**

Parametric approaches are used to describe the data  $s(n)$  time series, which is represented by the rational assembly and two-step spectrum estimation procedure, as the output of the linear system [49],[50]. In AR modeling, the time history of a signal is used to extract useful information from the signal. To compute a time series power spectrum density function, the AR model can be used and then application of the DFT is made. The power spectrum provides information on the frequency output of a time series [51],[52]. The features of stationary stochastic systems are defined by AR models. The problems that best suit parametric algorithms have well-defined and predictable input data. The most popular parametric method is the AR method. The data in the AR technique can be represented as the result of a discrete causal filter, all poles, with white noise as the input. Each EEG signal sample is described by the autoregressive (AR) model as a linear mixture of earlier samples. AR model parameters and variance are used to generate the power spectrum and maximum covariance function [53]. The AR model predicts the present values of a time series based on its historical values. Autocorrelation is a process that will demonstrate the potential dependency on previous values [52].

Autocorrelation is the coupling of a data sample  $s[n]$  with a more advanced version of itself. Autocorrelation is the average of a data

sample's  $s[n]$  outputs with a version of itself that has been advanced by a lag time [52].

Autocorrelation is described by the equation [52]:

$$r_{ss}[k] = \frac{1}{N} \sum_{n=1}^{N-k} s[n]s[n+k] \quad (2.14)$$

In this case,  $r_{ss}[k]$  is the amount of autocorrelation at sample delay  $k$ , and  $N$  is the total number of observations.

The AR model [52],[54] can be viewed as a series of autocorrelation functions. Time series modelling is based on the assumption that current data points contain more information than past data points, and that each series value can be calculated as a weighted sum of the same series' prior values plus an error word "known as AR time series modelling". AR's model is characterized by the following:

$$s[n] = \sum_{i=1}^M a_i s[n-i] + e[n] \quad (2.15)$$

One-step prediction error,  $s[n]$  is the value in the selected time series,  $a_1, a_M$  is the weighting coefficient (predictor), and  $M$  is the order of the sequence (forecasting the present value based on a number of prior values), and  $e[n]$  is the difference between the expected value and the actual value.

### **2.2.3 Subspace Methods (High-Resolution Techniques)**

One of the most crucial processes in the signal processing field is estimating the problem's parameters of a particular signal. This is important since high-resolution DOA estimation is used in a variety

of applications such as radar systems, sonar systems, navigating systems, tracking systems, etc. The estimation of high-resolution frequency is termed “*Super Resolution*” technique, which is useful in many contemporary applications. One of the most common techniques is “*Maximum Likelihood (ML)*” [55] and “*Maximum Entropy (ME)*” [56] are (super) high resolution methods. However, these techniques have limitations related to sensitivity when estimating parameters is attempted.

Eigenanalysis is widely used in the literature for different applications including parameters, estimation of signals. The early literature showed involving eigenanalysis in estimating parameters such as in the works of Pisarenko [17] and Schmidt [18].

One of the most widely used high-resolution algorithms is Root-MUSIC (*Multiple Signal Classification*). The literature showed that it is the most efficient and promising algorithm due to many reasons. For instance, it is characterized by eigenvectors that enable splitting between the noise subspace and signal subspace, which is useful in many applications [57].

The Eigen-based analysis are utilized to approximate the characteristics of the sinusoidal signal. Two subspaces can be created using Eigen-analysis to separate the Eigenvector and Eigen-values of the autocorrelation matrix of the noise signal [58]:

1. Signal subspace: An important part of the signal dimensionality is made up of the primary Eigenvectors that are linked to the highest Eigenvalues.

2. Noise subspace : The smallest Eigenvalues indicated the noise's dimensionality.

The Eigen-vector approach is able to estimate complex exponential frequencies in such a noise amongst many other methods [59],[60].

### 2.2.3.1 Matrices

Multiplying and adding numbers and other abstract quantities can be done using a matrix, which is a rectangular table with a fixed number of elements (or entries). Matrices are used to define linear equations, maintain track of linear transformation coefficients, and record data dependently on numerous factors. The study of matrices is known as matrix theory.' Additionally, matrices are a crucial notion in linear algebra because they may be added, multiplied, and deconstructed.

A matrix is a data structure that is able to contain different data types of different dimensions. For instance, a matrix of  $(m \times l)$  has  $n$  rows and  $m$  columns as shown in (2.16):

$$\mathbf{B} = \{b_{ij}\} = \begin{bmatrix} b_{11} & b_{12} & \dots & b_{1m} \\ b_{21} & b_{22} & \dots & b_{2m} \\ \dots & \dots & \dots & \dots \\ b_{n1} & b_{n2} & \dots & b_{nm} \end{bmatrix} \quad (2.16)$$

If  $m=l$ , the matrix is said to be a squared matrix because the number of rows equals the number of columns. The transpose matrix of  $\mathbf{B}$  is termed  $\mathbf{B}^T$  with a size of  $m \times l$ , which is obtained by exchanging the M's columns with its rows such that  $b_{ij}$  becomes  $b_{ji}$ .

Moreover, for squared matrices, when a matrix is equal to its transpose, it is called “*Symmetric Matrix*” ( $\mathbf{B}=\mathbf{B}^T$ ) [60]. The “*Hermitian Transpose*” of a complex matrix is the complex conjugate transpose such that  $\mathbf{B}^H=(\mathbf{B}^*)^T=(\mathbf{B}^T)^*$ . It should be mentioned that a matrix is called “*Hermitian*” when a “*Square Complex*” value equals its Hermitian transpose.

### 2.2.3.2 Autocorrelation Matrices [60, 62, 63]

Signals in communication systems may include environment-based noise that is originated from a different source, which makes the noise uncorrelated. In the context of autocorrelation matrices, the correlation sequence for  $s(n)$  can be formulated as follows:

$$r_{ss}(k) = \sum_{n=-\infty}^{\infty} s(n-k)s^*(n) \quad (2.17)$$

when ( $Length(s(n))=N$ ), it can be reformulated as follows:

$$\hat{r}_{ss}(k) = \sum_{n=0}^{N-1} s(n-k)s^*(n) \quad (2.18)$$

Then, the autocorrelation sequence can be represented as follows:

Let ( $s$ ) be a data sequence (samples), then:

$$\mathbf{s} = [s(0), s(1), s(2), \dots, s(N-1)]^T \quad (2.19)$$

The correlation matrix becomes:

$$\mathbf{V}_y = E\{\mathbf{s}\mathbf{s}^H\} \quad (2.20)$$

This equation determines the “*Degree of Correlation*” of data signals, and the term  $E\{\}$  represents the “*Statistical Expectation*”. The symbol  $H$  reflects the transpose of the complex conjugate. Now, the term  $\mathbf{ss}^H$  is the  $N \times N$  can be represented as follows:

$$\mathbf{ss}^H = \begin{bmatrix} s(0)s^*(0) & s(0)s^*(1) & \dots & s(0)s^*(N-1) \\ s(1)s^*(0) & s(1)s^*(1) & \dots & s(1)s^*(N-1) \\ \dots & \dots & \dots & \dots \\ s(N-1)s^*(0) & s(N-1)s^*(1) & \dots & s(N-1)s^*(N-1) \end{bmatrix}$$

... (2.21)

Considering the aforementioned description, the autocorrelation matrix leads to product the  $N \times N$  becomes:

$$\mathbf{V}_y = E\{\mathbf{ss}^H\} = \begin{bmatrix} r_{ss}(0) & r_{ss}^*(1) & r_{ss}^*(2) & \dots & r_{ss}^*(N-1) \\ r_{ss}(1) & r_{ss}^*(0) & r_{ss}^*(1) & \dots & r_{ss}^*(N-2) \\ r_{ss}(2) & r_{ss}^*(1) & r_{ss}^*(0) & \dots & r_{ss}^*(N-3) \\ \dots & \dots & \dots & \dots & \dots \\ r_{ss}(N-1) & r_{ss}^*(N-2) & r_{ss}^*(N-3) & \dots & r_{ss}^*(0) \end{bmatrix} \quad (2.22)$$

### 2.2.3.3 Eigenvectors and Eigenvalues [59, 62]

Eigenvalues and Eigenvectors are used to extract useful information from matrices. Eigenvectors can be also used in distinguishing noise subspace and signal subspace. This decomposition is effectively used in Root-MUSIC algorithms.

Given that  $\mathbf{B}$  is a matrix of dimension  $(m \times m)$ , then;

$$\mathbf{B}\mathbf{u} = \lambda\mathbf{u} \quad (2.23)$$

Where  $\lambda$  is a constant value. The above equation is re-formalized to be a set of homogeneous linear as follows:

$$(\mathbf{B} - \lambda\mathbf{I})\mathbf{u} = 0 \quad (2.24)$$

For a non-zero vector, the terms  $(\mathbf{B} - \lambda\mathbf{I})$  should not have an inverse (singular matrix). For this reason, the determinant should be:

$$\det(\mathbf{B} - \lambda\mathbf{I}) = 0 \quad (2.25)$$

The above equation includes the features of  $\mathbf{B}$  and its  $n$  roots. The values of  $\lambda_i$  are the eigenvalues of the matrix  $\mathbf{B}$  for  $i=1, 2, 3, \dots, n$ , and for each of which, the matrix will be singular and there exists a *non-zero vector* (at least one). Therefore, Equation 2.25 is re-formalized and becomes as follows:

$$\mathbf{B}\mathbf{u}_i = \lambda_i\mathbf{u}_i \quad (2.26)$$

The Eigenvectors in the above equation are represented by  $\mathbf{u}_i$  for matrix  $\mathbf{B}$ . For any given  $\mathbf{u}_i$ ,  $\alpha\mathbf{u}_i$  is also an eigenvector for any  $\alpha$  (constant). The eigenvector can be normalized as  $\|\mathbf{u}_i\|=1$

#### ***2.2.3.4 Eigendecomposition of Autocorrelation Matrices [60, 63]***

As shown in the previous sections, estimating the spectrum can be performed using a variety of methods based on some parameters. Other methods may use the characteristics of the process in addition to the assumed parameters. In a practical context, for the autocorrelation matrix, these methods perform “*EigenDecomposition*” into noise and signal subspaces. Given that a

single frequency and complex exponential with white noise (equal intensity at different frequencies):

$$s(n) = h \exp(jn\omega_1) + q(n) \quad (2.27)$$

The complex exponential amplitude is represented by  $h_1$  and the white noise is represented by  $q(n)$ . The white noise variance is  $\sigma_q^2$ , the  $s(n)$  autocorrelation sequence can be formalized as follows:

$$r_{ss}(k) = P_1 \exp(jk\omega_1) + \sigma_q^2 \delta(k)$$

$$k = 0, \pm 1, \dots, \pm(M-1) \quad \dots \dots (2.28)$$

where  $P_1 = |h|^2$ , which is the complex exponential power. Now, the autocorrelation matrix  $V_y$  of dimension  $M \times M$  is the sum of the signal-based matrix ( $V_s$ ) and noise-based matrix ( $V_q$ ) as follows:

$$V_y = V_s + V_q \quad (2.29)$$

The  $V_s$  matrix is as follows:

$$V_s = P_1 \begin{bmatrix} 1 & e^{-j\omega_1} & e^{-j2\omega_1} & \dots & e^{-j(M-1)\omega_1} \\ e^{j\omega_1} & 1 & e^{-j\omega_1} & \dots & e^{-j(M-2)\omega_1} \\ e^{j2\omega_1} & e^{j\omega_1} & 1 & \dots & e^{-j(M-3)\omega_1} \\ \dots & \dots & \dots & \dots & \dots \\ e^{j(M-1)\omega_1} & e^{j(M-2)\omega_1} & e^{j(M-3)\omega_1} & \dots & 1 \end{bmatrix} \quad \dots \dots (2.30)$$

The noise matrix is diagonal and the signal matrix has a rank of one:

$$V_q = \sigma_q^2 I \quad (2.31)$$

The above equation is considered full-rank; and:

$$\mathbf{a}_1 = [1, e^{j\omega_1}, e^{j2\omega_1}, \dots, e^{j(M-1)\omega_1}]^T \quad (2.32)$$

Then  $\mathbf{V}_s$  is a signal vector of dimension  $M$  in terms of Equation (2.32) which becomes:

$$\mathbf{V}_s = P_1 \mathbf{a}_1 \mathbf{a}_1^H \quad (2.33)$$

Based on the rank of  $\mathbf{V}_s$  and the non-zero Eigenvalue, then:

$$\mathbf{V}_s \mathbf{a}_1 = P_1 (\mathbf{a}_1 \mathbf{a}_1^H) \mathbf{a}_1 = P_1 \mathbf{a}_1 (\mathbf{a}_1^H \mathbf{a}_1) = MP_1 \mathbf{a}_1 \quad (2.34)$$

The  $MP_1$  is the non-zero Eigenvalue and the Eigenvector is  $\mathbf{a}_1$ . The  $\mathbf{V}_s$  is “Hermitian”, the rest of Eigenvectors “ $\mathbf{u}_2, \mathbf{u}_3, \mathbf{u}_4, \dots, \mathbf{u}_m$ ” are orthogonal to  $\mathbf{a}_1$  as follows:

$$\mathbf{a}_1^H \mathbf{u}_i = 0; \quad \text{where } i = 2, 3, 4, \dots, M \quad (2.35)$$

when the  $\lambda_i^s$  are the Eigenvalues of  $\mathbf{V}_s$ , the following formula is obtained:

$$\mathbf{V}_y \mathbf{u}_i = (\mathbf{V}_s + \sigma_q^2 \mathbf{I}) \mathbf{u}_i = \lambda_i^s \mathbf{u}_i + \sigma_q^2 \mathbf{u}_i = (\lambda_i^s + \sigma_q^2) \mathbf{u}_i \quad (2.36)$$

The Eigenvector of  $\mathbf{V}_s$  is similar in  $\mathbf{V}_y$ :

$$\lambda_i = \lambda_i^s + \sigma_q^2 \quad (2.37)$$

The maximum Eigenvalues in  $\mathbf{V}_y$  is as follows:

$$\lambda_{max} = MP_1 + \sigma_q^2 \quad (2.38)$$

The above description is extended to  $M$ -frequencies in white noise and  $M > p$ , then the correlation sequence becomes as follows:

$$r_{ss}(k) = \sum_{i=1}^p P_i \exp(ik\omega_1) + \sigma_q^2 \delta(k) \quad (2.39)$$

The parameters of the above equation have been defined before and the new formula is written below:

$$\mathbf{V}_y = \mathbf{V}_s + \mathbf{V}_q = \sum_{i=1}^p P_i \mathbf{a}_i \mathbf{a}_i^H + \sigma_q^2 \mathbf{I} \quad (2.40)$$

Where  $\mathbf{a}_i$  is formalized as follows

$$\mathbf{a}_i = [1, e^{j\omega_i}, e^{j2\omega_i}, e^{j3\omega_i}, \dots, e^{j(M-1)\omega_i}]^T$$

$$i = 1, 2, 3, \dots, M \quad (2.41)$$

This is a set of M independent vectors.

Alternatively, this decomposition can be expressed as follows:

$$\mathbf{V}_y = \mathbf{A} \mathbf{P} \mathbf{A}^H + \sigma_q^2 \mathbf{I} \quad (2.42)$$

Where  $\mathbf{A} = [\mathbf{a}_1, \dots, \mathbf{a}_M]$  is  $M \times p$  matrix with p signal vectors and  $\mathbf{P} = \text{diag}\{P_1, \dots, P_p\}$  would hold the signal power diagonal matrix.

The eigenvalues of  $\mathbf{V}_y$

$$\lambda_i = \lambda_i^s + \sigma_q^2 \quad (2.43)$$

Where  $\lambda_i^s$ : eigenvalues of  $\mathbf{V}_s$

Since  $\mathbf{V}_s$  is a matrix of rank M, and  $\mathbf{V}_y$  has M eigenvalues, the first p eigenvalues will be larger than  $\sigma_q^2$  and the last M-p will be equal to a  $\sigma_q^2$ . Hence there are two kinds of Eigenvectors of  $\mathbf{V}_y$ : the signal Eigenvectors  $\mathbf{u}_1, \dots, \mathbf{u}_p$ , with eigenvalues larger than  $\sigma_q^2$  and the noise eigenvectors  $\mathbf{u}_{p+1}, \dots, \mathbf{u}_M$ , which have eigenvalues equal to  $\sigma_q^2$ . So, here's how we would break out  $\mathbf{V}_y$  :

$$\mathbf{V}_y = \sum_{i=1}^p (\lambda_i^s + \sigma_q^2) \mathbf{u}_i \mathbf{u}_i^H + \sum_{i=p+1}^M \sigma_q^2 \mathbf{u}_i \mathbf{u}_i^H \quad (2.44)$$

Matrix notation can be used to express this decomposition as:

$$\mathbf{V}_y = \mathbf{U}_s \mathbf{U}_s^H + \mathbf{U}_q \mathbf{U}_q^H \quad (2.45)$$

A signal eigenvectors  $M \times p$  matrix called  $\mathbf{U}_s$  is used here.

$$\mathbf{U}_s = [\mathbf{u}_1, \mathbf{u}_2, \dots, \mathbf{u}_p] \quad (2.46)$$

The noise eigenvectors'  $M \times (M-p)$  matrix is also known as  $\mathbf{U}_q$ .

$$\mathbf{U}_q = [\mathbf{u}_{p+1}, \mathbf{u}_{p+2}, \dots, \mathbf{u}_M] \quad (2.47)$$

Complex exponential frequencies can be estimated by using the orthogonality of the signal and noise subspaces, as was previously demonstrated for single complex exponential signal with white noise. As known, all signal eigenvectors  $\mathbf{a}_1, \dots, \mathbf{a}_p$  are in the subspace of the signal, hence the orthogonality includes  $\mathbf{a}_i$  is orthogonal to a noise eigenvectors:

$$\mathbf{a}_i^H \mathbf{u}_k = 0; \quad i=1,2,\dots,p \quad k=p+1, p+2, \dots, M \quad (2.48)$$

An estimation of the frequencies is given by using the following frequency estimation function:

$$\hat{P}(e^{j\omega}) = \frac{1}{\sum_{k=p+1}^M c_k |\mathbf{a}^H \mathbf{u}_k|^2} \quad (2.49)$$

Where  $c_k$  is a positive weight.

It is possible to estimate the direction of sources using array's steering vectors which are orthogonal to the noise subspace by detecting the peaks in the spatially power spectrum based on the eigendecomposition method.

### 2.2.3.5 Pisarenko Harmonic Decomposition Algorithm (PHD) [60, 63]

The PHD algorithm was first suggested by Pisarenko [17] in 1973 as a high-resolution method and was based on eigenanalysis of the autocorrelation matrix of the data model. The main reason behind developing this algorithm is to fill the gaps that existed in the classical approaches. The estimation was based on Eigen analysis of the  $V_y$ , where the eigenvector of  $V_y$  is used to derive the frequency. The PHD algorithm considers the sum of a known complex exponentials  $p$  in “white noise”  $s(n)$ . Also, it considers that the values  $(p+1)$  of the correlation sequence are already estimated or known. Then, given that a correlation matrix  $((p+1) \times (p+1))$ , the noise subspace dimension is 1, it is spanned by the Eigen corresponding to the minimum eigenvalue:

$$\lambda_{min} = \sigma_q^2 \quad (2.50)$$

The eigenvector  $\mathbf{u}_{min}$  is orthogonal to signal vectors  $\mathbf{a}_i$  as follows:

$$\mathbf{a}_i^H \mathbf{u}_{min} = \sum_{k=0}^p u_{min}(k) e^{-jk\omega_i} = 0 \quad (2.51)$$

Where  $i=1, 2, 3, \dots, p$  and then,

$$U_{min}(e^{j\omega}) = \sum_{k=0}^p u_{min}(k) e^{-jk\omega} = 0 \quad (2.52)$$

The above equation equals 0 at each  $\omega_i$ . Now, the z-transform of the eigenvector of the noise is called “Eigen Filter” and on the unit, a circle has  $p$  zeros.

$$U_{min}(z) = \sum_{k=0}^p u_{min}(k)z^{-k} = \prod_{k=1}^p (1 - e^{-jk\omega}z^{-1}) \quad (2.53)$$

In the above equation, the value of  $z=e^{j\omega}$  and the frequency is derived from the “Eigen Filter Roots”. The estimation function of the frequency is formalized as follows:

$$\hat{P}_{PHD}(e^{j\omega}) = \frac{1}{|\mathbf{a}^H \mathbf{u}_{min}|^2} \quad (2.54)$$

It should be mentioned that the term  $\hat{P}_{PHD}(e^{j\omega})$  is large and the location of the peaks in it is used for estimating the frequencies. Also, this term is called “*Eigenspectrum*” or sometimes “*Pseudospectrum*” that does not include information about the noise components or the complex exponentials. After determining the frequencies,  $P_i$  will be extracted from the  $\mathbf{V}_y$  eigenvalues. The details of this process are described as follows:

Consider the Eigenvectors of the signal subspace ( $u_1, \dots, u_p$ ) can be normalized as:

$$\mathbf{u}_i^H \mathbf{u}_i = 1 \quad (2.55)$$

And,

$$\mathbf{V}_y \mathbf{u}_i = \lambda_i \mathbf{u}_i \quad (2.56)$$

where  $i = 1, 2, 3, \dots, p$  and by multiplying both sides with  $\mathbf{u}_i^H$ , it becomes as follows:

$$\mathbf{u}_i^H \mathbf{V}_y \mathbf{u}_i = \lambda_i \mathbf{u}_i^H \mathbf{u}_i = \lambda_i \quad (2.57)$$

By substituting  $\mathbf{V}_y$  with  $\mathbf{A} \mathbf{P} \mathbf{A}^H + \sigma_w^2 \mathbf{I}$ , the above equation becomes:

$$\mathbf{u}_i^H \mathbf{V}_y \mathbf{u}_i = \mathbf{u}_i^H \left\{ \sum_{k=1}^p P_k \mathbf{a}_k \mathbf{a}_k^H + \sigma_q^2 \mathbf{I} \right\} \mathbf{u}_i = \lambda_i \quad (2.58)$$

The above formula can be re-written as follows:

$$\sum_{k=1}^p P_k |\mathbf{a}_k^H \mathbf{u}_i|^2 = \lambda_i - \sigma_q^2 \quad (2.59)$$

Where  $|\mathbf{a}_k^H \mathbf{u}_i|^2$  is the squared magnitude of the DT-FT that is calculated at frequency  $\omega_k$ . of the Eigenvector ( $\mathbf{u}_i$ ) of the signal subspace:

$$|\mathbf{a}_k^H \mathbf{u}_i|^2 = |U_i(e^{j\omega_k})|^2 \quad (2.60)$$

And,

$$U_i(e^{j\omega_k}) = \sum_{l=0}^p u_i(l) e^{-jl\omega} \quad (2.61)$$

Thus, Equation (2.59) can be re-written as follows:

$$\sum_{k=1}^p P_k |U_i(e^{j\omega_k})|^2 = \lambda_i - \sigma_q^2 \quad (2.62)$$

Now, the above equation is a set of a linear equation and takes the following form:

$$\begin{bmatrix} |U_1(e^{j\omega_1})|^2 & |U_1(e^{j\omega_2})|^2 & \dots & |U_1(e^{j\omega_p})|^2 \\ |U_2(e^{j\omega_1})|^2 & |U_2(e^{j\omega_2})|^2 & \dots & |U_2(e^{j\omega_p})|^2 \\ \dots & \dots & \dots & \dots \\ |U_p(e^{j\omega_1})|^2 & |U_p(e^{j\omega_2})|^2 & \dots & |U_p(e^{j\omega_p})|^2 \end{bmatrix} \begin{bmatrix} P_1 \\ P_2 \\ \dots \\ P_p \end{bmatrix} = \begin{bmatrix} \lambda_1 - \sigma_q^2 \\ \lambda_2 - \sigma_q^2 \\ \dots \\ \lambda_p - \sigma_q^2 \end{bmatrix} \quad (2.63)$$

The PHD can perform the estimation using peaks' locations in  $\hat{P}_{PHD}(e^{j\omega})$  or the roots of the Eigen filter. However, the PHD struggles with computation cost when it comes to high-order

problems. Also, the PHD has some limitations related to the availability of prior-knowledge about the signal's number of complex exponentials.

### ***2.2.3.6 Multiple Signal Classification (MUSIC) Algorithm [60, 62, 63]***

As explained above, the previous algorithm (PHD) is restricted by some limitations. Therefore, it becomes necessary to adopt an algorithm that is able to overcome the aforementioned limitations. The “Multiple Signal Classification (MUSIC)” comes for this purpose and has been suggested by Schmidt [18]. There is algorithm method is called Root-MUSIC to find frequencies we have moved its application towards DOA.

The detailed work of the MUSIC algorithm is described in this section. Consider having a random process  $s(n)$  that includes “Complex exponentials ( $p$ )” in “White-Noise” and variance of  $\sigma_q^2$ . Also, consider that the autocorrelation matrix ( $M \times M$ ) is  $V_y$  such that ( $M \geq p+1$ ). Moreover,  $\lambda_1 \geq \lambda_2 \geq \lambda_3 \geq \dots \geq \lambda_M$  are the ascending order of the  $V_y$  eigenvalues, and the corresponding eigenvectors are  $\mathbf{u}_1, \mathbf{u}_2, \mathbf{u}_3, \dots, \mathbf{u}_M$ , then, these vectors are partitioned into:

- The “*signal eigenvectors*” ( $p$ ) of the largest eigenvalues; and,
- The “*noise eigenvector*” ( $M-p$ ) of the eigenvalues that are equal to  $\sigma_q^2$ .

Hence the estimation of power spectrum using MUSIC method is [60, 62, 63]:

$$\hat{P}_{MU}(e^{j\omega}) = \frac{1}{\sum_{i=p+1}^M |\mathbf{a}^H \mathbf{u}_i|^2} \quad (2.64)$$

The above equation is used to find the positions of the largest peaks ( $M$ ), which are the frequency estimates of the complex exponentials.

### ***2.2.3.7 Root-MUSIC Algorithm***

It is an updated version of the MUSIC algorithm that has been proposed by Barabell [19]. The root of the polynomial in the MUSIC spectrum is utilized in the “*Angle of Arrival (AOA)*” estimation, a signal's direction of arrival, such as its radio, optical, or acoustic component, is known as its angle of arrival (AoA). The main difference between the MUSIC and Root-MUSIC is that MUSIC always provides the results as visual plots, but the Root-MUSIC provides the results as numbers.

Using a polynomial search for zeros instead of searching for maxima in the case of MUSIC, this method provides a direct estimate of the DoA. This strategy is only applicable to networks of linear antennas that are evenly spaced. By leveraging certain features of the received signals, it allows for a reduction in computation time and hence an increase in angular resolution. This approach uses a polynomial of degree  $2(M-1)$  to extract the roots [64]-[65] from a given polynomial. The estimation of signal arrival directions corresponds to the search for max. pseudo-spectrum  $F(\theta)$  values of MUSIC [72]:

$$F_{MUSIC}(\theta) = \frac{1}{\mathbf{a}^H(\theta) \mathbf{V}_q \mathbf{V}_q^H \mathbf{a}(\theta)} \quad (2.65)$$

Where  $\mathbf{V}_q$  is the matrix of eigenvectors that span the noise subspace. Let  $\mathbf{D} = \mathbf{V}_q \mathbf{V}_q^H$  is the projection matrix and  $\mathbf{a}^H(\theta) \mathbf{V}_q \mathbf{V}_q^H \mathbf{a}(\theta)$  is the noise subspace projection of the  $\mathbf{a}(\theta)$  vector.

According to (2.65), the following relation describes the steering vector's projection onto the noise subspace:

$$F_{MUSIC}^{-1}(\theta) = g_{R-MUSIC}(\theta) = \mathbf{a}^H(\theta) \mathbf{V}_q \mathbf{V}_q^H \mathbf{a}(\theta) \quad (2.66)$$

Equation (2.66) can be written:

$$F_{MUSIC}^{-1}(\theta) = g_{R-MUSIC}(\theta) = \mathbf{a}^H(\theta) \cdot \mathbf{D} \cdot \mathbf{a}(\theta) \quad (2.67)$$

Analysis and expression of steering vectors are used in this kind of representation  $\mathbf{a}_n(\theta) = e^{\frac{i2\pi d(n-1) \sin \theta}{\Psi}}$  of the  $n^{th}$  element of the linear array ( $n= 1, 2, \dots, N$ ), where  $\Psi$  is the wavelength, So [66]:

$$F_{MUSIC}^{-1}(\theta) = g_{R-MUSIC}(\theta) = \sum_{n=1}^M \sum_{p=1}^M e^{\frac{-i2\pi(n-1)d \sin \theta}{\Psi}} \mathbf{D}_{np} e^{\frac{i2\pi(p-1)d \sin \theta}{\Psi}} \quad (2.68)$$

Where  $\mathbf{D}_{np}$  refers to the elements of the  $n^{th}$  row and the  $p^{th}$  column of  $\mathbf{D}$  [66]. Root-MUSIC Algorithm is represented by a Linear Algebraic and the roots are obtained after equating (2.68) to zero. The following equation is generated by combining both amounts from (2.68):

$$F_{MUSIC}^{-1}(\theta) = g_{R-MUSIC}(\theta) = \sum_{L=-M+1}^{M-1} D_L e^{\frac{-2\pi L d \sin \theta}{\Psi}} \quad (2.69)$$

Where  $D_L = \sum_{n-p=L} \mathbf{D}_{np}$

The Root-MUSIC polynomial, a function of  $z$ , can be derived from Equation (2.69) [66], as follows:

$$R(z) = \sum_{L=-M+1}^{M-1} \mathbf{D}_L z^L \quad (2.70)$$

Where  $z = e^{\frac{-i2\pi d \sin \theta}{\Psi}}$

The problem is to find the  $2(M-1)$  double roots of the polynomial whose usable zeros are located on the unit circle because the directions of arrival of signals are functions of  $z$ . These complex root phases are consistent with the electrical phase shifts that are desired. From the following equation, the angles of signal arrival can be deduced [73]:

$$\theta_m = \sin^{-1} \left( \frac{\Psi}{2\pi d} \arg(z_m) \right) \quad (2.71)$$

Roots of the unit circle,  $z_m$  are the  $m$ -th nearest to the unit circle.

Now, calculating the root of the polynomial given in the values for  $\mu$ . The zero polynomial is considered in terms of  $(N-1)$  pairs within the unit circle. As a result, the closest roots ( $d$ ) to the circle unit are selected. Lastly, the values of AOA can be calculated according to the following formula:

$$\theta = \sin^{-1} \left[ \frac{\Psi}{2\pi d} \mu \right] \quad (2.72)$$

### 2.3 Direction of Arrival (DOA) Estimation

Recently a great revolution in wireless technologies has been witnessed. These technologies have been widely used in many different applications (e.g., tracking, environment monitoring, sensor

networks, etc.). This revolution introduces many policies that control the demand and use of these technologies. Most of the to be mentioned applications aim to determine the location of the source/target. This kind of request raises the demand for the Direction of Arrival (DOA) in communications systems [67].

According to the existing literature, the demand for DOA has increased in recent years. The most recent applications are “Mobile Wireless Communications” and “*Biomedical Signal Processing*” [68],[69]. Also, an antenna array is involved in most of these applications aiming to measure the incoming signals.

Furthermore, the DOA estimation can be performed for single or multiple sources of signals. Sensor arrays are usually involved in the estimation process. The literature on the field shows a lot of approaches proposed to find the DOA of signals based on sensor arrays and these approaches are categorized into: conventional (e.g., Fourier Transform) and subspace (e.g., Root-MUSIC).

### **2.3.1 Model of the Data**

The assumptions considered in this study algorithms for estimating DOA are:

- Linear Transmission Medium and Non-Isotropic: The transmission medium between signal sources and antenna array in all the directions does not have of the same physical features.
- Far-Field: This assumption states that the sources of signals are located far from the sensors. This means that the sources’

waves arrive at all sensors in equal directions. This situation is obtained by setting a larger space than the antenna array dimensions between the array and the sources. This leads to have a distance larger than  $2D^2/\lambda$ , where  $\lambda$  represents the signal's wavelength and  $D$  denotes the array's dimension.

- Narrowband: Signals of different sources  $p$  and their carrier have the same frequency. The contents of frequency are focused in the proximity of “*Carrier Frequency ( $f_c$ )*”. The coming signals can be formulated as follows:

$$s_i^r(t) = h_i(t)\cos[2\pi f_c t + \beta_i(t)] \quad (2.73)$$

Where  $1 \leq i \leq p$ ,  $r$  is used for narrowband,  $h_i(t)$  is the amplitudes, and  $\beta_i(t)$  is an arbitrary phase.

AWGN Channel: The features of the signals assumed are: zero mean, Gaussian complex white noise, and spatially uncorrelated with the signal. The white noise variance is  $\sigma^2$ .

### 2.3.2 Antenna Array

An antenna array is a set of antennas involved in receiving/transmitting signals [70]. The term “*Array Element*” is used to refer to a single antenna. In a receiving array, all elements receive the signal and merge them for processing (e.g., DOA estimation). Figure 2.1 depicts an antenna array of 3 elements (element\_1, element\_2, and element\_3). In the figure, element\_1 is called the “*Reference Element*”. The distance between any given two elements is denoted by  $d$ . The far distances of the sources (i.e., far-field) enable the path lines of the elements to be parallel [71].

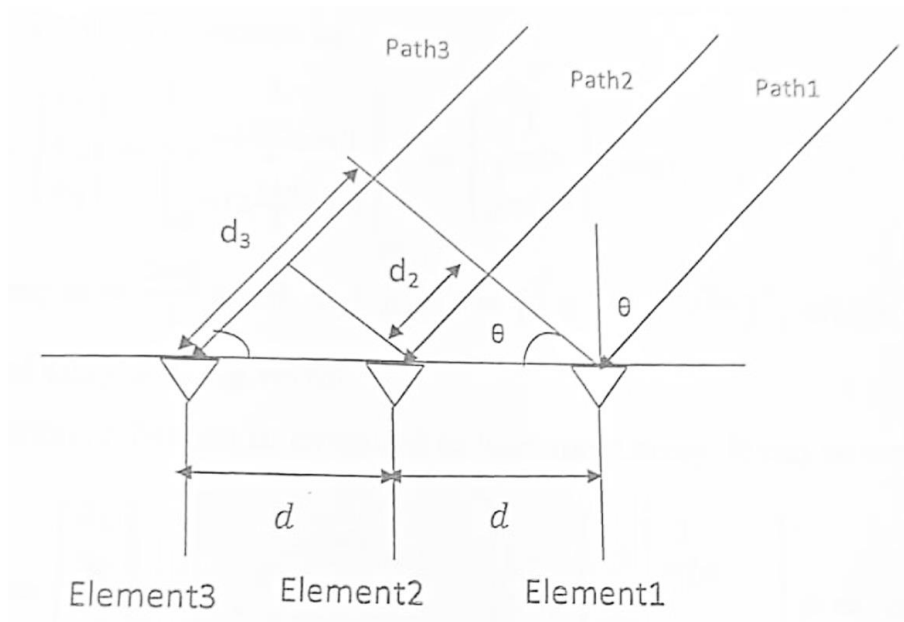


Figure 2.1: An antenna of 3 elements.

The path lines from the reference element to both elements 2 and 3 are explained in the following equation:

$$d_2 = d \cdot \sin \theta \quad (2.74 \text{ a})$$

$$d_3 = 2d \cdot \sin \theta \quad (2.74 \text{ b})$$

In general  $d_n = (n - 1)d \cdot \sin \theta \quad (2.75)$

Where  $\theta$  is the angle of waves impinging on the array and  $n=1, 2, 3$ . Moreover, consider that the wave received by the reference element is as follows:

$$s_1 = h \quad (2.76)$$

The waves received by the other two elements can be expressed as follows (considering no additive noise):

$$s_2 = h e^{-j\beta d_2} = h e^{-j\frac{2\pi d}{\Psi} \sin \theta} \quad (2.77)$$

And,

$$s_3 = h e^{-j\beta d_3} = h e^{-j2\frac{2\pi d}{\Psi} \sin \theta} \quad (2.78)$$

The term  $\beta = \frac{2\pi d}{\Psi}$  is the “*Phase Shift*” constant of the disseminating wave with  $\Psi$  of wavelength. The term  $e^{-j\beta d_n}$  in both of the above equations reflects the outcome of the difference between the reference element compared to the path lines (the additional mentioned distance). The receiving signals by the aforementioned elements can be generalized as follows:

$$\mathbf{s} = \begin{bmatrix} s_1 \\ s_2 \\ s_3 \end{bmatrix} = \begin{bmatrix} 1 \\ e^{-j\frac{2\pi d}{\Psi} \sin \theta} \\ e^{-j2\frac{2\pi d}{\Psi} \sin \theta} \end{bmatrix} h = \begin{bmatrix} 1 \\ e^{-j\mu} \\ e^{-j2\mu} \end{bmatrix} h = \mathbf{a}(\mu)h \quad (2.79)$$

Where  $\mathbf{a}(\mu) = [1 \ e^{-j\mu} \ e^{-j2\mu}]^T$  is called “*Array Steering Vector*”, and  $\mu = \frac{2\pi d}{\Psi}$ . The above equation can be extended as follows:

$$\mathbf{s} = \begin{bmatrix} s_1 \\ s_2 \\ \dots \\ s_N \end{bmatrix} = \begin{bmatrix} 1 \\ e^{-j\frac{2\pi d}{\Psi} \sin \theta} \\ \dots \\ e^{-j(N-1)\frac{2\pi d}{\Psi} \sin \theta} \end{bmatrix} h = \begin{bmatrix} 1 \\ e^{-j\mu} \\ \dots \\ e^{-j(N-1)\mu} \end{bmatrix} h = \mathbf{a}(\mu)h \quad (2.80)$$

Where N is the number of antenna elements.

Also the term  $\mathbf{a}(\mu)$  becomes as follows [72]:

$$\mathbf{a}(\mu) = [1 \ e^{-j\mu} \ \dots \ e^{-j(N-1)\mu}]^T \quad (2.81)$$

### 2.3.3 DOA Problem Formulation

In this study, the term “*Uniform Linear Array (ULA)*” will be frequently used. To describe this array, it is assumed that the system depicted in figure 2.2 is used having source  $i$  that have generated a wave signal of narrowband type ( $s_i^r$ ). But Wideband systems support substantially higher data rate communications than narrowband systems, which often have lower data rate transmissions. Broadband networks, to put it simply, facilitate speedier communication. The impinging on the array by the source is at an angle  $\theta_i$ .

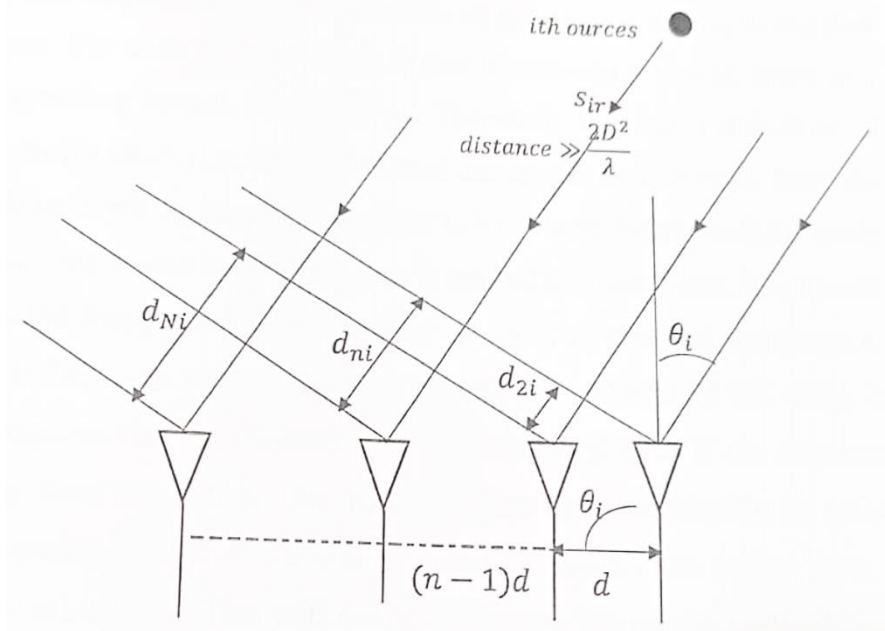


Figure 2.2: DOA estimation data model on  $N$  elements.

According to the previous section, the signal that is moving from the rightmost element takes a shorter distance compared to the other elements that consume additional distance that can be calculated using the following equation:

$$d_{ni} = (n - 1)d \sin \theta_i \quad (2.82)$$

Where  $n=1, 2, 3, \dots, N$ .

Furthermore, the difference between the signal received by the reference element (rightmost) and the  $n^{\text{th}}$  element is called “*Phase Shift Factor*” that can be formalized as  $e^{-j(n-1)\mu_i}$ . Also, this factor depends on the first element’s relative position and the spatial frequency ( $\mu_i$ ). In practice, there is a  $\mu_i$  for each incident angle  $\theta_i$  that detects the source. Accordingly the DOA estimation aims to investigate the signals received by the array and extract the spatial frequency ( $\mu_i$ ). These spatial frequencies are restricted by the following limitation:

$$-\pi \leq \mu_i \leq \pi \quad (2.83)$$

Also, the DOA potential range is limited by the following:

$$-90 \leq \theta_i \leq 90 \quad (2.84)$$

The above restriction intervals need the element spacing to hold the term  $d \leq \lambda/2$  [73]. In fact, this condition is necessary because if it does not hold, the estimation of DOA will be ambiguous since ( $\mu_i$ ) will lead to have two solutions for the angles. This specific case may lead to what is called “*Grating Lobes*” and it is also called “*Spatial Aliasing*”.

To generalize and formulate the noises and signals received by  $n^{\text{th}}$  elements, the following formula can be used [73]:

$$s_n = \sum_{i=1}^p S_i e^{-j(n-1)\mu_i} + q_{ni} \quad (2.85)$$

where  $n=1,2,3,\dots, N$ .

Now, differentiating the noise and the pure signal, the previous equation after calling the data, can be formalized as follows [73]:

$$\mathbf{S} = [\mathbf{a}(\mu_1), \mathbf{a}(\mu_2), \mathbf{a}(\mu_3), \dots, \mathbf{a}(\mu_M)] \begin{bmatrix} h_1 \\ h_2 \\ \dots \\ h_M \end{bmatrix} + \mathbf{q} = \mathbf{A}\mathbf{h} + \mathbf{q} \quad (2.86)$$

The data column vector received is denoted as  $\mathbf{s}$ , which is:  $\mathbf{S}=[\mathbf{s}_1, \mathbf{s}_2, \mathbf{s}_3 \dots \mathbf{s}_N]^T$ . Also, the signal column vector is denoted as  $\mathbf{s}$ , which is  $\mathbf{h}=[h_1, h_2, h_3 \dots h_N]^T$  and  $\mathbf{q}=[q_1, q_2, q_3 \dots q_N(t)]^T$  that represents a “Zero-Mean Spatially Uncorrelated Additive Noises” with the spatial covariance matrix of  $\sigma_N^2 \mathbf{I}_N$  [73]. Furthermore, the “Array Steering” column vector is denoted by  $\mathbf{a}(\mu_i)$  and formulated as follows [73]:

$$\mathbf{a}(\mu_i) = [1 \quad e^{j\mu_i} \quad e^{j2\mu_i} \quad \dots \quad e^{j(N-1)\mu_i}]^T \quad (2.87)$$

The steering matrix  $\mathbf{A}$  can be formalized based on the following equation [73]:

$$\begin{aligned} \mathbf{A} &= [\mathbf{a}(\mu_1) \quad \dots \quad \mathbf{a}(\mu_i) \quad \dots \quad \mathbf{a}(\mu_M)] \\ &= \begin{bmatrix} 1 & 1 & \dots & 1 \\ e^{j\mu_1} & e^{j\mu_2} & \dots & e^{j\mu_M} \\ \dots & \dots & \dots & \dots \\ e^{j(N-1)\mu_1} & e^{j(N-1)\mu_2} & \dots & e^{j(N-1)\mu_M} \end{bmatrix} \end{aligned} \quad (2.88)$$

# CHAPTER THREE

## Simulation Results

### 3.1 Introduction

In this chapter, simulation results are given for noiseless, and noisy data; and for both single and two emitting sources. The parameters required for DOA estimation methods are: number of samples,  $N$ , sampling interval,  $d$ , (equivalent to separation between receiving antennas or transducers), and the wavelength,  $\Psi$  of the transmitted signal from the source. The methods used are: the Fourier transform, also called a classical method, and the Root-MUSIC method, which is also considered as super resolution method. We are used computer software MATLAB program with m-file.

$$\theta_{\text{apparent}} = \sin^{-1}\left(\frac{((x_{\text{axis value}})/mk)*\Psi}{d}\right) \text{ for positive angle} \quad (3.1)$$

$$\theta_{\text{apparent}} = \sin^{-1}\left(\frac{((-x_{\text{axis value}})/mk)*\Psi}{d}\right) \text{ for negative angle} \quad (3.2)$$

Where  $mk=180^\circ$ .

The percentage error in all methods is determined by using the following equation:

$$\% \text{ Error} = \frac{|\theta_{\text{apparent}} - \theta_{\text{actual}}|}{|\theta_{\text{actual}}|} * 100 \quad (3.3)$$

## 3.2 Simulation Results with Noiseless Data

### 3.2.1 Single Source for DOA Estimation.

Figure (3.1) shows the result of using a single source. The Fourier transform (FFT) algorithm is applied. The values of parameters used here are  $N=12$ ,  $d=0.6$  cm,  $\Psi=2$  cm.

Figure (3.2) illustrates the effect of using only one source of information. Fourier transform (FFT) is used. The parameters utilized here are  $N=11$ ,  $d=0.6$  cm,  $\Psi=2$  cm, and the angle  $\theta_{\text{actual}}$  is  $37^\circ$ .

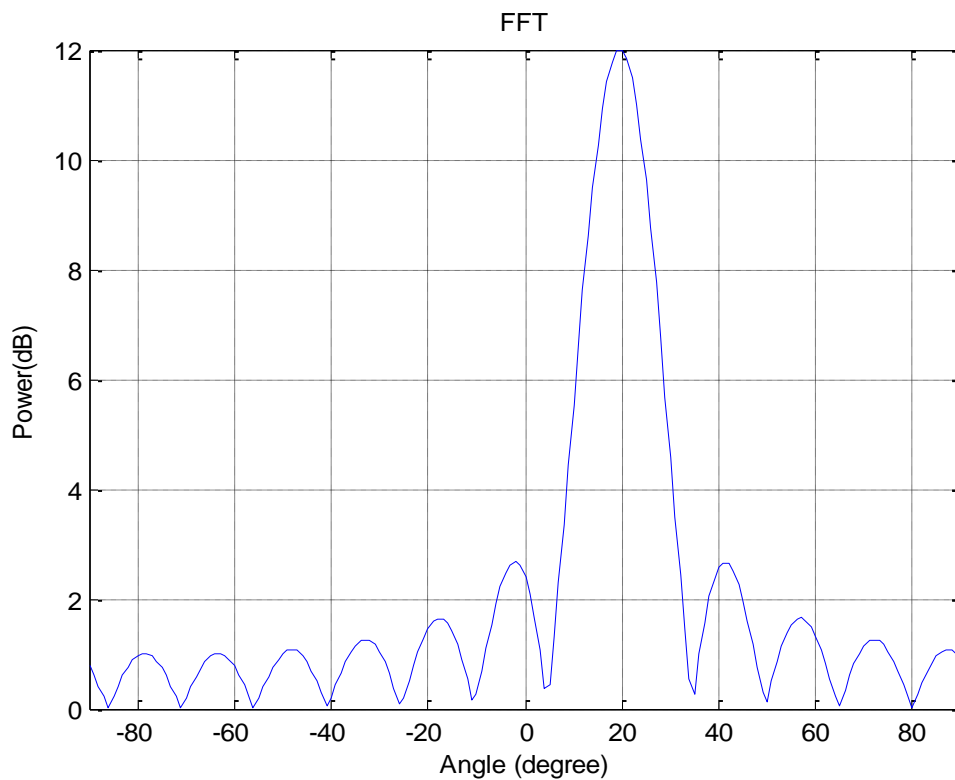


Figure (3.1) Magnitude (power(dB)) versus angle (degree) for a single-source angle  $\theta = 20^\circ$  using the FFT method ( $N=12$ ).

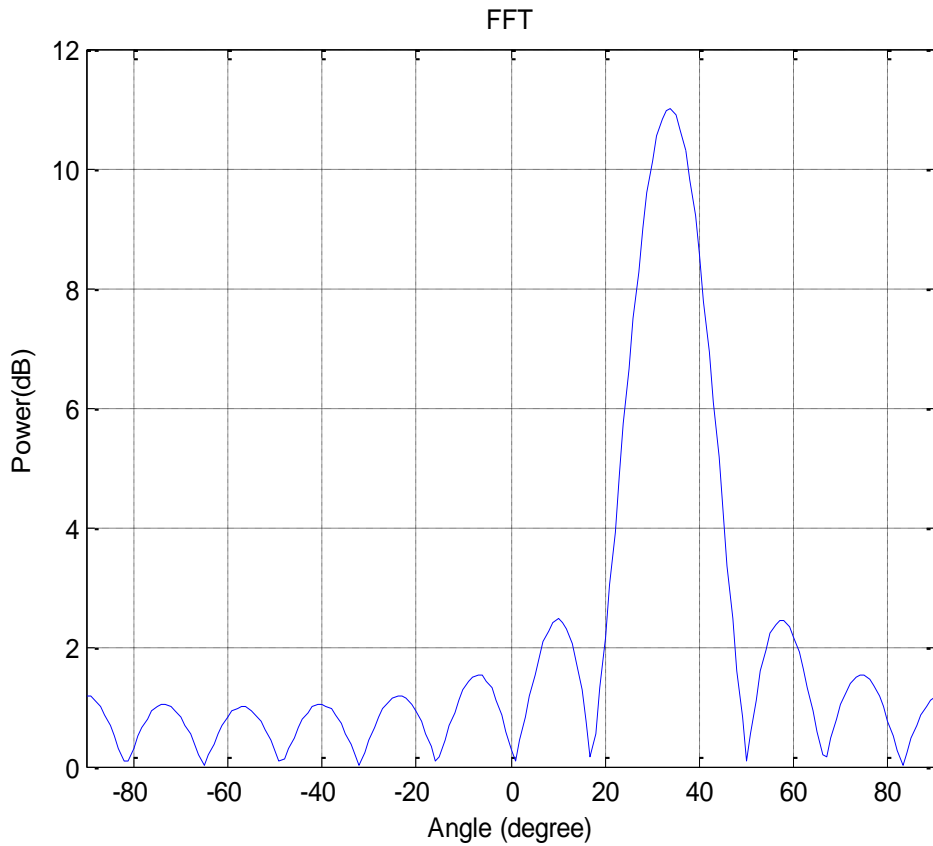


Figure (3.2) Magnitude (power(dB)) versus angle (degree) for a single-source angle  $\theta = 37^\circ$  using the FFT method (N=11)..

Using a single source yields the results shown in Figure (3.3). The Fourier transform procedure is used. N=10, d=0.6 cm,  $\Psi=2$  cm, and  $\theta_{\text{actual}} = -50^\circ$  are the parameters utilized in this example.

Figure (3.4) shows the result of using a single source. The Fourier transform (FFT ) algorithm is applied. The values of parameters used here are N=12, d=0.2 cm,  $\Psi=0.8$  cm, and the angle,  $\theta_{\text{actual}}$  is equal to  $6^\circ$ .

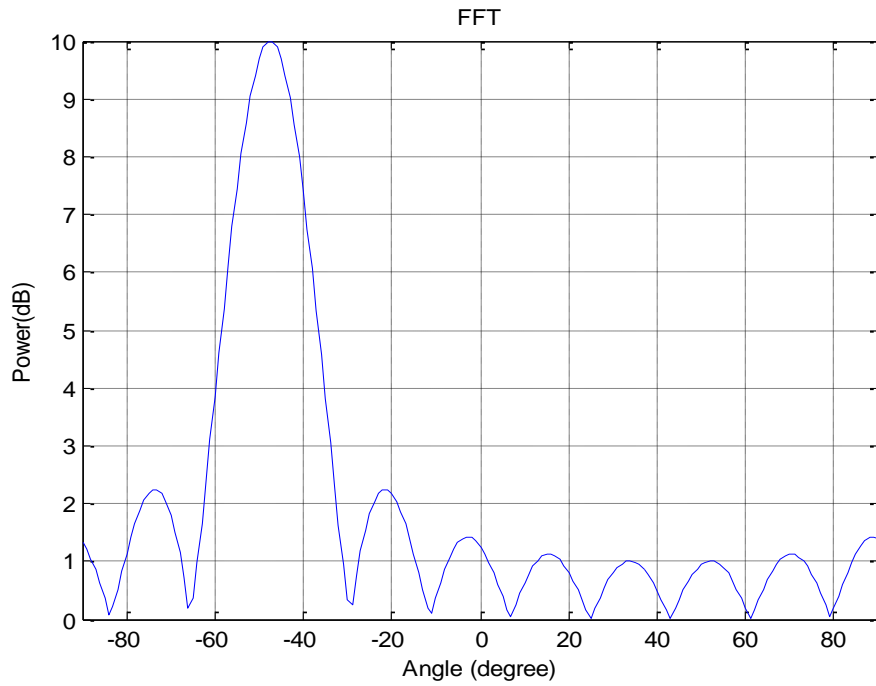


Figure (3.3) Magnitude (power(dB)) versus angle (degree) for a single-source angle  $\theta = -50^\circ$  using the FFT method (N=10).

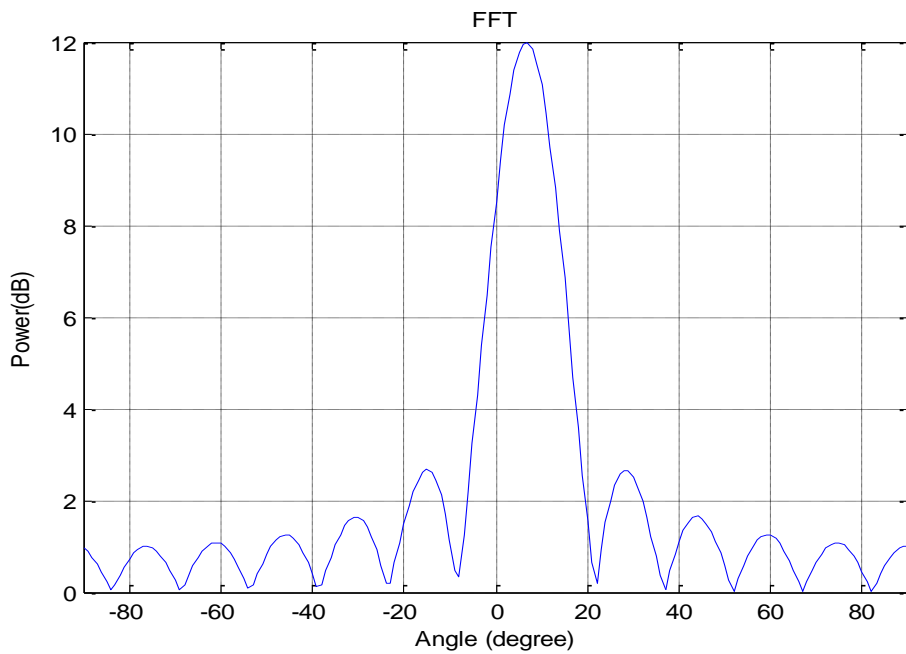


Figure (3.4) Magnitude (power(dB)) versus angle (degree) for a single-source angle  $\theta = 6^\circ$  using the FFT method (N=12).

In Figure (3.5), a single source is shown. The Fourier transform procedure is used.  $N=10$ ,  $d=0.2$  cm,  $\Psi=0.8$  cm, and  $\Theta_{\text{actual}} = -10^\circ$  are the values of parameters utilized here.

The use of one source is depicted in Figure (3.6). One method for doing this is through the use of an algorithm called Fourier transform (FFT).  $N=8$ ,  $d=0.2$  cm,  $\Psi = 0.8$  cm, and  $\Theta_{\text{actual}} = -11^\circ$  are the values of the parameters used in this example.

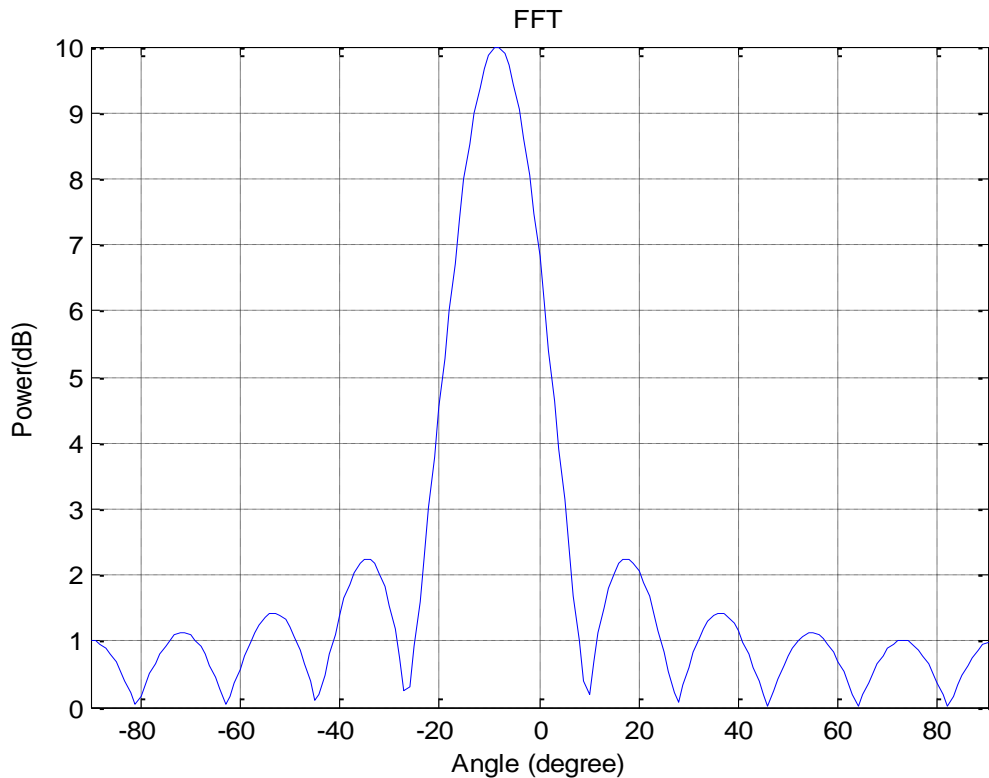


Figure (3.5) Magnitude (power(dB)) versus angle (degree) for a single-source angle  $\Theta = -10^\circ$  using the FFT method ( $N=10$ ).

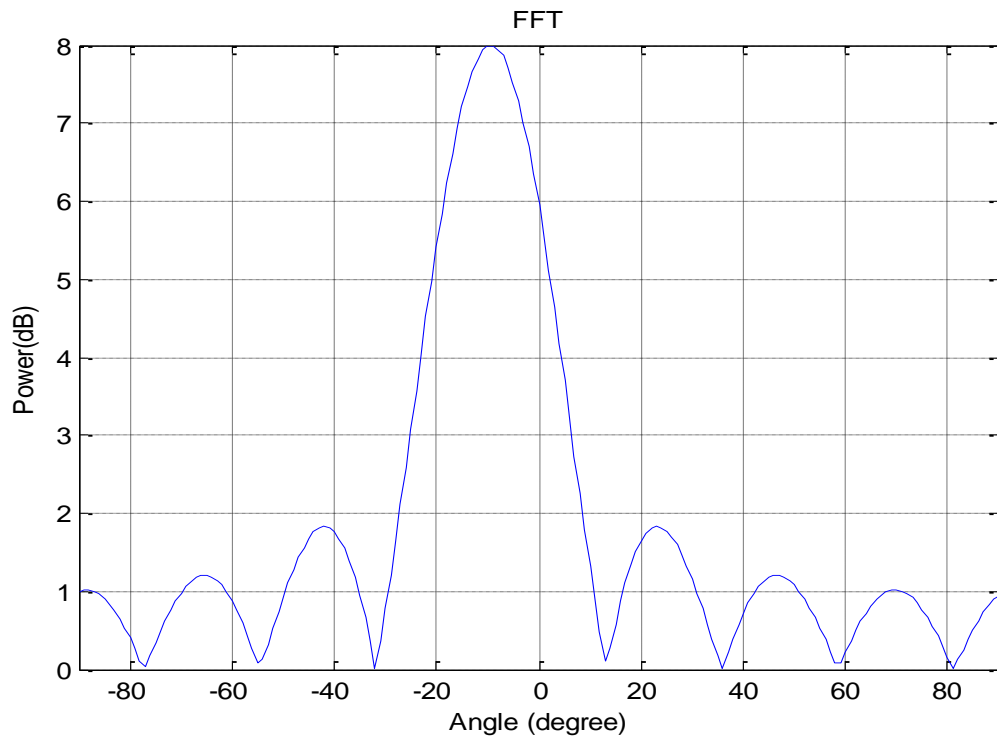


Figure (3.6) Magnitude (power(dB)) versus angle (degree) for a single-source angle  $\theta = -11^\circ$  using the FFT method (N=8).

We conclude from all the above figures that indicate to the relationship between Amplitude versus angles with noiseless data for a single source a sidelobe is clear, and this is the disadvantage of the FFT technique. Also, it is noticed that, from the resulting curve using the FFT method, the peak corresponding to the apparent (measured) angle is not sharp enough.

Figures (3.7) indicate (3D) plot to the relationship between the percentage error and the number of samples, N, and angles (Theta) with noiseless data for a single source for the FFT algorithm method. It is noticed that the percentage error is a constant level for the FFT algorithm method. For the Root-MUSIC, the percentage error equals

zero at all points of N (number of samples) and the order equals  $n=2$ . It means that  $N_{min}=5$  for the Root-MUSIC method. When using the Root-MUSIC method, it is found that the appearing value of  $\theta$  is equal exactly to its real value.

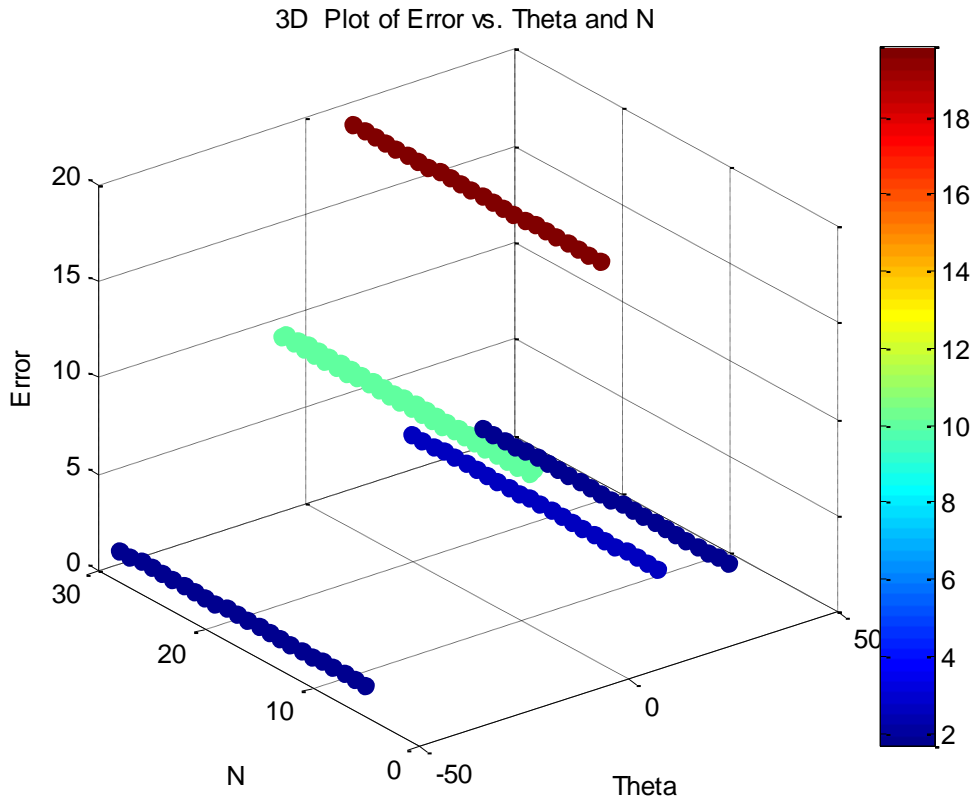


Figure (3.7) Percentage error of versus N and angles (Theta) for a single source DOA Estimation for (FFT) algorithm method.

### ***3.2.2 Double (two) emitting Sources for DOA Estimation.***

In figure (3.8) two sources are used to show the result of using the FFT algorithm method. The two sources can not be distinguished when the difference between two angles is (20 degrees) when  $N < 9$ .

A side lobe is clear and this is a problem of the FFT technique. when  $\theta_1=17^\circ$ ,  $\theta_2=37^\circ$ ,  $N=8$ ,  $d=0.6\text{cm}$ , and  $\Psi=2\text{cm}$ .

In figure (3.9) above, two sources are used to show the result of using the FFT algorithm method. It can recognize between two sources when the difference between two angles is (20 degrees) when  $N \geq 9$ . A side lobe is clear and this is a drawback of the FFT technique. when  $\theta_1=17^\circ$ ,  $\theta_2=37^\circ$ ,  $N=12$ ,  $d=0.6\text{cm}$  and  $\Psi=2\text{cm}$ .

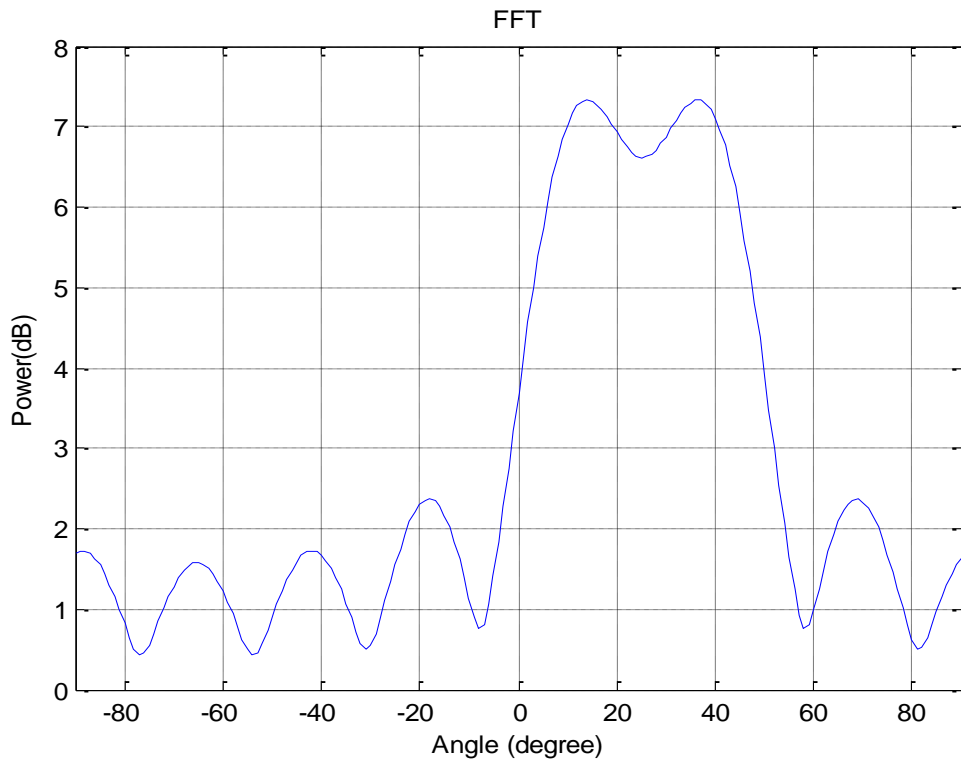


Figure (3.8) Magnitude (power(dB)) versus angle (degree) for a double (two)-source angle ( $\theta_1=17^\circ$ ,  $\theta_2=37^\circ$ ) using the FFT method ( $N=8$ ).

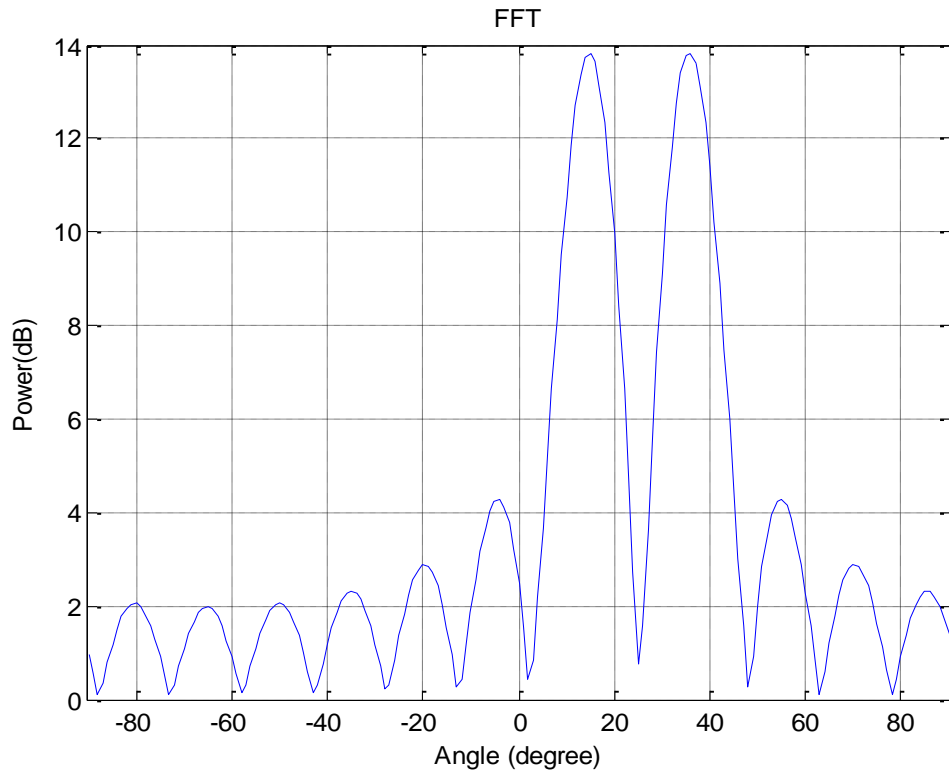


Figure (3.9) Magnitude (power(dB)) versus angle (degree) for a double (two)-source angle ( $\theta_1=17^\circ$  ,  $\theta_2=37^\circ$ ) using the FFT method ( $N=12$ ).

For the FFT algorithm method with noiseless double (two) sources, the relationship between the percentage error and  $N$  (number of samples) is shown in figure (3.10) when the first actual angle is equal to  $\theta_1=17^\circ$  and the second actual angle is equal to  $\theta_2=37^\circ$ . For the Root-MUSIC algorithm method, the percentage error of the first and second source is equal to zero at all points of  $N$  (number of samples) and the order is equal to  $n=3$ . It means that  $N_{min} = 8$  for the Root-MUSIC method.

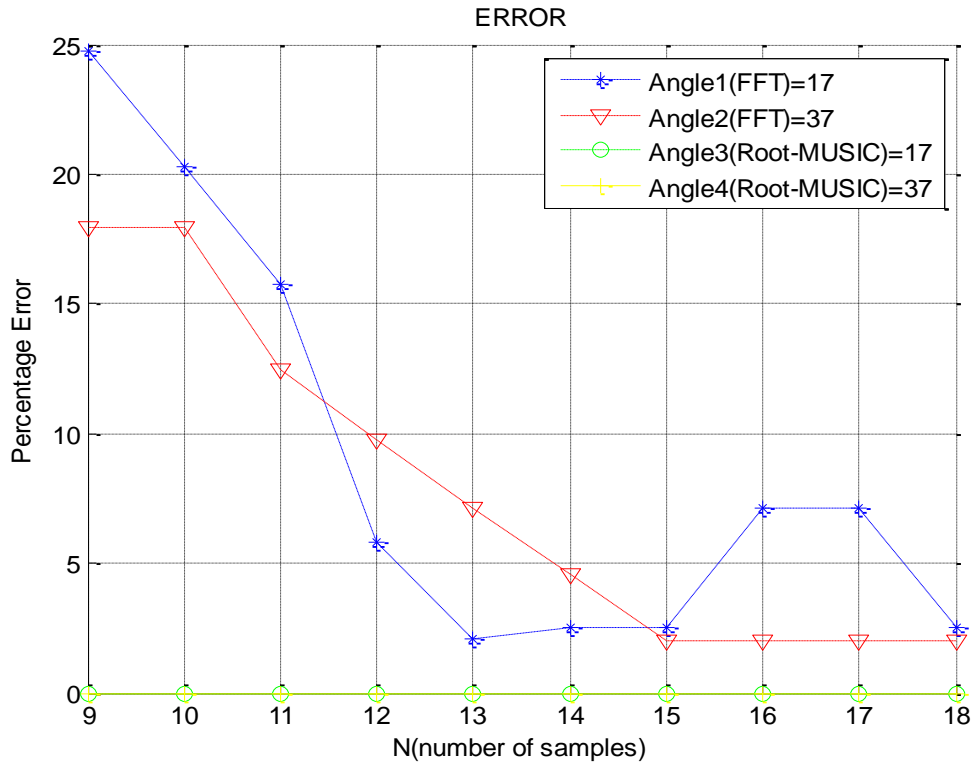


Figure (3.10) Percentage error of angle versus N for double (two) sources ( $\theta_1=17^\circ$ ,  $\theta_2=37^\circ$ ) for DOA Estimation.

Using the FFT algorithm approach, the results are shown in Figure (3.11) using two sources. If the difference between the two angles is (15 degrees) when  $N < 12$ , the two sources can not be distinguished. When  $\theta_1=20^\circ$ ,  $\theta_2=35^\circ$ ,  $N=11$ ,  $d=0.6\text{cm}$ , and  $\Psi=2\text{cm}$ , the FFT approach has a visible side lobe.

Using the FFT algorithm approach, the results are shown in figure (3.12) using two sources. If the difference between the two angles is (15 degrees) when  $N \geq 12$ , the two sources can be distinguished. When  $\theta_1=20^\circ$ ,  $\theta_2=35^\circ$ ,  $N=15$ ,  $d=0.6\text{cm}$ , and  $\Psi=2\text{cm}$ , the FFT approach has a visible side lobe.

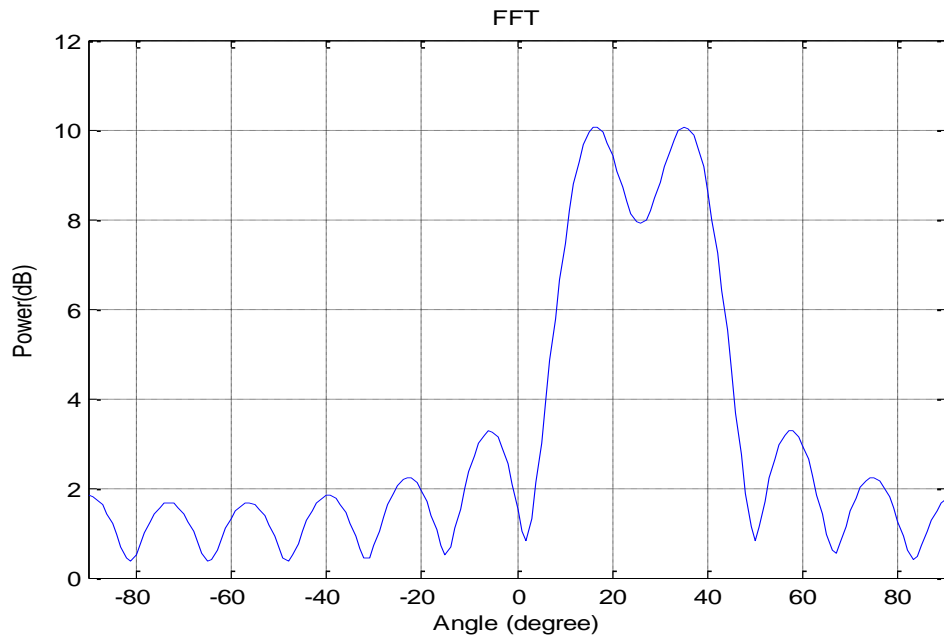


Figure (3.11) Magnitude (power(dB)) versus angle (degree) for a double (two)-source angle ( $\theta_1=20^\circ$ ,  $\theta_2=35^\circ$ ) using the FFT method (N=11).

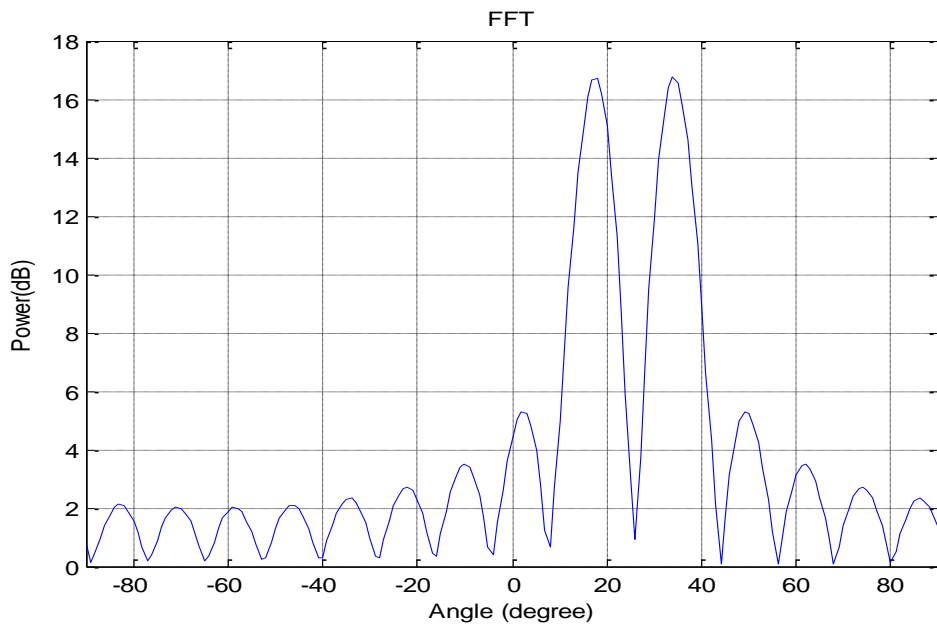


Figure (3.12) Magnitude (power(dB)) versus angle (degree) for a double (two)-source angle ( $\theta_1=20^\circ$ ,  $\theta_2=35^\circ$ ) using the FFT method (N=15).

Figure (3.13) refers to the relationship between the percentage error and N (number of samples) for the FFT algorithm method with noiseless double (two) sources when the first actual angle is equal to  $\theta_1=20^\circ$  and the second actual angle is equal to  $\theta_2=35^\circ$ . For the Root-MUSIC algorithm method, the percentage error of the first and second source is equal to zero at all points of N (number of samples) and the order is equal to  $n=3$ . It means that  $N_{min} = 8$  for the Root-MUSIC method.

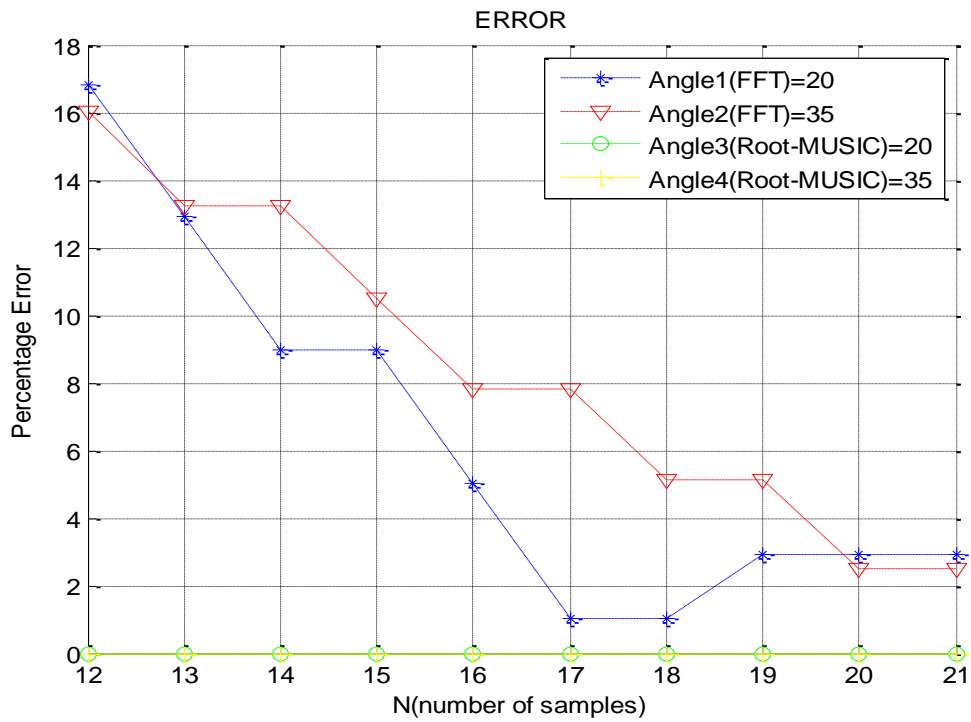


Figure (3.13) Percentage error of angle versus N for double (two) sources ( $\theta_1=20^\circ$ ,  $\theta_2=35^\circ$ ) for DOA Estimation.

In figure (3.14), the FFT algorithm results from two different sources are shown.  $N < 17$  allows it for not distinguishing between two sources when the difference in angles is 10 degrees. When  $\theta_1 =$

$25^\circ$ ,  $\theta_2=-35^\circ$ ,  $N=16$ ,  $d=0.6\text{cm}$ , and  $\Psi =2\text{cm}$ , there is a visible side lobe, which is one of the limitations of using the FFT method.

In figure (3.15), the FFT algorithm results from two different sources are shown.  $N \geq 17$  allows it for distinguishing between two sources when the difference in angles is 10 degrees. When  $\theta_1=-25^\circ$ ,  $\theta_2=-35^\circ$ ,  $N=22$ ,  $d=0.6\text{cm}$ , and  $\Psi =2\text{cm}$ , there is a visible side lobe, which is one of the limitations of using the FFT method.

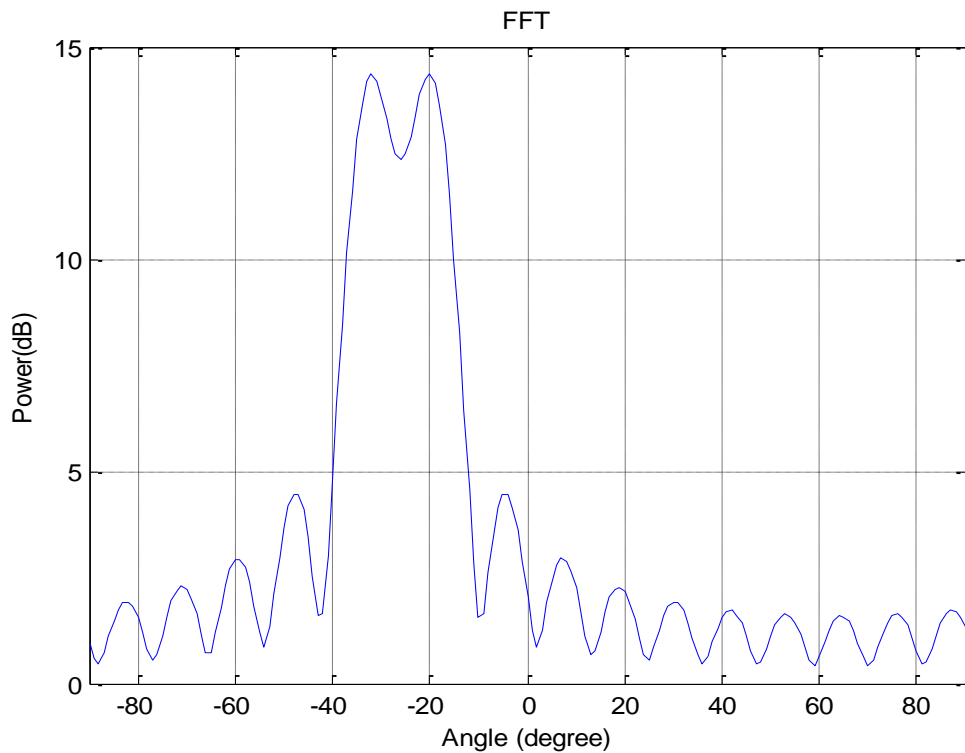


Figure (3.14) Magnitude (power(dB)) versus angle (degree) for a double (two)-source angle ( $\theta_1=-25^\circ$ ,  $\theta_2=-35^\circ$ ) using the FFT method ( $N=16$ ).

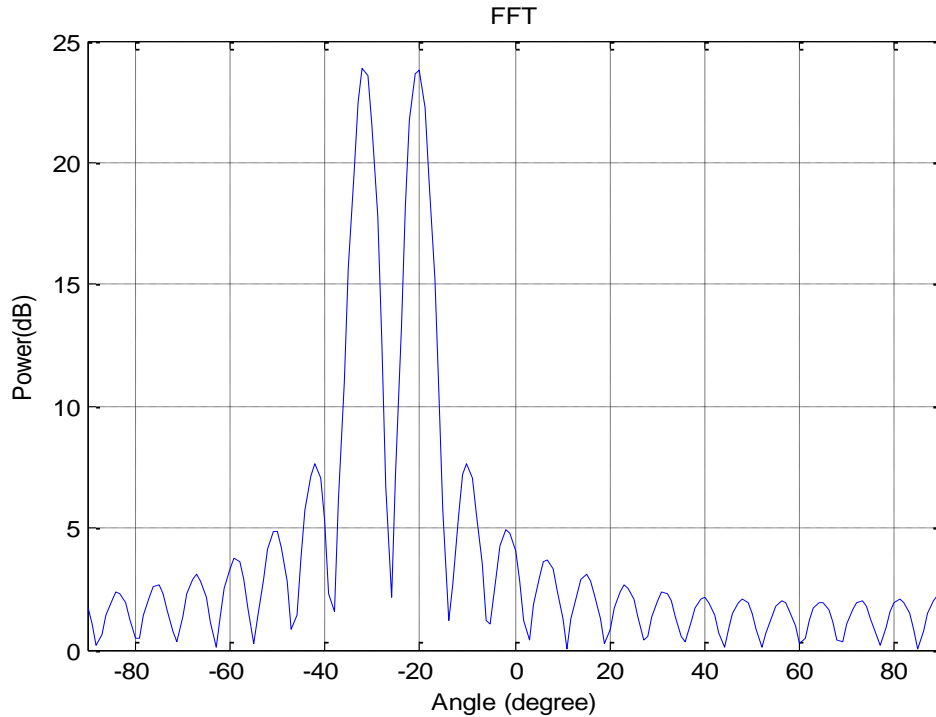


Figure (3.15) Magnitude (power(dB)) versus angle (degree) for a double (two)-source angle ( $\theta_1=-25^\circ$ ,  $\theta_2=-35^\circ$ ) using the FFT method ( $N=22$ ).

The relationship between the percentage error and  $N$  (number of samples) for the FFT algorithm method with noiseless double (two) sources, when the first actual angle is equal to  $\theta_1=-25^\circ$  and the second actual angle is equal to  $\theta_2=-35^\circ$ , is depicted in figure (3.16). It noticed that the percentage error is maximum at minimum  $N$  (number of samples) and then decreases at maximum  $N$  (number of samples). When using the Root-MUSIC algorithm approach, the order is equal to  $n=3$ , and the percentage error of the first and second sources is equal to zero at all points of  $N$  (number of samples). It indicates that for the Root-MUSIC approach,  $N_{\min}=8$ .

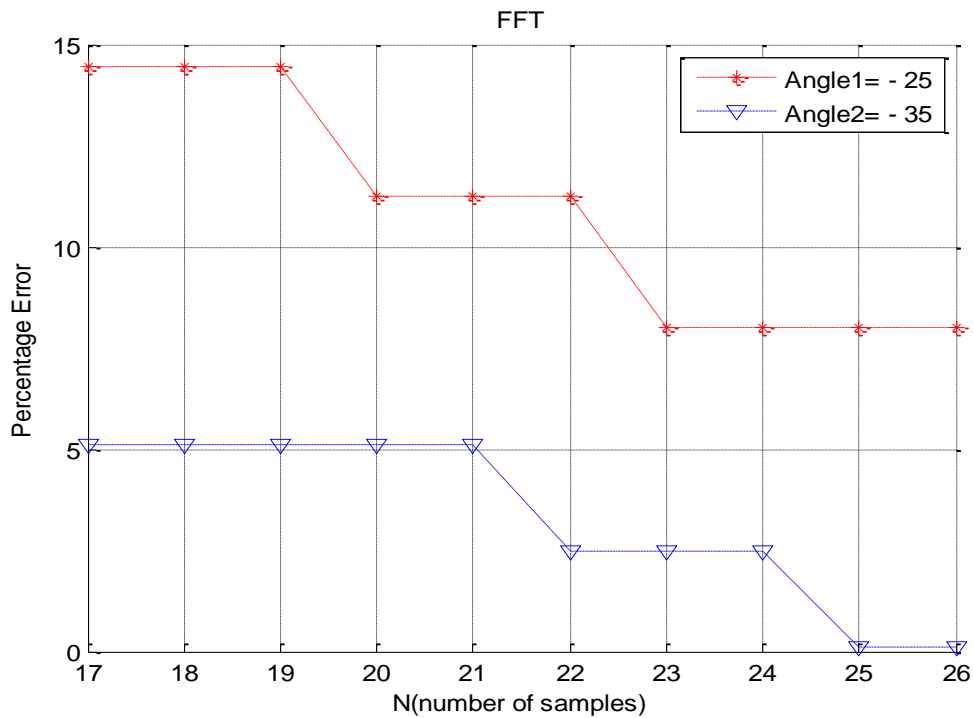


Figure (3.16) Percentage error of angle versus N for double (two) sources ( $\theta_1=-25^\circ$ ,  $\theta_2=-35^\circ$ ) for DOA Estimation.

Figure (3.17) shows the FFT algorithm results from two different sources. When the difference between the two angles is (25 degrees) when  $N \leq 8$ , the two sources can not be distinguished. When  $\theta_1=-15^\circ$ ,  $\theta_2=-40^\circ$ ,  $N=8$ ,  $d=0.6\text{cm}$ , and  $\Psi =2\text{cm}$ , a side lobe is clearly visible, which is one of the downsides of the FFT method.

Figure (3.18) shows the FFT algorithm results from two different sources. When the difference between the two angles is (25 degrees) when  $N > 8$ , the two sources can be distinguished. When  $\theta_1=-15^\circ$ ,  $\theta_2=-40^\circ$ ,  $N=17$ ,  $d=0.6\text{cm}$ , and  $\Psi =2\text{cm}$ , a side lobe is clearly visible, which is one of the downsides of the FFT method.

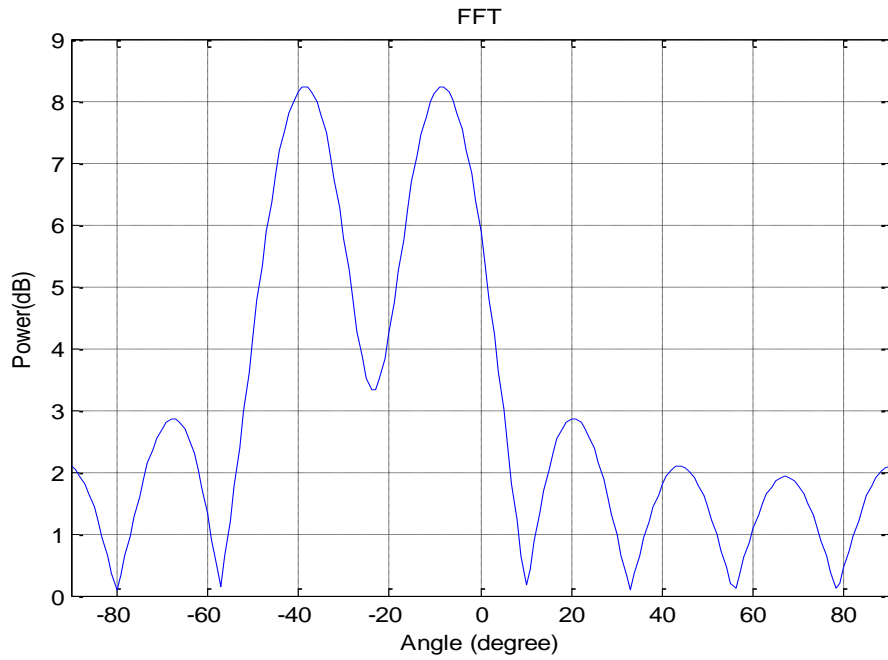


Figure (3.17) Magnitude (power(dB)) versus angle (degree) for a double (two)-source angle ( $\theta_1=-15^\circ$ ,  $\theta_2=-40^\circ$ ) using the FFT method ( $N=8$ ).

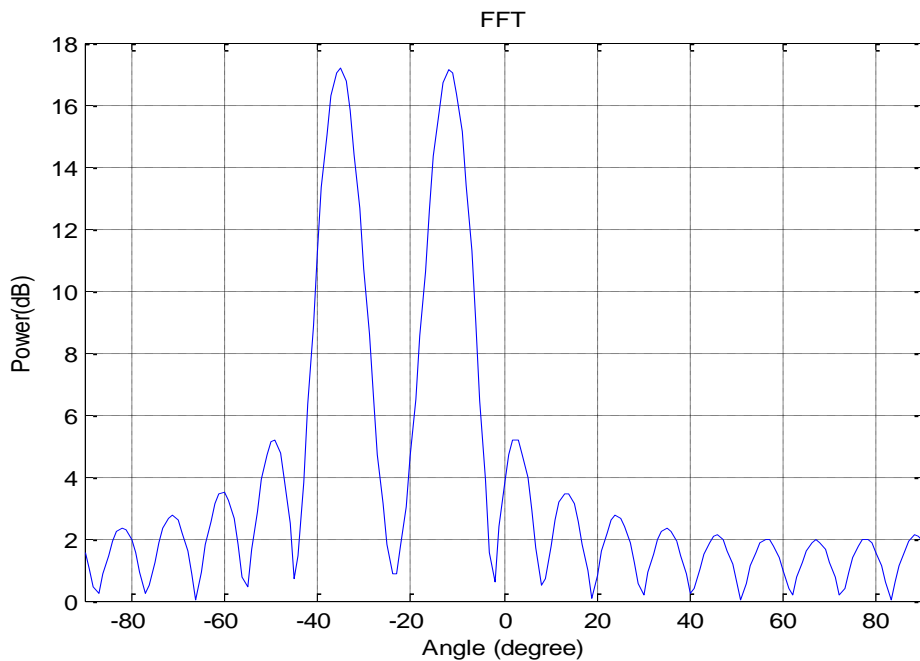


Figure (3.18) Magnitude (power(dB)) versus angle (degree) for a double (two)-source angle ( $\theta_1=-15^\circ$ ,  $\theta_2=-40^\circ$ ) using the FFT method ( $N=17$ ).

Using the FFT algorithm approach with noiseless double (two) sources and a first angle of  $\theta_1=-15^\circ$  and a second angle of  $\theta_2=-40^\circ$ , figure (3.19) shows the relationship between percentage error and N (number of samples). It was observed that the percentage error peaks at the lowest number of samples, N, and subsequently falls at the highest number of samples, N. The order is equivalent to  $n=3$  when employing the Root-MUSIC algorithm technique, and the first and second sources' percentage errors are always equal to zero (number of samples = N). It suggests that  $N_{\min}=8$  for the Root-MUSIC method.

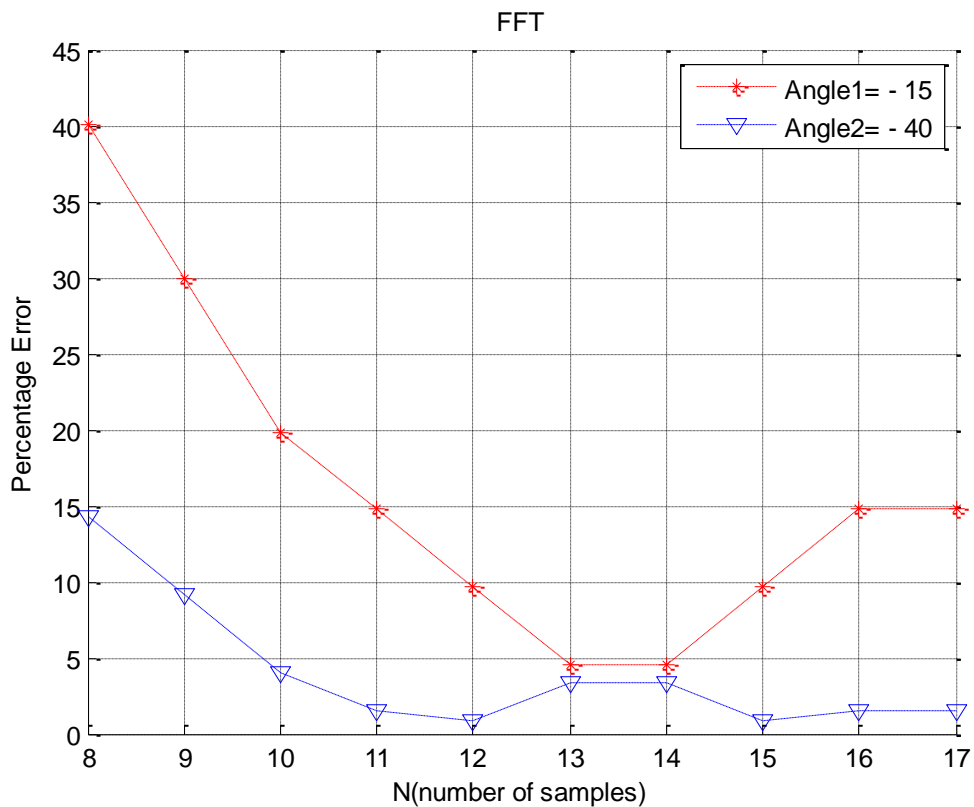


Figure (3.19) Percentage error of angle versus N for double (two) sources ( $\theta_1=-15^\circ, \theta_2=-40^\circ$ ) for DOA Estimation.

Figure (3.20) shows the results of utilizing the FFT algorithm approach employing two sources. When  $N$  is less than or equal to 5, it may not distinguish between two sources when the angle difference between the two is (30 degrees). When  $\theta_1=-17^\circ$ ,  $\theta_2=13^\circ$ ,  $N=5$ ,  $d=0.6\text{cm}$ , and  $Y=2\text{cm}$ , a side lobe is clearly visible and this is a downside of the FFT technique.

Figure (3.21) shows the results of utilizing the FFT algorithm approach employing two sources. When  $N$  is more than or equal to 6, it may distinguish between two sources when the angle difference between the two is (30 degrees). When  $\theta_1=-17^\circ$ ,  $\theta_2=13^\circ$ ,  $N=14$ ,  $d=0.6\text{cm}$ , and  $Y=2\text{cm}$ , a side lobe is clearly visible and this is a downside of the FFT technique.

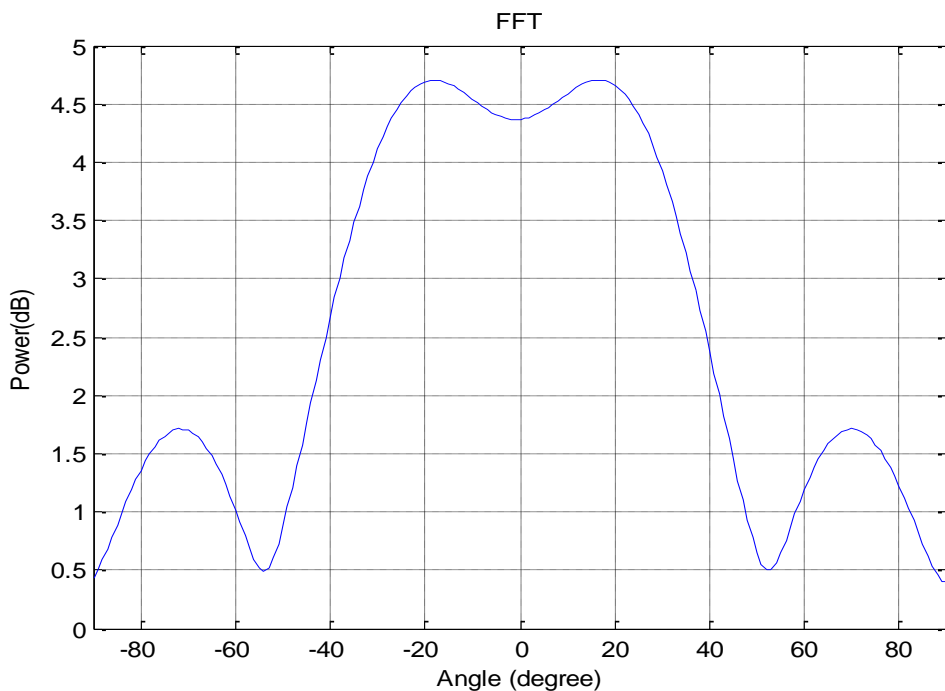


Figure (3.20) Magnitude (power(dB)) versus angle (degree) for a double (two)-source angle ( $\theta_1=-17^\circ$ ,  $\theta_2=13^\circ$ ) using the FFT method ( $N=5$ ).

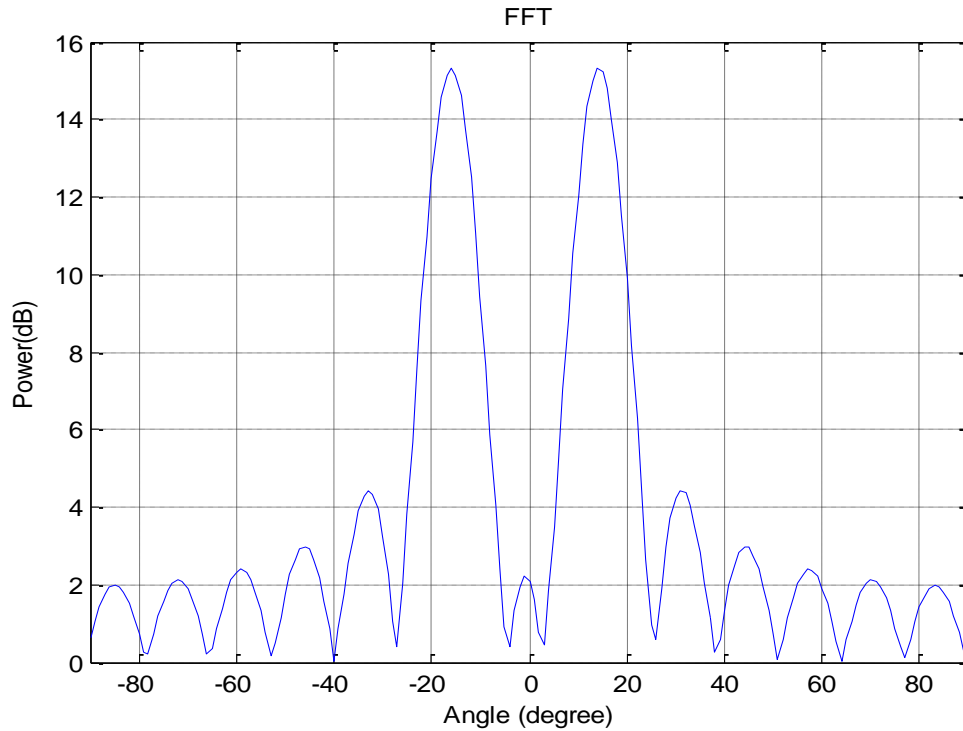


Figure (3.21) Magnitude (power(dB)) versus angle (degree) for a double (two)-source angle ( $\theta_1=-17^\circ$ ,  $\theta_2=13^\circ$ ) using the FFT method ( $N=14$ ).

The relationship between percentage error and  $N$  (number of samples) for the FFT algorithm method with noiseless double (two) sources when the first actual angle is equal to  $\theta_1=-17^\circ$  and the second actual angle is equal to  $\theta_2=13^\circ$ , is depicted in figure (3.22). It was observed that at minimal  $N$  (number of samples), the percentage error is at its maximum, and at maximum  $N$  (number of samples), it declines. When employing the Root-MUSIC algorithm approach, the first and second sources' percentage errors are equal to zero over the whole  $N$  (number of samples) range, and the order is equal to  $n=3$ . It shows that  $N_{\min}=8$  for the Root-MUSIC method.

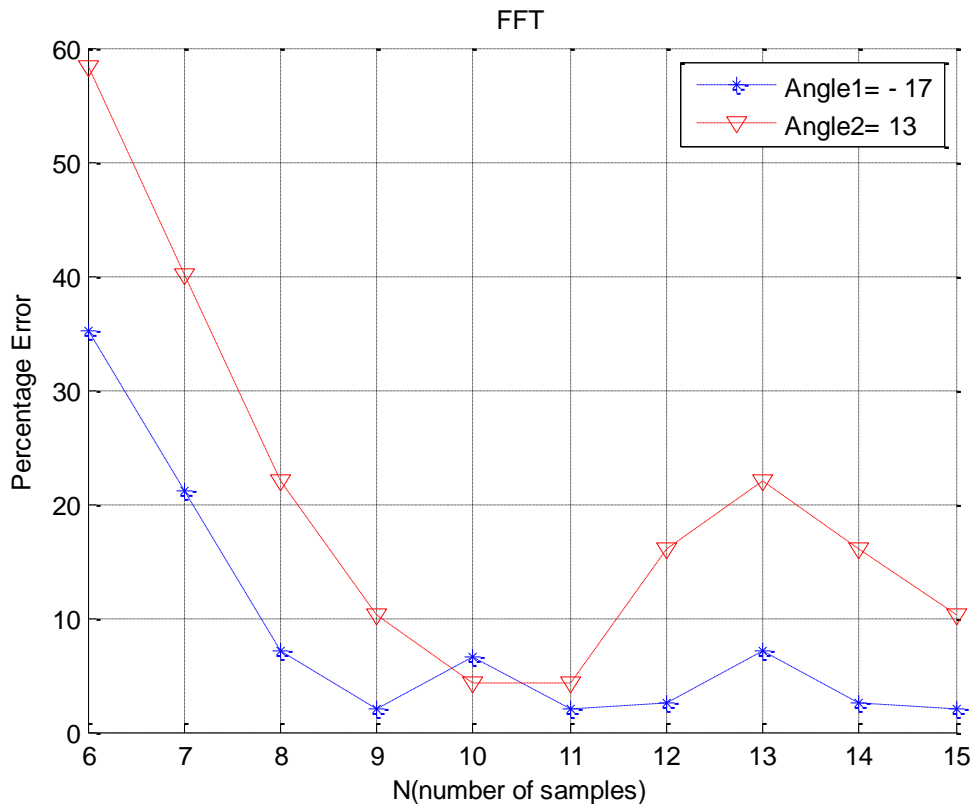


Figure (3.22) Percentage error of angle versus N for double (two) sources ( $\theta_1=-17^\circ$ ,  $\theta_2=13^\circ$ ) for DOA Estimation.

Figure (3.23) shows the result of utilizing the FFT algorithm approach with two sources. When the difference between the two angles is (25 degrees) when  $N < 7$ , the two sources can not be distinguished. Because of this, when  $\theta_1=-10^\circ$ ,  $\theta_2=15^\circ$ ,  $N=6$ ,  $d=0.6\text{cm}$ ,  $\Psi=2\text{cm}$ , the FFT approach has certain issues.

Figure (3.24) shows the result of utilizing the FFT algorithm approach with two sources. When the difference between the two angles is (25 degrees) when  $N \geq 7$ , the two sources can be distinguished. Because of this, when  $\theta_1=-10^\circ$ ,  $\theta_2=15^\circ$ ,  $N=17$ ,  $d=0.6\text{cm}$ ,  $\Psi=2\text{cm}$ , the FFT approach has certain issues.

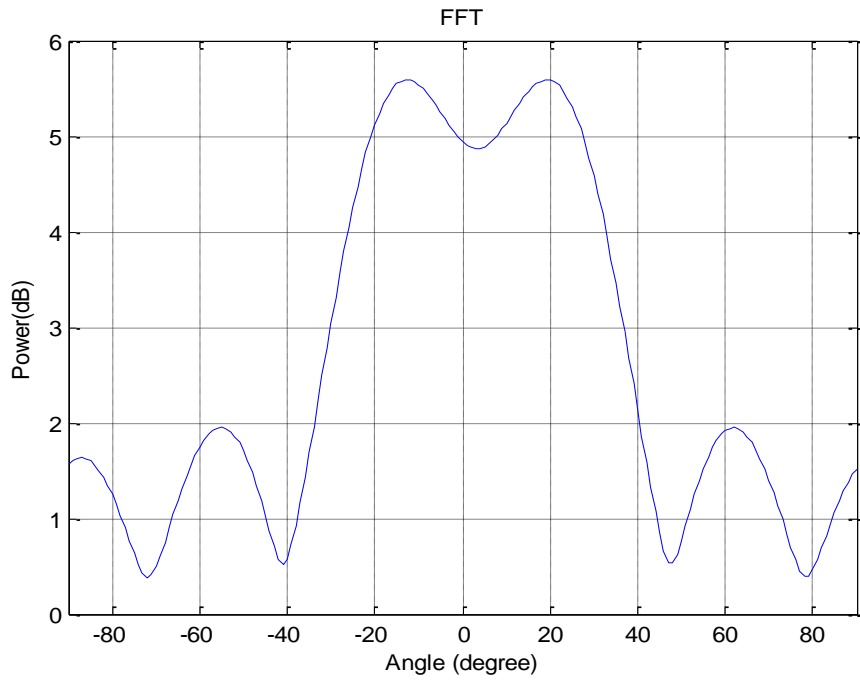


Figure (3.23) Magnitude (power(dB)) versus angle (degree) for a double (two)-source angle ( $\theta_1=-10^\circ$ ,  $\theta_2=15^\circ$ ) using the FFT method (N=6).

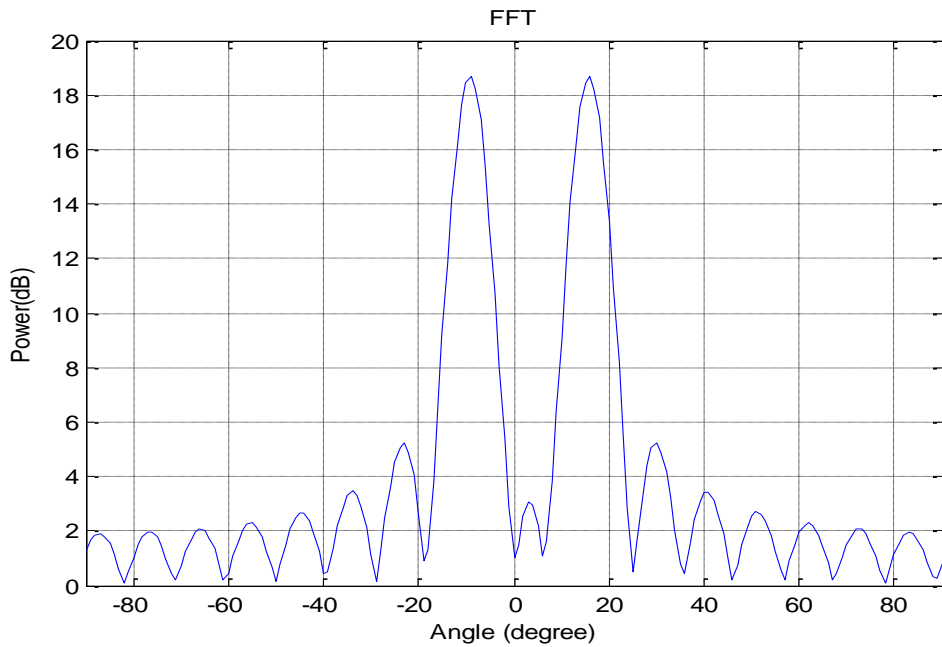


Figure (4.24) Magnitude (power(dB)) versus angle (degree) for a double (two)-source angle ( $\theta_1=-10^\circ$ ,  $\theta_2=15^\circ$ ) using the FFT method (N=17).

The relationship between the percentage error and N (number of samples) for the FFT algorithm method with noiseless double (two) sources when the first actual angle is equal to  $\theta_1=-10^\circ$  and the second actual angle is equal to  $\theta_2=15^\circ$  is illustrated in figure (3.25). The percentage error was found to peak at the lowest number of samples, or N, and to fall at the highest number of samples, or N. When the Root-MUSIC algorithm approach is applied, the first and second source's percentage error is equal to zero at all locations within N (the number of samples), and the order is equal to  $n=3$ . According to it,  $N_{\min}=8$  for the Root-MUSIC method.

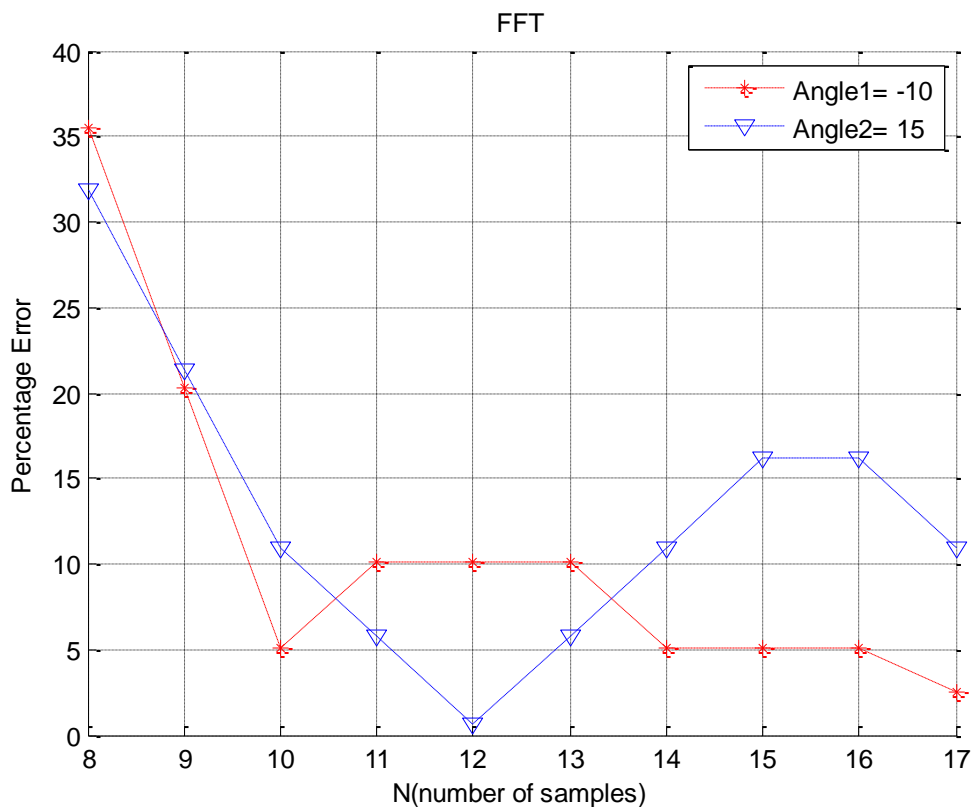


Figure (3.25) Percentage error of angle versus N for double (two) sources ( $\theta_1=-10^\circ$ ,  $\theta_2=15^\circ$ ) for DOA Estimation.

As seen in figure (3.26), the FFT algorithm method yields the desired results. When  $N \leq 5$ , it can not distinguish between two sources when the difference in the two angles is (55 degrees). When  $\theta_1 = -29^\circ$ ,  $\theta_2 = 26^\circ$ ,  $N$  is 5,  $d$  is 0.2cm, and  $\Psi$  is 0.8cm, a side lobe is clearly visible. This is a shortcoming of the FFT technique.

As seen in figure (3.27), the FFT algorithm method yields the desired results. When  $N > 5$ , it can distinguish between two sources when the difference in two angles is (55 degrees). When  $\theta_1 = -29^\circ$ ,  $\theta_2 = 26^\circ$ ,  $N$  is 14,  $d$  is 0.2cm, and  $\Psi$  is 0.8cm, a side lobe is clearly visible. This is a shortcoming of the FFT technique.

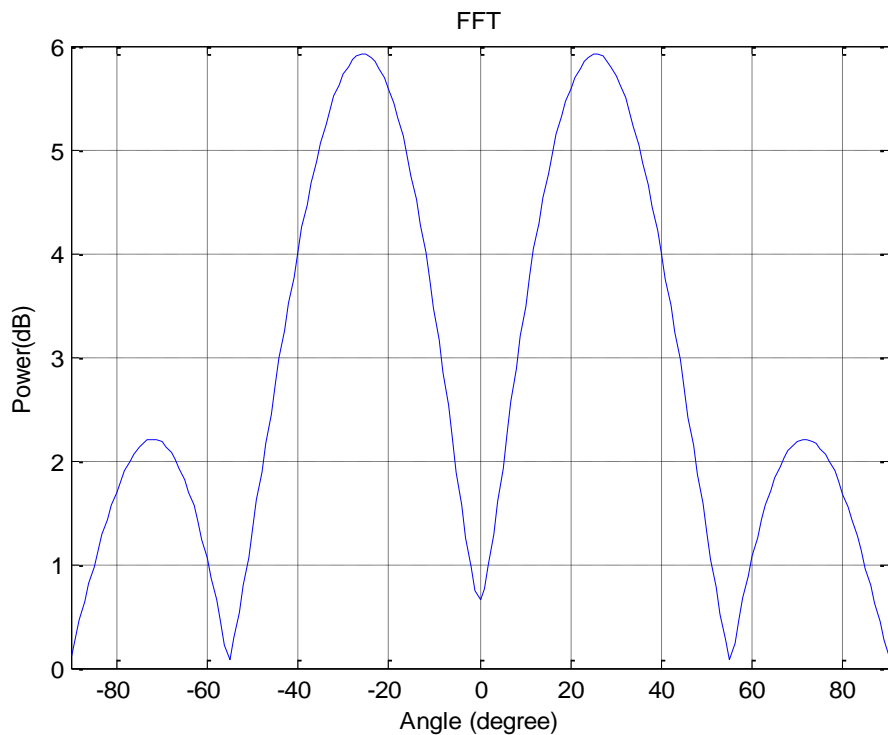


Figure (3.26) Magnitude (power(dB)) versus angle (degree) for a double (two)-source angle ( $\theta_1 = -29^\circ$ ,  $\theta_2 = 26^\circ$ ) using the FFT method ( $N=5$ ).

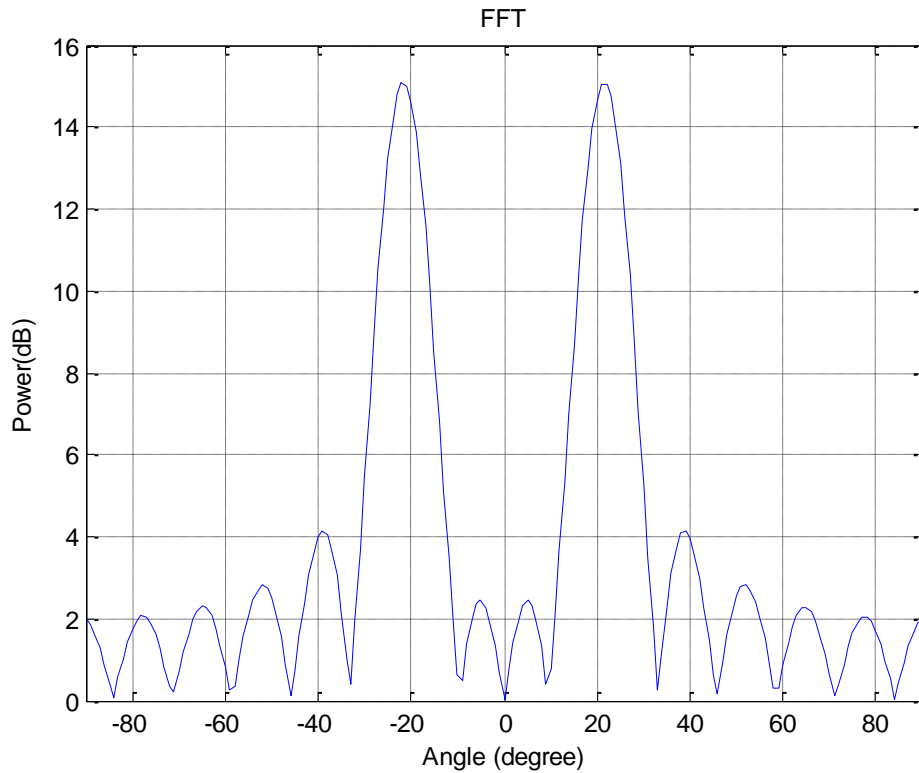


Figure (3.27) Magnitude (power(dB)) versus angle (degree) for a double (two)-source angle ( $\theta_1=-29^\circ$ ,  $\theta_2=26^\circ$ ) using the FFT method ( $N=14$ ).

It is shown in figure (3.28) that when the first actual angle is equal to  $\theta_1=-29^\circ$  and the second actual angle is equal to  $\theta_2=26^\circ$ , the percentage error and  $N$  (number of samples) are related. As the number of samples increases, so does the percentage error, starting at the smallest  $N$  and decreasing in the case of the largest  $N$ . (number of samples). The Root-MUSIC algorithm approach has zero percent error in the first and second sources at all places of  $N$ . (number of samples) and the order is equal to  $n=3$ . It means that  $N_{min} = 8$  for the Root-MUSIC method.

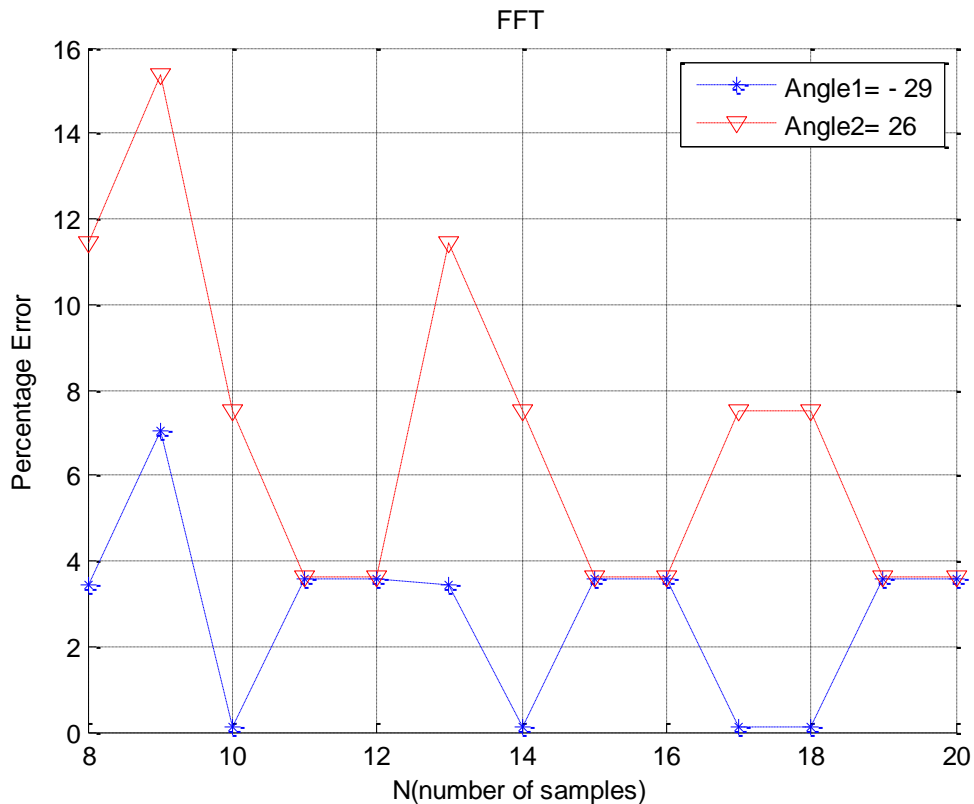


Figure (3.28) Percentage error of angle versus N for double (two) sources ( $\theta_1=-29^\circ$ ,  $\theta_2=26^\circ$ ) for DOA Estimation.

As seen in figure (3.29), the FFT algorithm method yields the desired results. When  $N \leq 8$ , it can distinguish between two sources when the difference in two angles is (24 degrees). When  $\theta_1=-10^\circ$ ,  $\theta_2=14^\circ$ , N is 8, d is 0.2cm, and  $\Psi$  is 0.8cm, a side lobe is clearly visible. This is a shortcoming of the FFT technique.

As seen in figure (3.30), the FFT algorithm method yields the desired results. When  $N > 8$ , it can distinguish between two sources when the difference in two angles is (24 degrees). When  $\theta_1=-10^\circ$ ,  $\theta_2=14^\circ$ , N is 20, d is 0.2cm, and  $\Psi$  is 0.8cm, a side lobe is clearly visible. This is a shortcoming of the FFT technique.

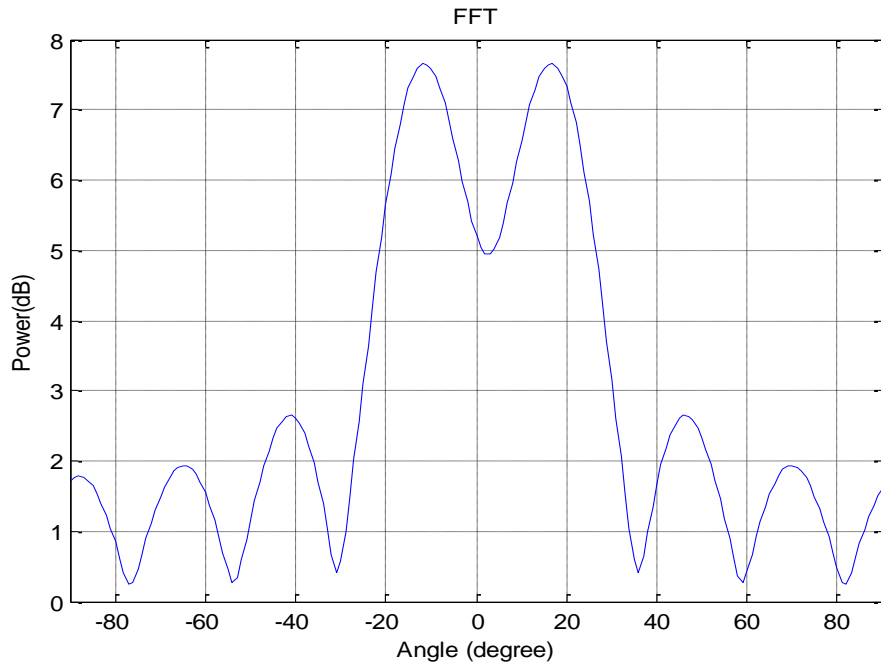


Figure (3.29) Magnitude (power(dB)) versus angle (degree) for a double (two)-source angle ( $\theta_1=-10^\circ$ ,  $\theta_2=14^\circ$ ) using the FFT method (N=8).

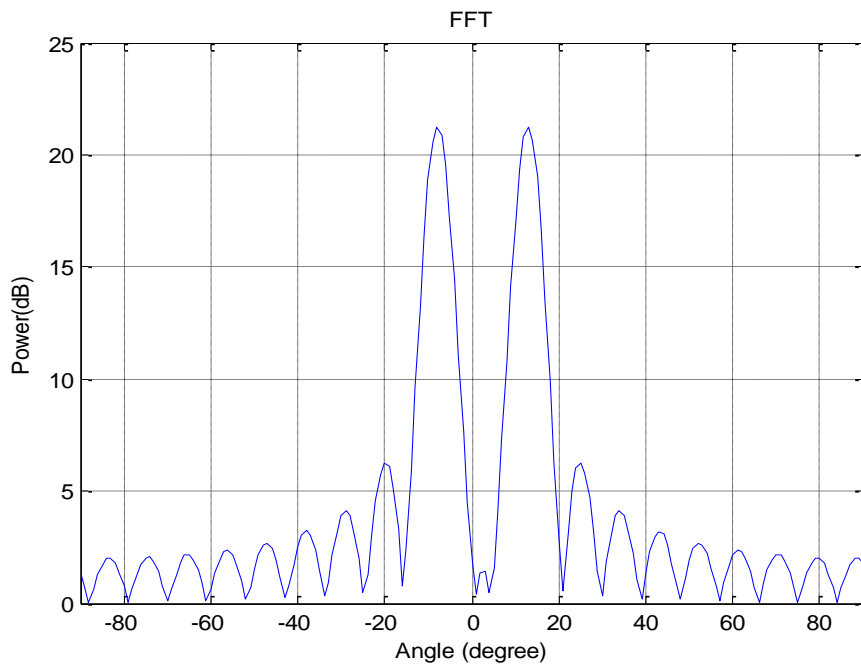


Figure (3.30) Magnitude (power(dB)) versus angle (degree) for a double (two)-source angle ( $\theta_1=-10^\circ$ ,  $\theta_2=14^\circ$ ) using the FFT method (N=20).

The relationship between the percentage error and N (number of samples) for the FFT algorithm method with noiseless double (two) sources is illustrated in figure (3.31) when the first actual angle is equal to  $\theta_1 = -10^\circ$  and the second actual angle is equal to  $\theta_2 = 14^\circ$ . It was observed that the percentage error is greatest at the smallest N (number of samples) and reduces to the greatest N. (number of samples). The percentage error of the first and second sources is equal to zero for the Root-MUSIC algorithm approach at all positions of N. (number of samples) and the order is equal to  $n=3$ . It means that  $N_{min} = 8$  for the Root-MUSIC method.

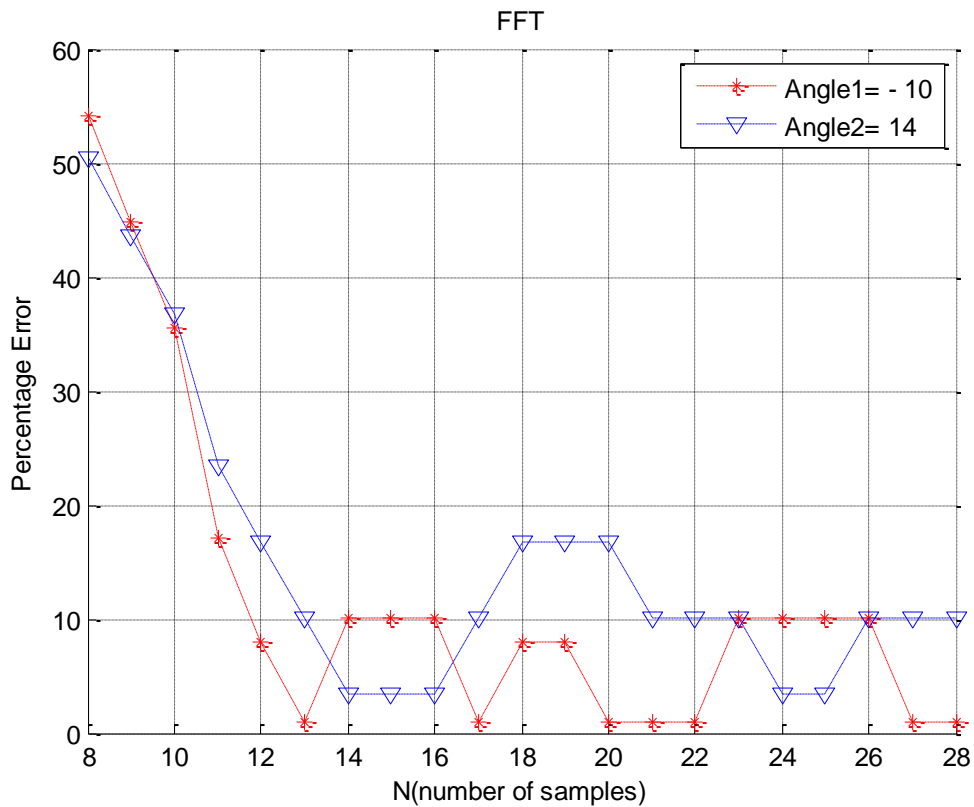


Figure (3.31) Percentage error of angle versus N for double (two) sources ( $\theta_1 = -10^\circ$ ,  $\theta_2 = 14^\circ$ ) for DOA Estimation.

Figure (3.32) refers to the relationship between the difference angle on the y-axis and the minimum number of samples  $N_{min}$  on the x-axis for the first angle is equal to  $20^\circ$  and the second angle is varied between  $25^\circ$  and  $50^\circ$  for double (two) sources with the FFT algorithm method. It is noticed that the minimum difference angle needs a maximum number of samples while the maximum difference angle needs a minimum one. For Root-MUSIC when order  $n=3$ , it is found that the difference approaches less than  $1^\circ$  (up to  $0.5^\circ$ ) for  $N_{min}=8$ .

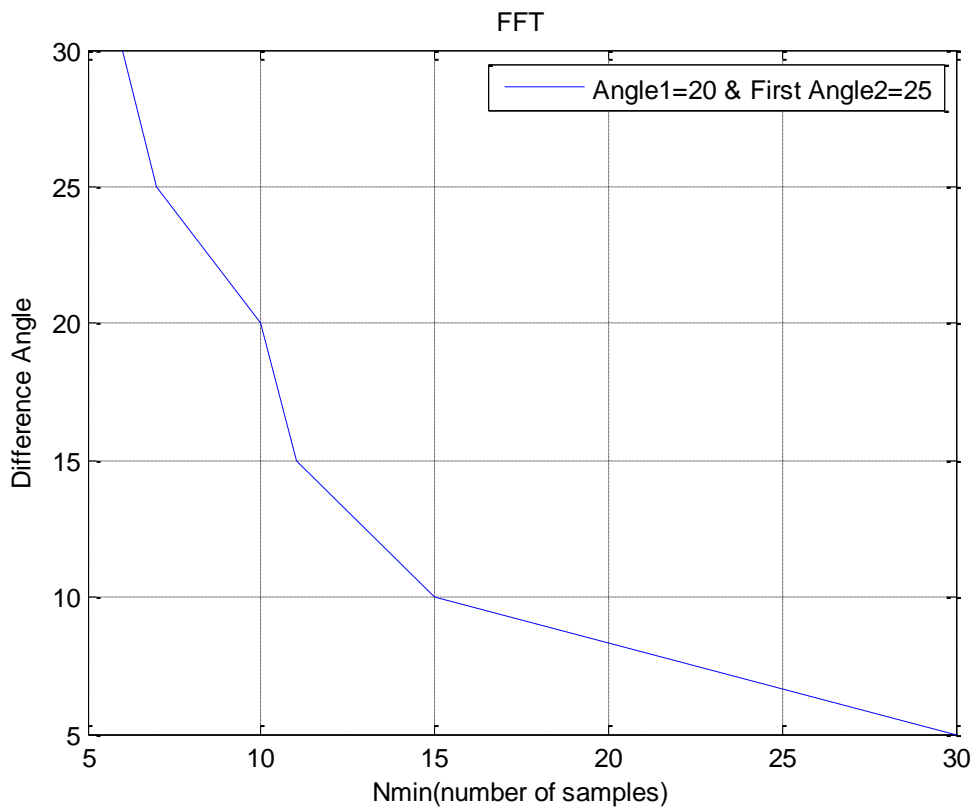


Figure (3.32) Relationship between Difference Angle and minimum number of samples  $N_{min}$  for noiseless double (two) sources.

### 3.3 Simulation Results with Noise Data.

#### 3.3.1 Single Source for DOA Estimation.

Figure (3.33) refers to the relationship between the percentage error and N (number of samples) for the FFT algorithm method and Root-MUSIC algorithm method with a noise single source when the actual angle of this single source is  $\theta=20^0$  and the value of the signal to noise ratio SNR=10dB and noticed that the percentage error is maximum at minimum N (number of samples) and then decreases at maximum N (number of samples). It means that the percentage error of the Root-MUSIC algorithm method is less than that of the FFT algorithm method.

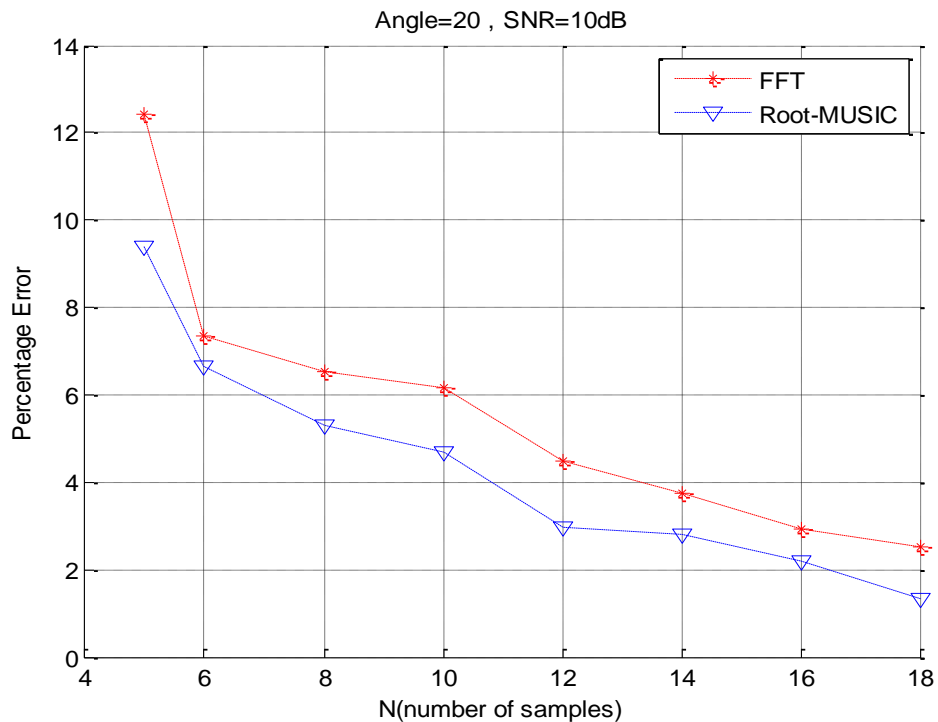


Figure (3.33) Percentage error of angle versus N for single angle source with  $\theta=20^0$ , SNR=10dB,  $d=0.6\text{cm}$ ,  $Y=2\text{cm}$  using DOA Estimation.

Figure (3.34) refers to the relationship between the percentage error and N (number of samples) for the FFT algorithm method and Root-MUSIC algorithm method with a noise single source when the actual angle of this single source is equal to  $\theta=20^0$  and the value of the signal to noise ratio SNR=5dB and noticed that the percentage error is maximum at minimum N (number of samples) and then decreases at maximum N (number of samples). It means that the percentage error of the Root-MUSIC algorithm method is less than that of the FFT algorithm method.

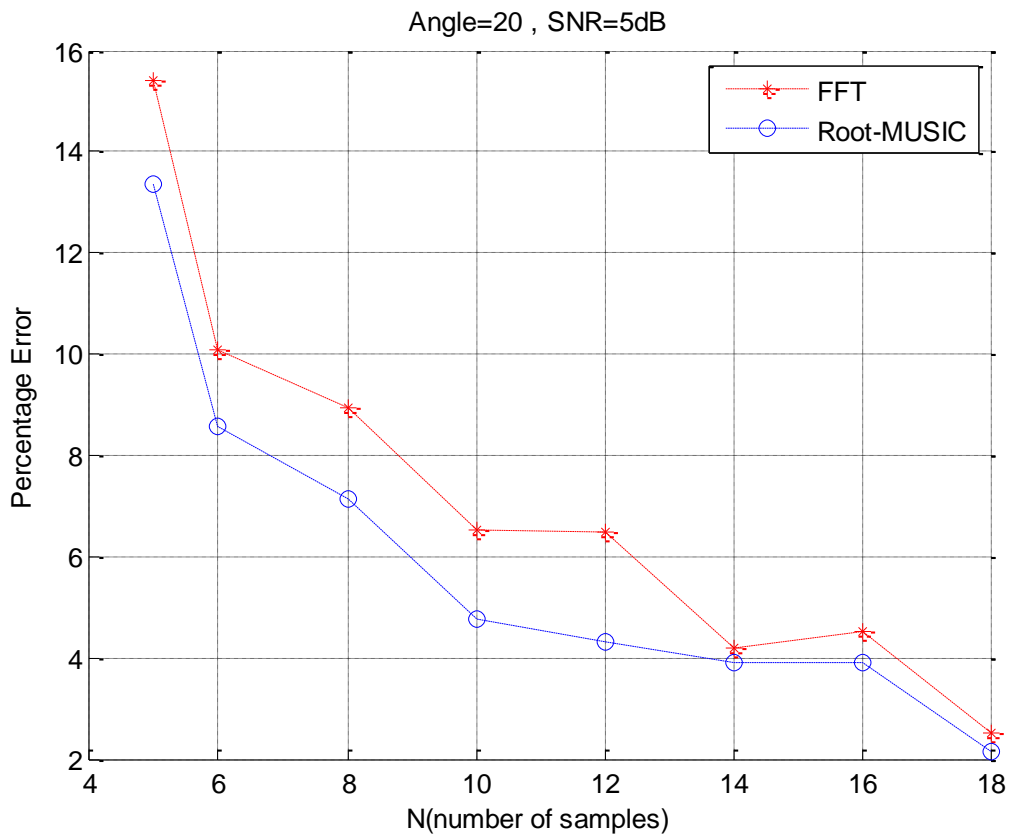


Figure (3.34) Percentage error of angle versus N for single angle source with  $\theta=20^0$ , SNR=5dB,  $d=0.6\text{cm}$ ,  $\Psi=2\text{cm}$  using DOA Estimation.

Figure (3.35) shows the FFT algorithm method and Root-MUSIC algorithm method with noise single source when the actual angle is  $=37^\circ$  and the value of the signal to noise ratio SNR=10 dB and observed that the percentage error reaches its maximum at the lowest number of samples, N, and then starts to decline at the highest number of samples, N. Compared to the FFT algorithm approach, the root-MUSIC algorithm method has a lower percentage inaccuracy.

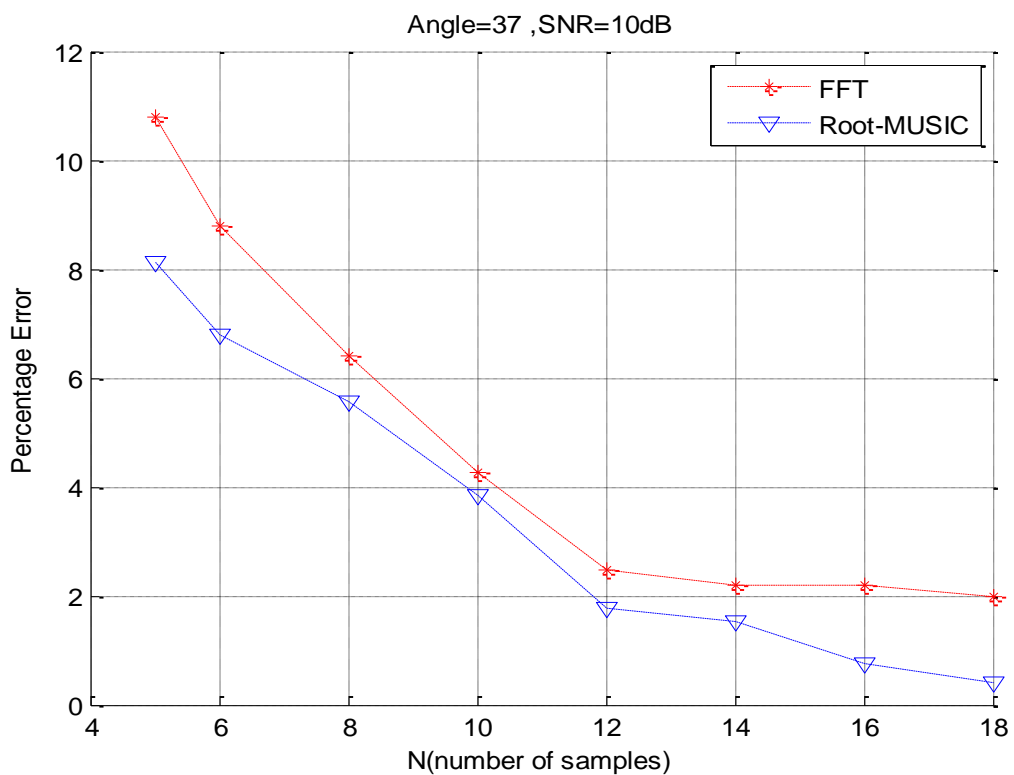


Figure (3.35) Percentage error of angle versus N for single angle source with  $\theta=37^\circ$ , SNR=10dB,  $d=0.6\text{cm}$ ,  $\Psi=2\text{cm}$  using DOA Estimation.

FFT algorithm method and Root-MUSIC algorithm method with a noise single source when the angle of this single source is equal to  $=37^\circ$  and the signal to noise value SNR is 5dB are shown in figure (3.36) and observed that the percentage error reaches its

maximum at the lowest number of samples, N, and then starts to decline at the highest number of samples, N. Compared to the FFT algorithm approach, the root-MUSIC algorithm method has a lower percentage inaccuracy.

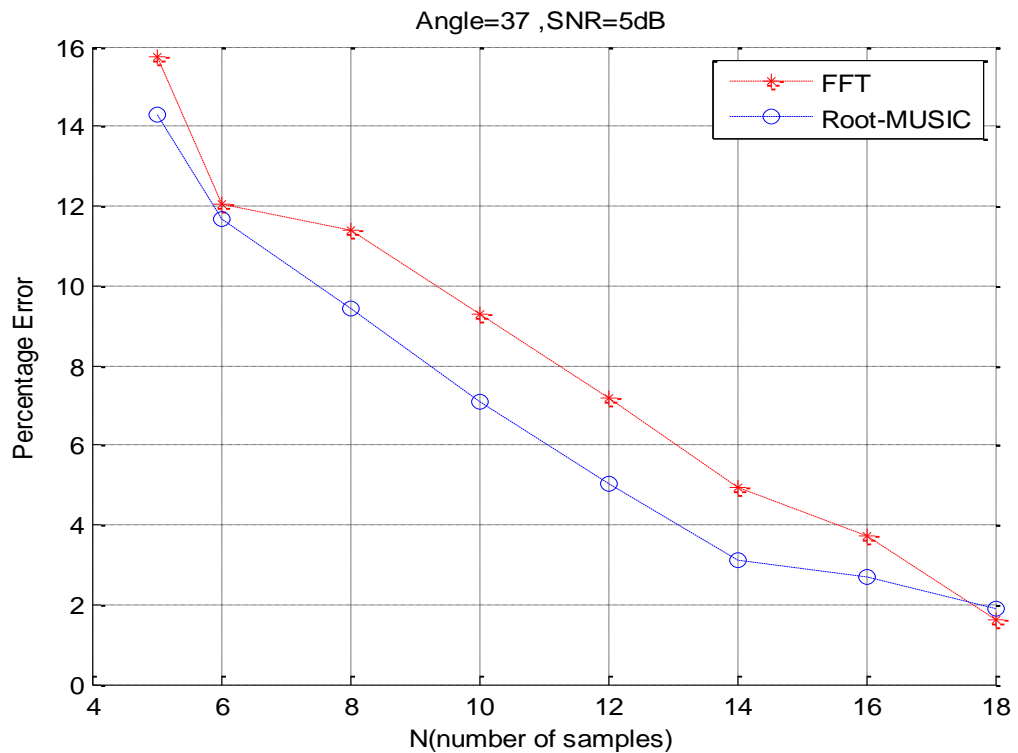


Figure (3.36) Percentage error of angle versus N for single angle source with  $\theta=37^0$ , SNR=5dB,  $d=0.6\text{cm}$ ,  $\Psi=2\text{cm}$  using DOA Estimation.

Using figure (3.37), we can see the relationship between the percentage error and N (number of samples) when the actual angle of the single source is  $\theta= -50^0$  and SNR=10dB, and we can see that the percentage error is highest when N is as low as possible, and then decreases when N is as high as possible (number of samples). It means that the Root-MUSIC algorithm method's percentage error is lower than the FFT algorithm method's percentage error.

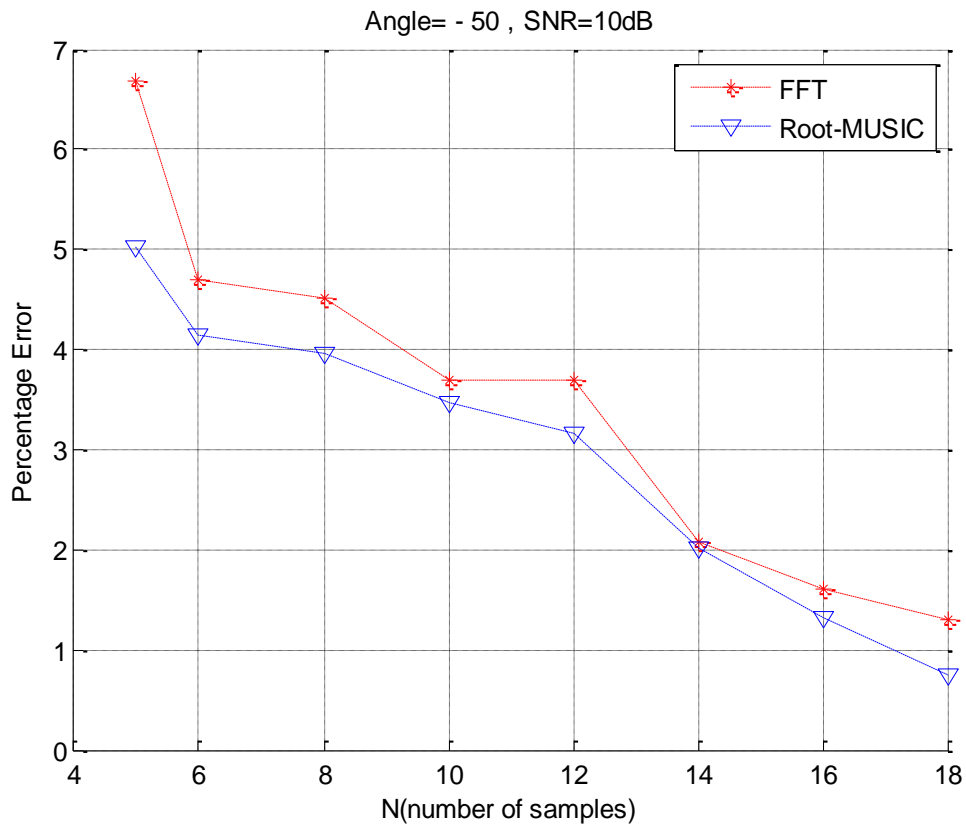


Figure (3.37) Percentage error of angle versus N for single angle source with  $\theta = -50^\circ$ , SNR=10dB,  $d=0.6\text{cm}$ ,  $\Psi=2\text{cm}$  using DOA Estimation.

For the FFT algorithm method with a single noise source at an actual angle of  $\theta = -50^\circ$  and a signal-to-noise ratio of SNR=5dB, see figure (3.38), where the relationship between the percentage error and the number of samples is shown, and it's seen that the percentage error reaches its maximum at minimum N (number of samples) and then decreases at maximum N. (number of samples). This means that the Root-MUSIC algorithm approach has a lower percentage error than the FFT algorithm method.

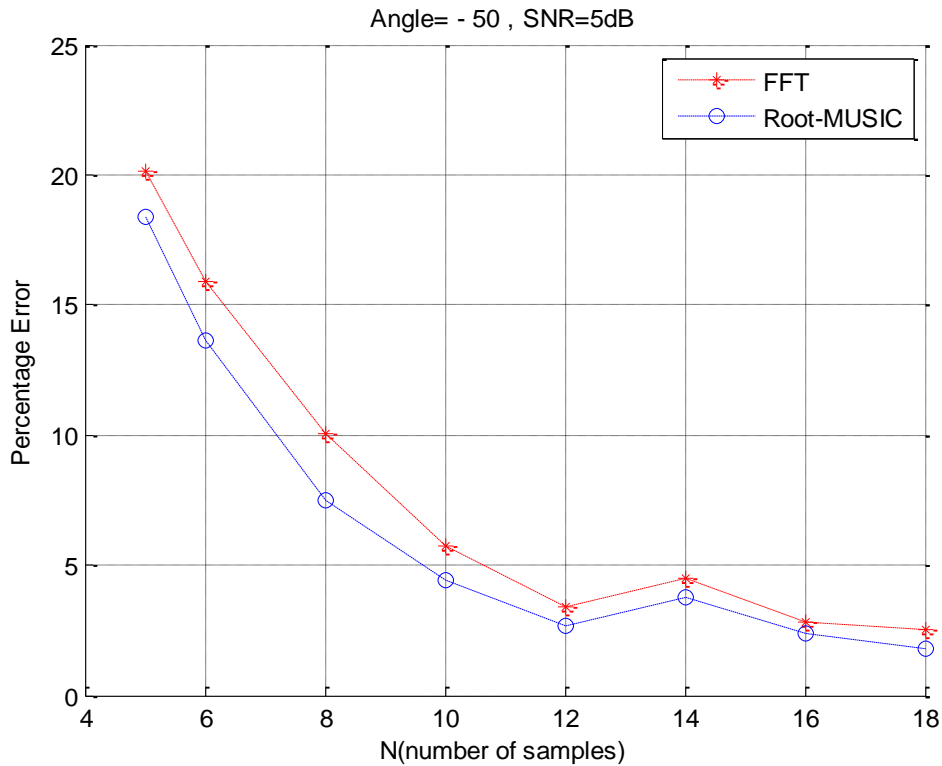


Figure (3.38) Percentage error of angle versus N for single angle source with  $\theta=-50^{\circ}$ , SNR=5dB,  $d=0.6\text{cm}$ ,  $\Psi=2\text{cm}$  using DOA Estimation.

### 3.3.2 Double (two) Sources for DOA Estimation.

For different N (number of samples), figure (3.39) shows the relationship between the percentage error and N (number of samples) for both FFT and Root-MUSIC algorithm methods, with noise double (two) sources ( $\theta_1=17^{\circ}$ ,  $\theta_2=37^{\circ}$ ),  $d=0.6\text{cm}$ ,  $\Psi=2\text{cm}$  for the first actual angle ( $\theta_1=17^{\circ}$ ) and the value of the signal to noise ratio SNR=10dB. It is found that the greatest error requires the minimum N (number of samples) while the minimum error requires the maximum N (number of samples). There is a less error rate with the

Root-MUSIC algorithm than there is with the FFT algorithm; as a result, it is more accurate than the FFT approach.

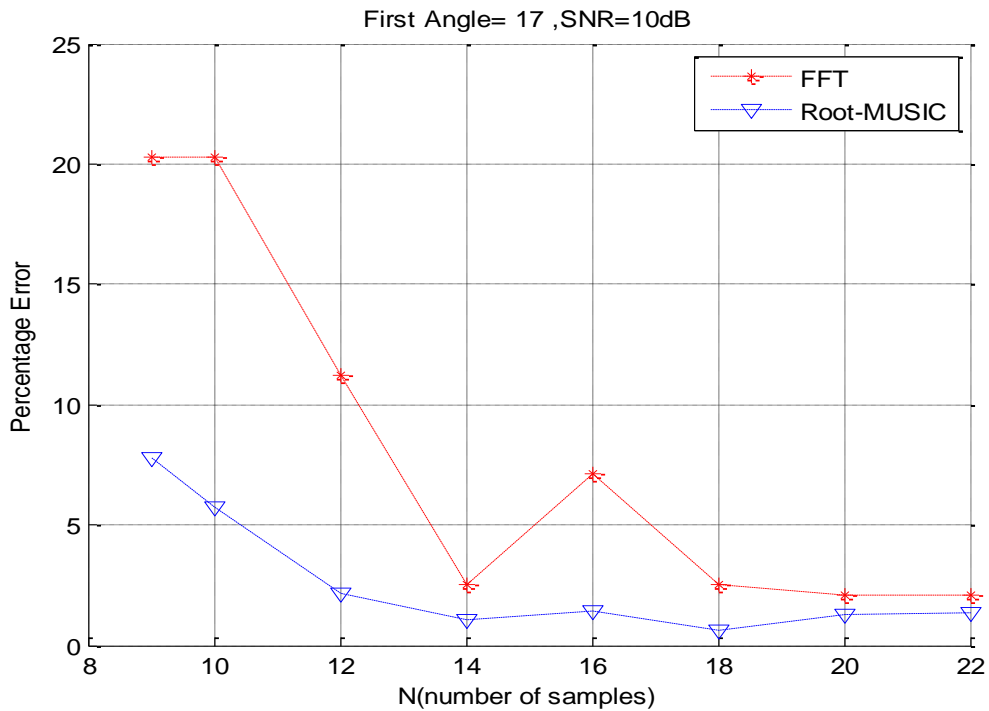


Figure (3.39) Percentage error of angle versus N for double (two) sources ( $\theta_1=17^\circ$ ,  $\theta_2=37^\circ$ ) for the first actual angle ( $\theta_1=17^\circ$ ), SNR=10dB for DOA Estimation.

Figure (3.40) shows the relationship between percentage error and N (number of samples) for both FFT and Root-MUSIC algorithms for various N (number of samples) with noise double (two) sources ( $\theta_1=17^\circ$ ,  $\theta_2=37^\circ$ ),  $d=0.6\text{cm}$ ,  $\Psi=2\text{cm}$  for the second actual angle ( $\theta_2=37^\circ$ ) and the value of the signal to noise ratio SNR=10dB. It has been discovered that the maximum percentage error requires a minimum number of samples, whereas the minimum percentage error requires a maximum number of samples (number of

samples). It signifies that the Root-MUSIC technique has a lower percentage error than the FFT method, making the Root-MUSIC algorithm method superior to the FFT algorithm method.

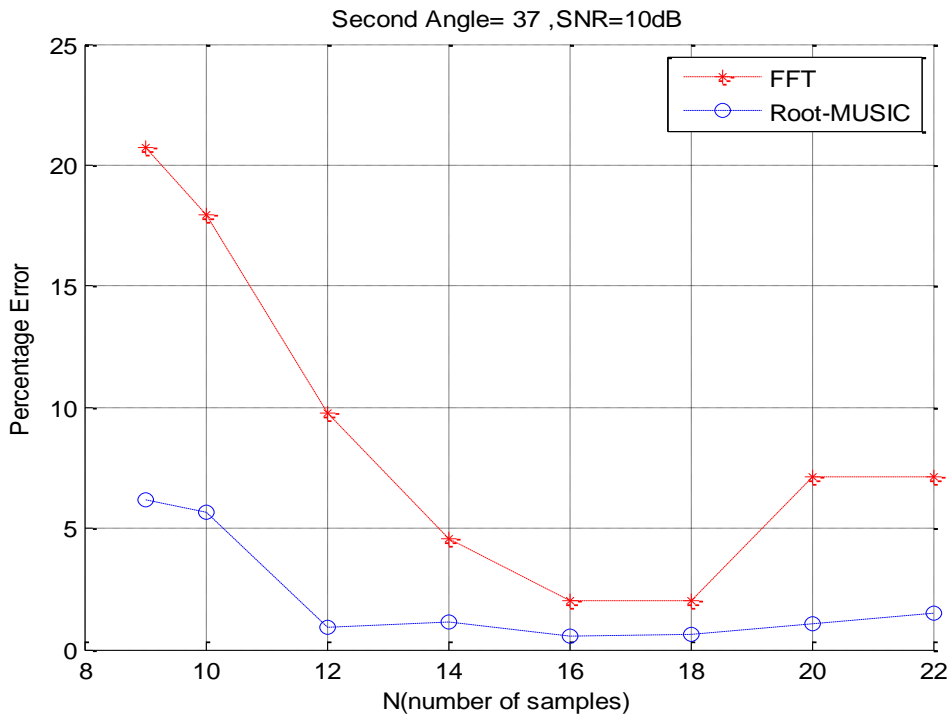


Figure (3.40) Percentage error of angle versus N for double (two) sources ( $\theta_1=17^\circ$ ,  $\theta_2=37^\circ$ ) for the second actual angle ( $\theta_2=37^\circ$ ), SNR=10dB for DOA Estimation.

Figure (3.41) refers to the relationship between the percentage error and N (number of samples) for both the FFT algorithm method and Root-MUSIC algorithm method for different N (number of samples) with noise double (two) sources ( $\theta_1=17^\circ$ ,  $\theta_2=37^\circ$ ),  $d=0.6\text{cm}$ ,  $\Psi=2\text{cm}$  for the first actual angle ( $\theta_1=17^\circ$ ) and the value of the signal to noise ratio SNR=5dB. It is noticed that the maximum percentage error requires the minimum N (number of samples) while the minimum percentage error requires the maximum N (number of

samples). It means that the percentage error of the Root-MUSIC method is less than that of the FFT method for this reason the Root-MUSIC method is better than the FFT method.

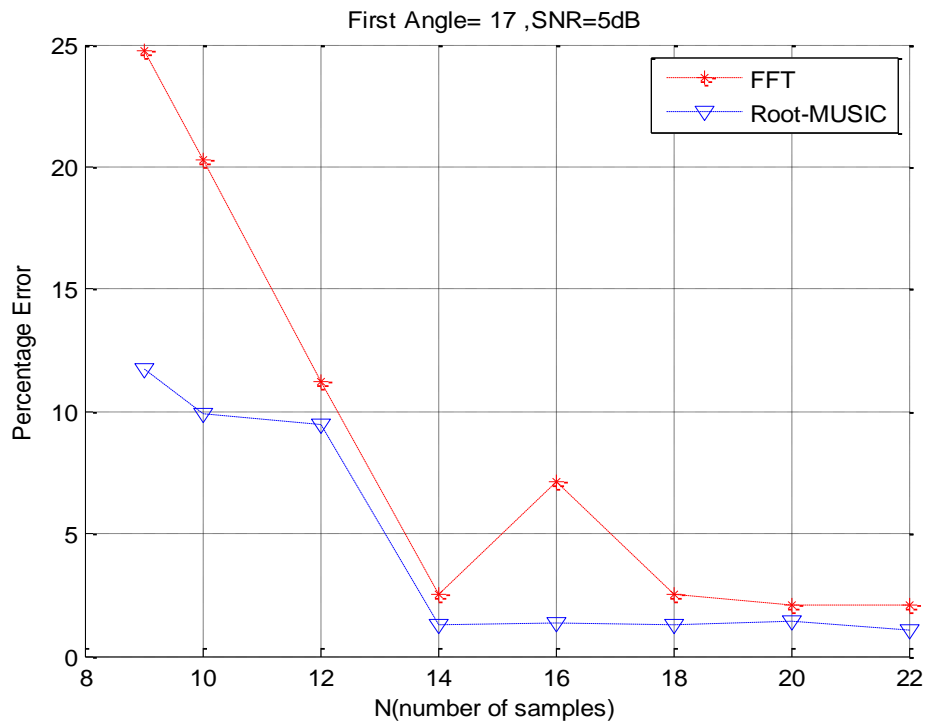


Figure (3.41) Percentage error of angle versus N for double (two) sources ( $\theta_1=17^\circ$ ,  $\theta_2=37^\circ$ ) for the first actual angle ( $\theta_1=17^\circ$ ), SNR=5dB for DOA Estimation.

For varying N (number of samples) with noise double (two) sources ( $\theta_1=17^\circ$ ,  $\theta_2=37^\circ$ ),  $d=0.6\text{cm}$ ,  $\Psi=2\text{cm}$  for the second actual angle ( $\theta_2=37^\circ$ ), SNR=5dB. Figure (3.42) shows the relationship between the percentage error and N (number of samples) for both the FFT algorithm technique and the Root-MUSIC algorithm method. It is found that the highest error requires the least number of samples, while the minimum error requires the maximum number of samples (number of samples). As a result, the Root-MUSIC algorithm

technique has a lower error % than the FFT algorithm method, for this reason, the Root-MUSIC method is better than the FFT method.

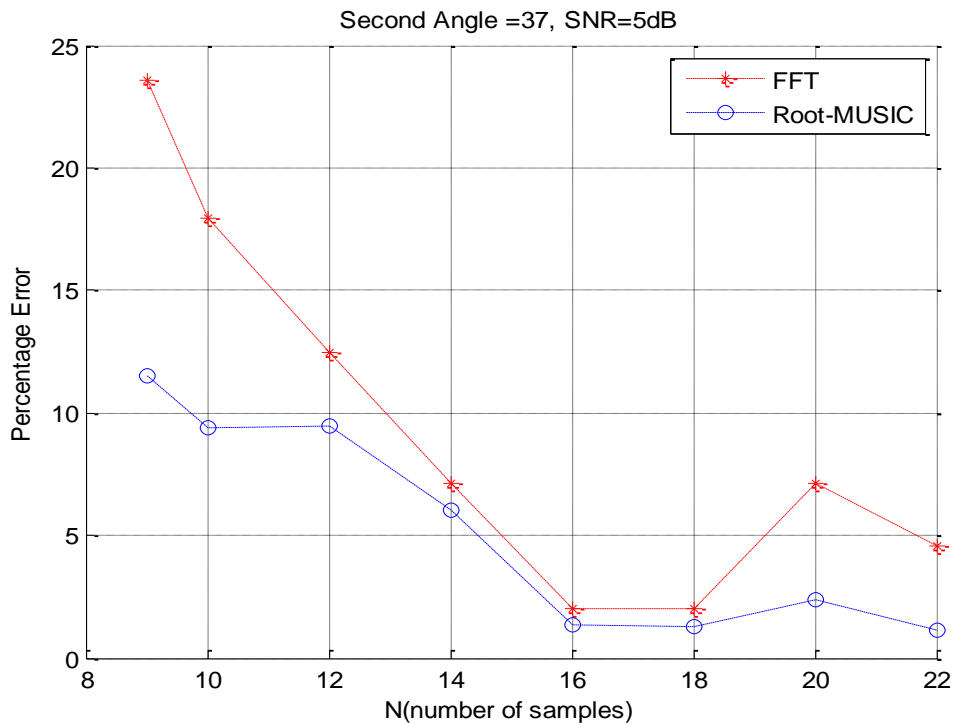


Figure (3.42) Percentage error of angle versus N for double (two) sources ( $\theta_1=17^\circ$ ,  $\theta_2=37^\circ$ ) for the second actual angle ( $\theta_2=37^\circ$ ), SNR=5dB for DOA Estimation.

For different N (number of samples), figure (3.43) shows the relationship between the percentage error and N (number of samples) for both FFT and Root-MUSIC algorithm methods, with noise double (two) sources ( $\theta_1=-15^\circ$ ,  $\theta_2=-40^\circ$ ),  $d=0.6\text{cm}$ ,  $Y=2\text{cm}$  for the first actual angle ( $\theta_1=-15^\circ$ ) and the value of the signal-to-noise ratio SNR=10dB. One thing that is found is that the maximum percentage error required the minimum N (number of samples), but that minimum percentage error required the maximum N. (number of

samples). Root-error MUSIC's percentage is lower than the FFT's, indicating that it is a superior method.

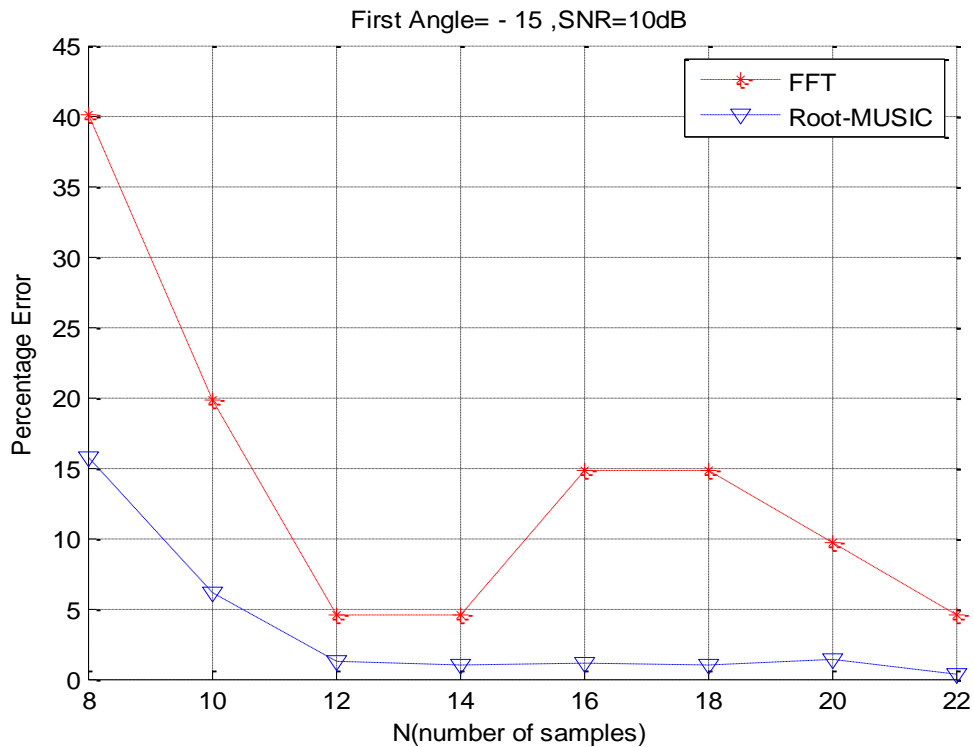


Figure (3.43) Percentage error of angle versus N for double (two) sources ( $\theta_1=-15^\circ$ ,  $\theta_2=-40^\circ$ ) for the first actual angle ( $\theta_1=-15^\circ$ ), SNR=10dB for DOA Estimation.

There is a relationship in figure (3.44) between the percentage error and the quantity N for the FFT algorithm method and the Root-MUSIC algorithm method for different quantities of N (number of samples) with noise double (two) noise sources ( $\theta_1=-15^\circ$ ,  $\theta_2=-40^\circ$ ),  $d=0.6\text{cm}$ ,  $\Psi=2\text{cm}$  for the second actual angle ( $\theta_2=-40^\circ$ ) and the value of SNR=10dB for both methods. Observedly, a maximum percent error require the minimum N (number of samples). As a result, the

Root-MUSIC algorithm method has a lower error percentage than the FFT algorithm method, and as a result, it is preferable to the latter.

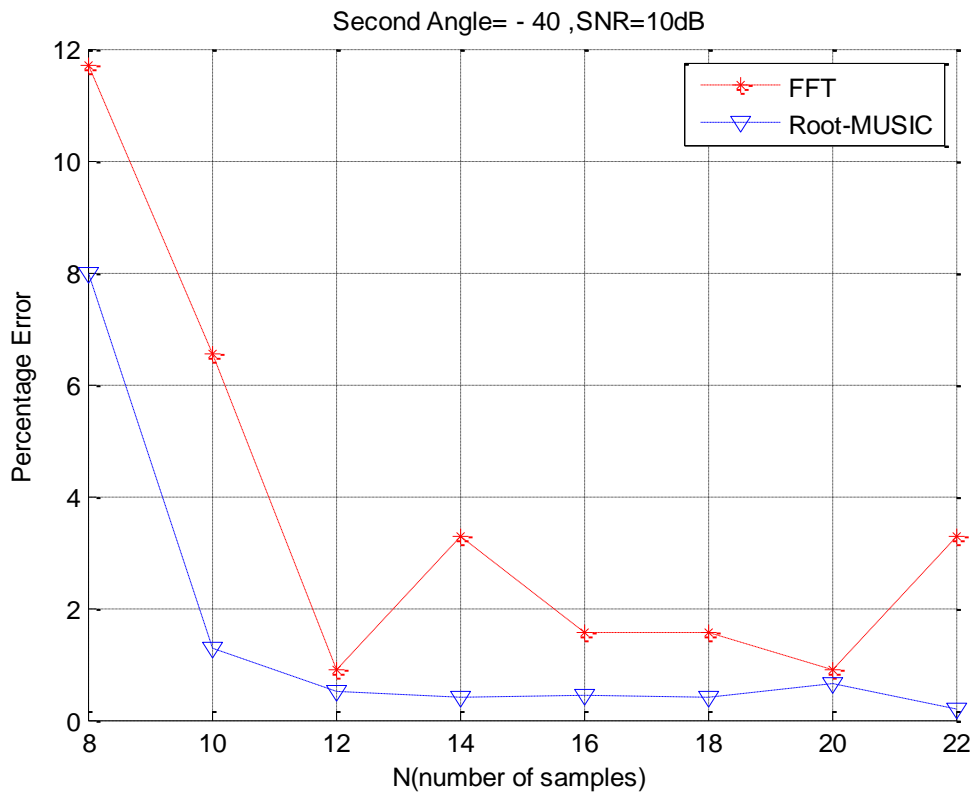


Figure (3.44) Percentage error of angle versus N for double (two) sources ( $\theta_1=-15^\circ$ ,  $\theta_2=-40^\circ$ ) for the second actual angle ( $\theta_2=-40^\circ$ ), SNR=10dB for DOA Estimation.

For different N (number of samples), figure (3.45) shows the relationship between the percentage error and N (number of samples) for both FFT and Root-MUSIC algorithm methods with noise double (two) sources ( $\theta_1=-15^\circ$ ,  $\theta_2=-40^\circ$ ),  $d=0.6\text{cm}$ ,  $\Psi=2\text{cm}$  for the first actual angle of ( $\theta_1=-15^\circ$ ) and the value of SNR=5dB. It is found that the maximum error requires the minimum number of samples, while the minimum error requires the maximum number of samples (number of samples). As a result, the Root-MUSIC algorithm method

has a lower error percentage than the FFT algorithm method, for this reason, the Root-MUSIC method is better than the FFT method.

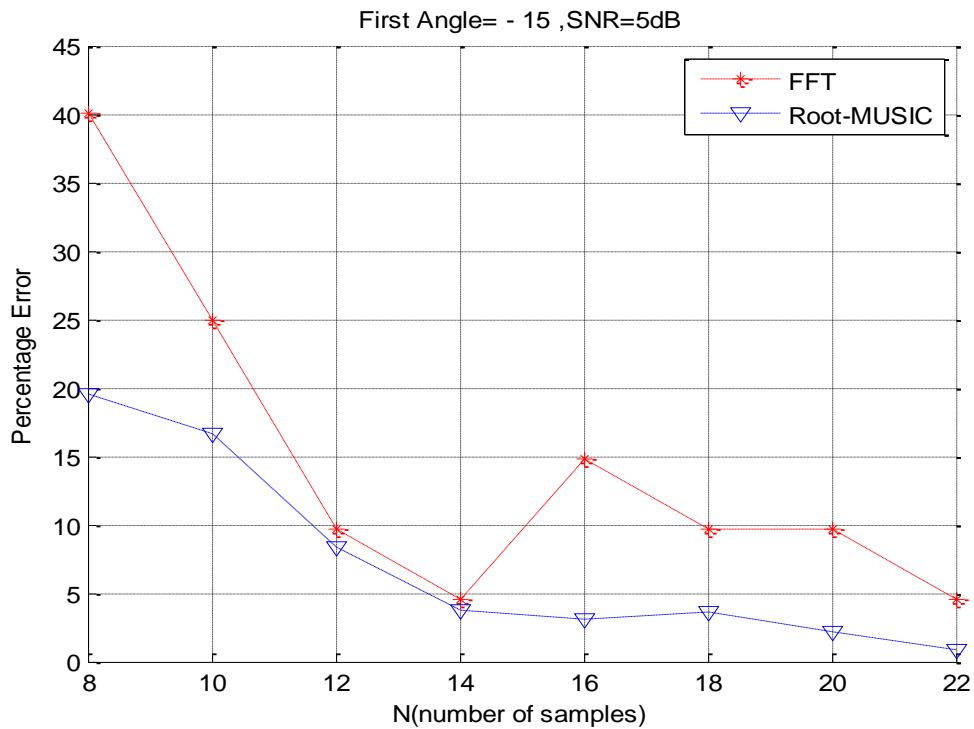


Figure (3.45) Percentage error of angle versus N for double (two) sources ( $\theta_1=-15^\circ$ ,  $\theta_2=-40^\circ$ ) for the first actual angle ( $\theta_1=-15^\circ$ ), SNR=5dB for DOA Estimation.

For different N (number of samples) with noise double (two) sources ( $\theta_1=-15^\circ$ ,  $\theta_2=-40^\circ$ ),  $d=0.6\text{cm}$ ,  $\Psi=2\text{cm}$  for the second actual angle ( $\theta_2=-40^\circ$ ) and the value SNR=5dB, figure (3.46) shows the relationship between the percentage error and N (number of samples) for the FFT algorithm method and Root-MUSIC algorithm method. It is discovered that whilst the minimum error needs the maximum N (number of samples), the maximum error requires the minimum N. The accuracy of the Root-MUSIC method is higher than that of the FFT algorithm because its error rate is lower.

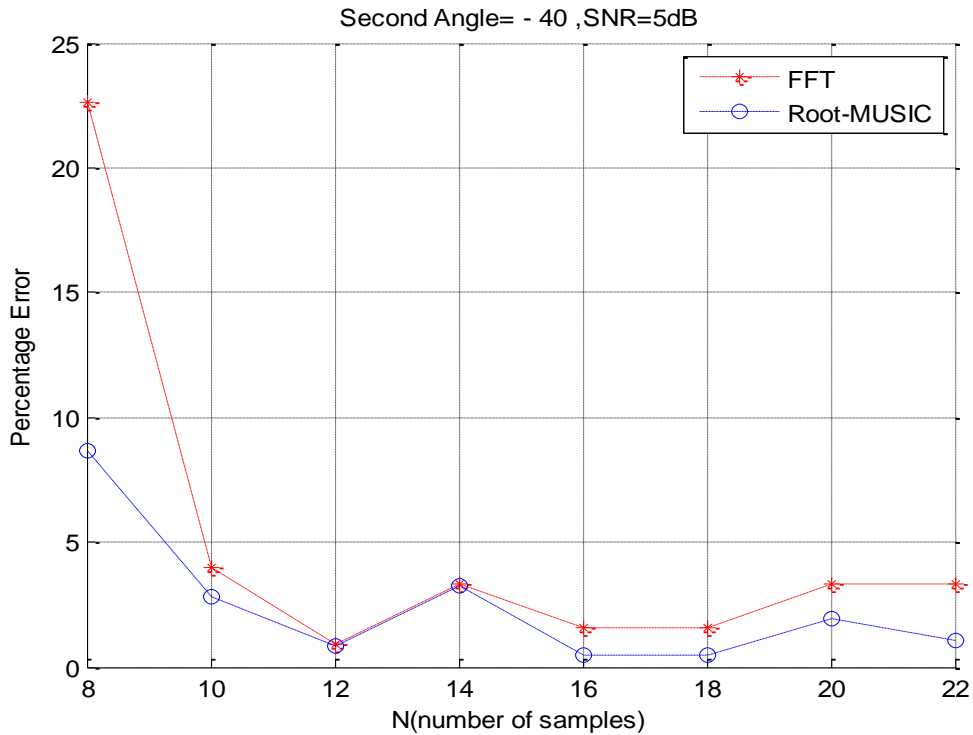


Figure (3.46) Percentage error of angle versus N for double (two) sources ( $\theta_1=-15^\circ$ ,  $\theta_2=-40^\circ$ ) for the second actual angle ( $\theta_2=-40^\circ$ ), SNR=5dB for DOA Estimation.

Figure (3.47), the relationship between the percentage error and N (number of samples) is shown for both the FFT algorithm and the Root-MUSIC algorithm with noise double (two) sources ( $\theta_1=-10^\circ$ ,  $\theta_2=15^\circ$ ),  $d=0.6\text{cm}$ ,  $\Psi=2\text{cm}$  for the first actual angle ( $\theta_1=-10^\circ$ ) and a signal-to-noise ratio SNR=10dB. A minimum of N (samples) is required for the maximum percentage error, whereas a maximum of N. (number of samples) is required for the minimum percentage error. This indicates that the Root-MUSIC approach is better than the FFT method because it has a smaller percentage inaccuracy.

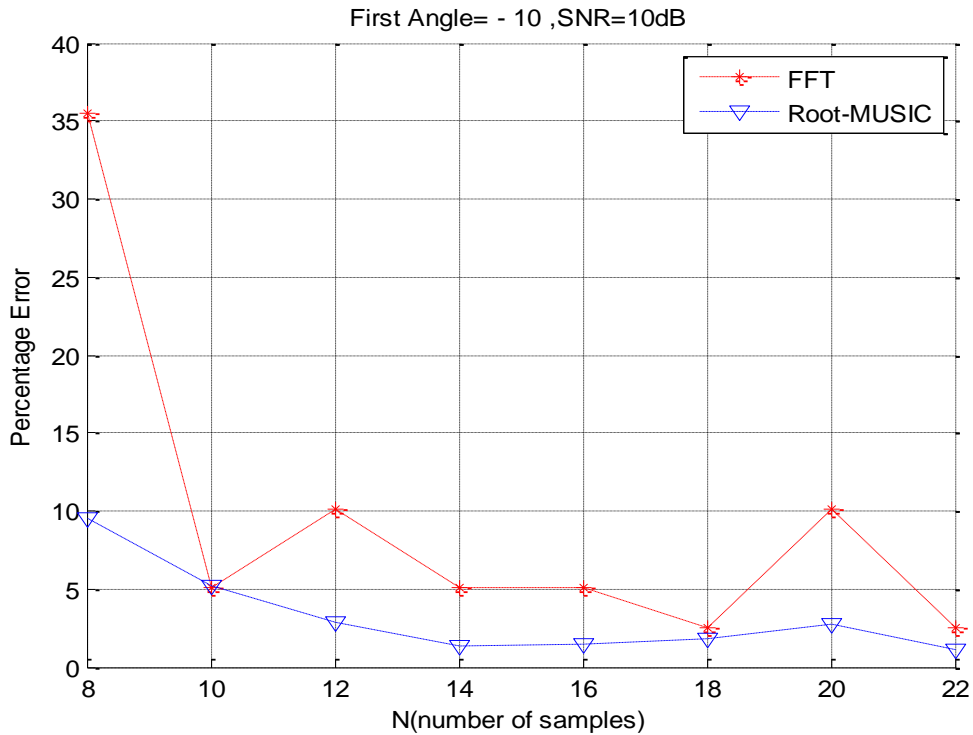


Figure (3.47) Percentage error of angle versus N for double (two) sources ( $\theta_1=-10^0, \theta_2=15^0$ ) for the first actual angle ( $\theta_1=-10^0$ ), SNR=10dB for DOA Estimation.

The relationship between the percentage error and N (number of samples) is depicted in figure (3.48) for both the FFT algorithm and the Root-MUSIC algorithm for different N (number of samples) with noise double (two) sources ( $\theta_1=-10^0, \theta_2=15^0$ ),  $d=0.6\text{cm}$ ,  $\Psi=2\text{cm}$  for the second actual angle ( $\theta_2=15^0$ ) and a signal-to-noise ratio SNR=10dB. A minimum of N (number of samples) is required for the maximum percentage error, whereas a maximum of N is required for the minimum percentage error (number of samples). This indicates that the Root-MUSIC algorithm technique is better

than the FFT algorithm method as its percentage error is lower in the former case.

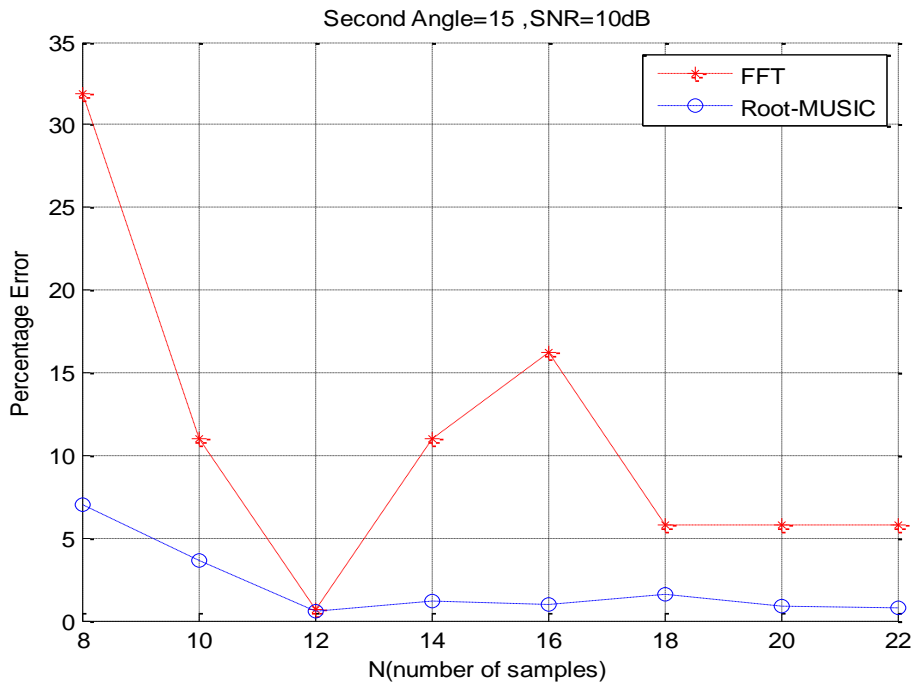


Figure (3.48) Percentage error of angle versus N for double (two) sources ( $\theta_1=-10^\circ$ ,  $\theta_2=15^\circ$ ) for the second actual angle ( $\theta_2=15^\circ$ ), SNR=10dB for DOA Estimation.

The relationship between the percentage error and N (number of samples) is depicted in figure (3.49) for both the FFT algorithm and the Root-MUSIC algorithm for different N (number of samples) with noise double (two) sources ( $\theta_1=-10^\circ$ ,  $\theta_2=15^\circ$ ),  $d=0.6\text{cm}$ ,  $\Psi=2\text{cm}$  for the first actual angle ( $\theta_1=-10^\circ$ ) and a signal-to-noise ratio SNR=5dB. Noted was the difference between the minimum and maximum percentage errors: the minimum requires a maximum of N (number of samples), while the maximum requires a minimum of N. By comparison, the Root-MUSIC algorithm methodology has a

lower percentage error than the FFT algorithm method, indicating its superiority.

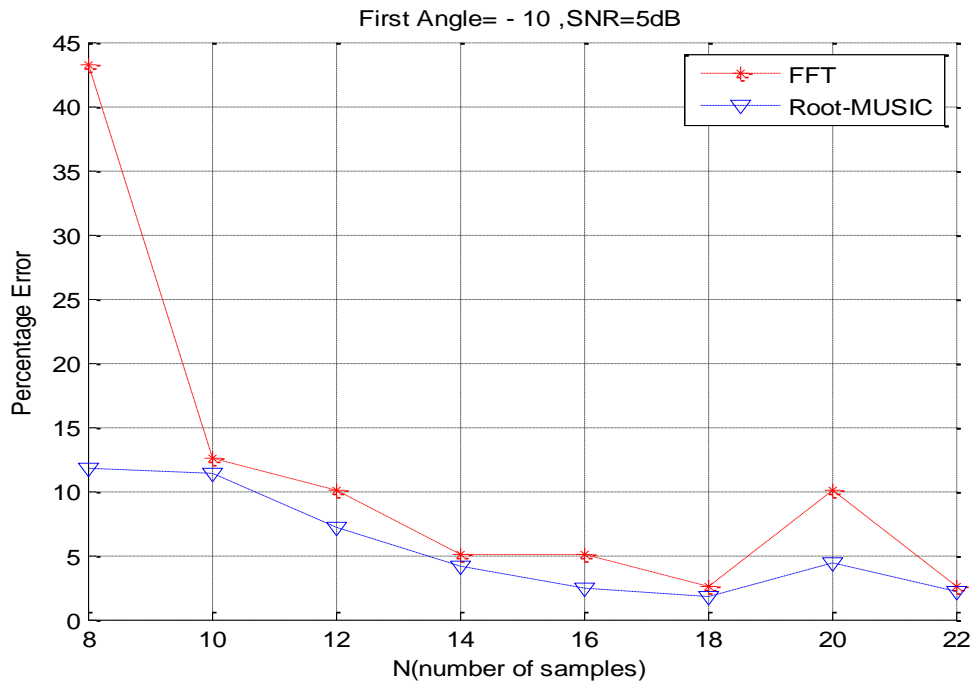


Figure (3.49) Percentage error of angle versus N for double (two) sources ( $\theta_1=-10^0$ ,  $\theta_2=15^0$ ) for the first actual angle ( $\theta_1=-10^0$ ), SNR=5dB for DOA Estimation.

The relationship between the percentage error and N (number of samples) is shown in figure (3.50) for both the FFT algorithm and the Root-MUSIC algorithm for different N (number of samples) with noise double (two) sources ( $\theta_1=-10^0$ ,  $\theta_2=15^0$ ),  $d=0.6\text{cm}$ ,  $\Psi=2\text{cm}$  for the second actual angle ( $\theta_2=15^0$ ) and a signal-to-noise ratio SNR=5dB. A minimum of N (number of samples) is required for the largest percentage error, while a maximum of N is needed for the smallest percentage error. This indicates that the Root-MUSIC

algorithm approach is better than the FFT algorithm method as the Root-MUSIC technique's percentage error is lower.

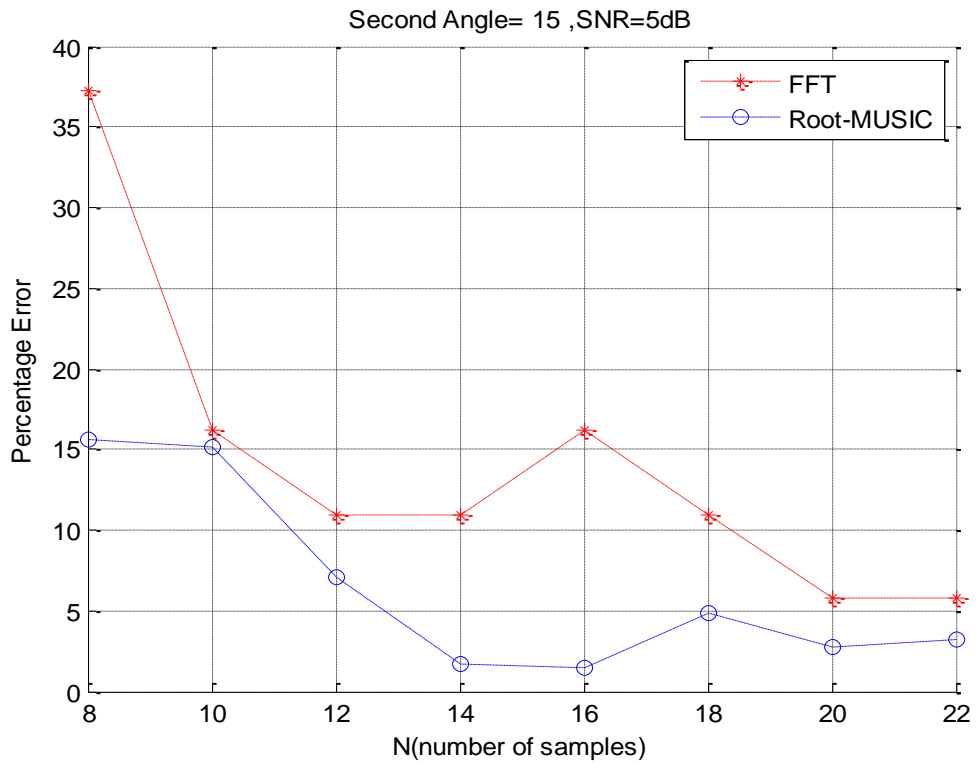


Figure (3.50) Percentage error of angle versus N for double (two) sources ( $\theta_1=-10^\circ$ ,  $\theta_2=15^\circ$ ) for the second actual angle ( $\theta_2=15^\circ$ ), SNR=5dB for DOA Estimation.

## **CHAPTER FOUR**

### ***Experimental Results***

#### ***4.1 Introduction***

This chapter presents experimental findings that assess the Root-MUSIC approach's effectiveness in calculating the DOA and contrast it with the FFT method. An ultrasonic transducer serves as the device for the practical system in this dissertation. The ultrasonic transducer's specifications and an overview are given. The ultrasonic DOA system, which is employed in the practical system and parameters, is introduced with a brief explanation. To execute the ultrasonic DOA estimation of a single source and two sources, several experiments were carried out.

#### **4.2 Ultrasonic Transducer**

There are numerous uses for the ultrasonic transducer, including channel level and air or water speed measurement. A gadget employs numerous detectors to measure direction and speed. It determines the speed based on the relative distances to airborne or waterborne particulate matter. This dissertation makes use of the air ultrasonic ceramic transducers depicted in figure (4.1) below.



Figure (4.1) Ultrasonic Ceramic Transducer.

### **4.3 The DOA Estimation System Using Ultrasound.**

The signal generator and transducers make up the initial section of the practical system. The 40kHz ultrasonic wave is produced by the signal generator. One transducer for a single source and two transducers for two sources convey the ultrasonic signal through the atmosphere.

The scanning receiver in the receiver uses a single transducer. The uniform linear array is the same as the receiver scanning procedure. The greatest distance between elements in a uniform linear array (ULA) is equal to or less than  $(\Psi / 2)$ , where  $\Psi$  is the wavelength. The ultrasonic wavelength is equivalent to 0.8cm. The distance between the ultrasonic transducer and the target must not be greater than 0.2 cm in order to meet ULA requirements.

## 4.4 Practical Experimental Results

The ultrasonic DOA estimate hardware experimental setup is depicted in figure (4.2). For the Direction Of Arrival (DoA) estimate test with one source and two sources, the ultrasonic transducers are used, and the received signal is obtained by scanning an ultrasonic transducer and taking a sample at ( $d$ ) interval. For DoA estimations, the FFT and Root-MUSIC methods are used.

A comparison between conventional and high-resolution methods is then made for different numbers of samples. The parameters of the system are as follows:  $N$  (number of samples),  $d$  (distance between two samples),  $f$  (frequency),  $\Psi$  (wavelength), and  $\theta$  (actual angle).

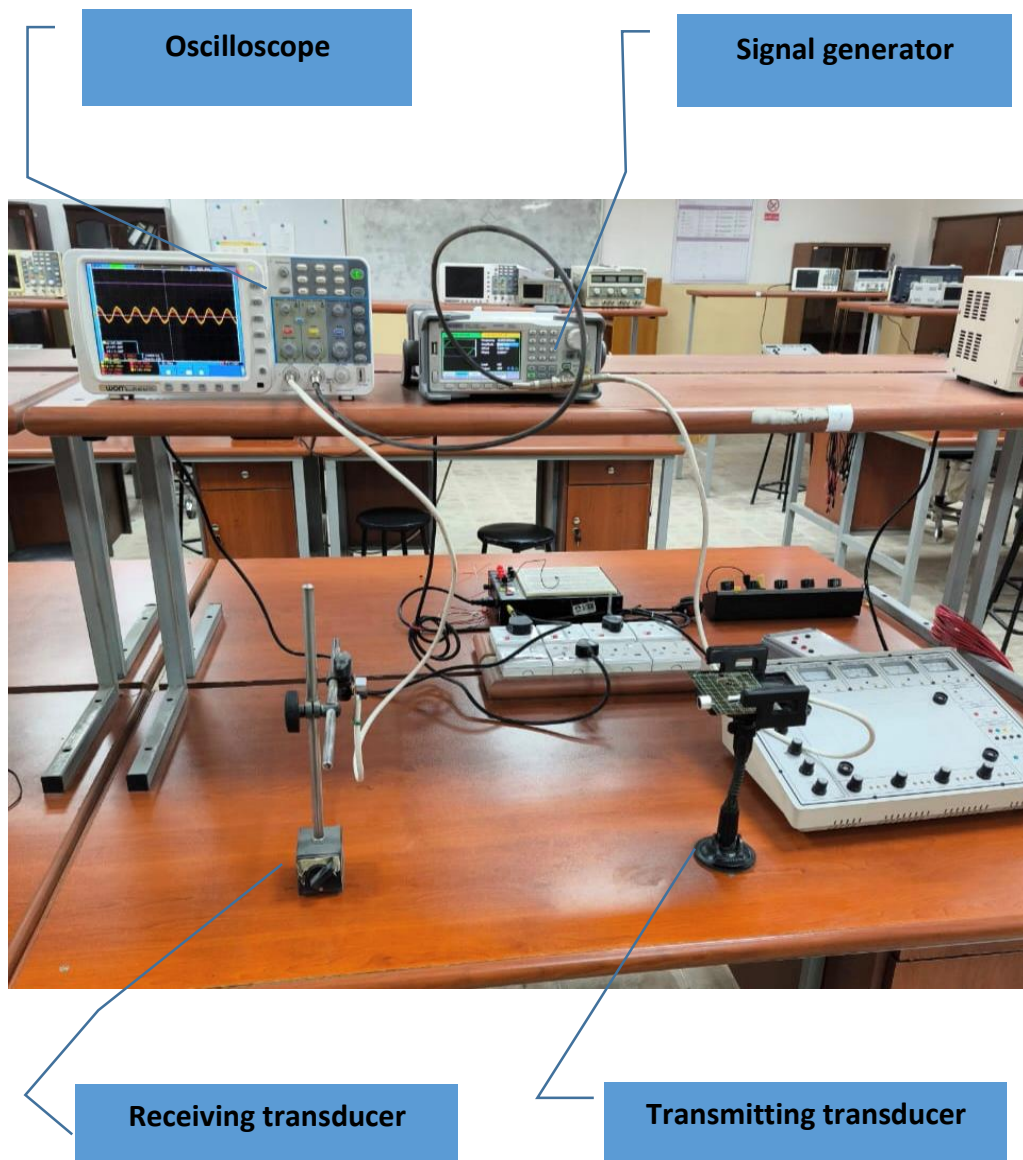


Figure (4.2) Hardware experimental system parts.

#### **4.5 Experimental with Single Source**

Three experiments for single-source are achieved, two of them are for a negative angle and the other is for a positive angle.

### 4.5.1 Single-Source with Negative Angle :

The experiment uses a single source with a negative angle. The actual angle is  $\theta = -10^\circ$ . The following parameters are used :  $N=11$ ,  $d=0.2$  cm,  $f=40$  KHz,  $Y=0.8$  cm. Figure (4.3) refers to the result of the FFT algorithm method. The practical (apparent) angle is equal to  $-6^\circ$ . The percentage error is very high and equal to 40%. Also, it is noticed, from the resulting curve using the FFT method, that the peak corresponding to the apparent (measured) angle is not sharp enough.

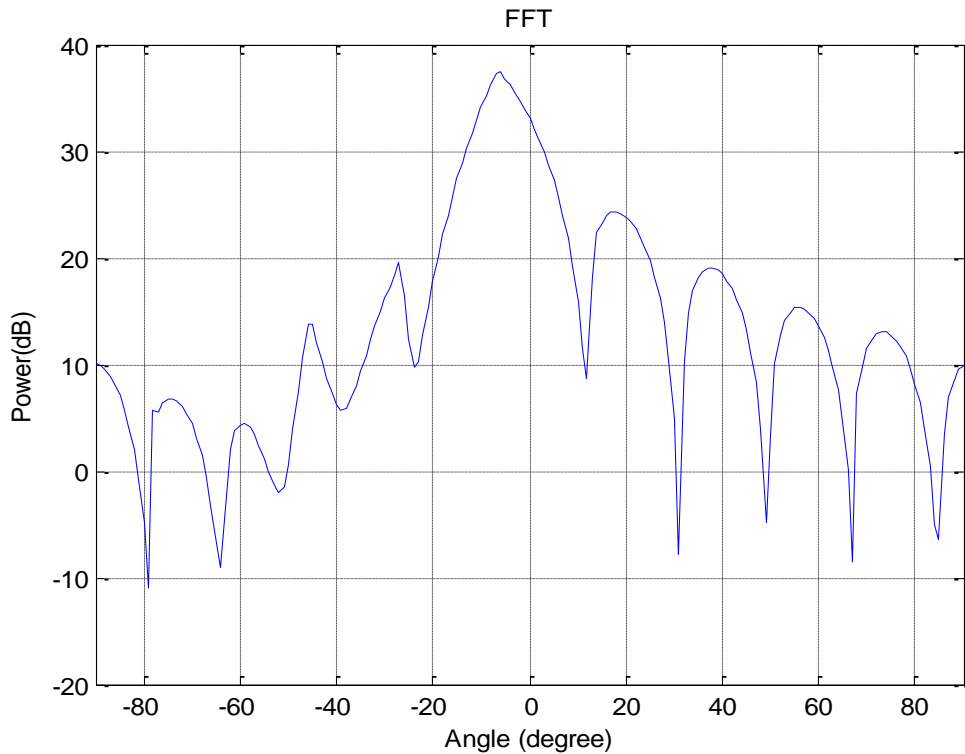


Figure (4.3) Magnitude (power (dB)) versus angle (degree) for a single-source ( $\theta = -10^\circ$ ) using the FFT approach ( $N=11$ ).

The other method that is used is the Root-MUSIC approach for the same number of samples,  $N=11$ . The practical (apparent) angle is  $-9.1190^\circ$ . Hence the percentage error is 8.81%. It means that the

percentage error of the Root-MUSIC approach is lower than that of the FFT approach. For this reason, the Root-MUSIC approach is better than the FFT approach. Moreover, the sidelobe that appears with the Root-MUSIC method is higher than 10 dB. Figure (4.4) shows the relationship between percentage error and N (number of samples) of both FFT and Root-MUSIC methods for a single source with  $\theta = -10^\circ$ . It is noticed that the percentage error for the FFT approach is much greater than that of the Root-MUSIC approach. The error for the FFT approach exceeds 30% and reaches up to 40% while for the Root-MUSIC approach is less than 20% and decreases down to less than 10%.

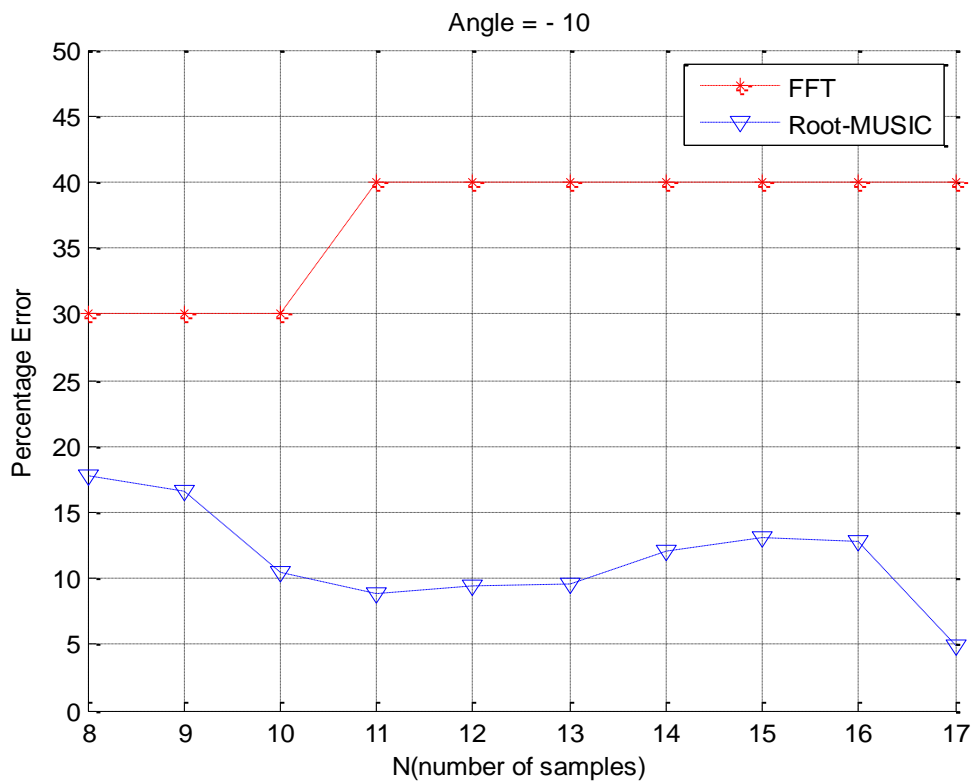


Figure (4.4) Percentage error of angle versus N for single source with  $\theta = -10^\circ$  for DOA Estimation.

The second experiment uses a single source with another negative angle. The actual angle is  $\theta = -11^\circ$ . The following parameters are used :  $N=18$ ,  $d=0.2$  cm,  $f=40$  KHz,  $\Psi=0.8$  cm.

Fig. (4.5) depicts the FFT algorithm method's output. The apparent (practical) angle is  $-12^\circ$ . The percentage mistake is 9.0909 percent, which is quite large. To put it in another way: The sidelobe is high, which means that it's at least 10% lower than the peak corresponding to the practical angle. The FFT algorithm has this shortcoming. Also, the peak corresponding to the apparent (measured) angle is not sharp enough in the resulting curve of employing the FFT approach.

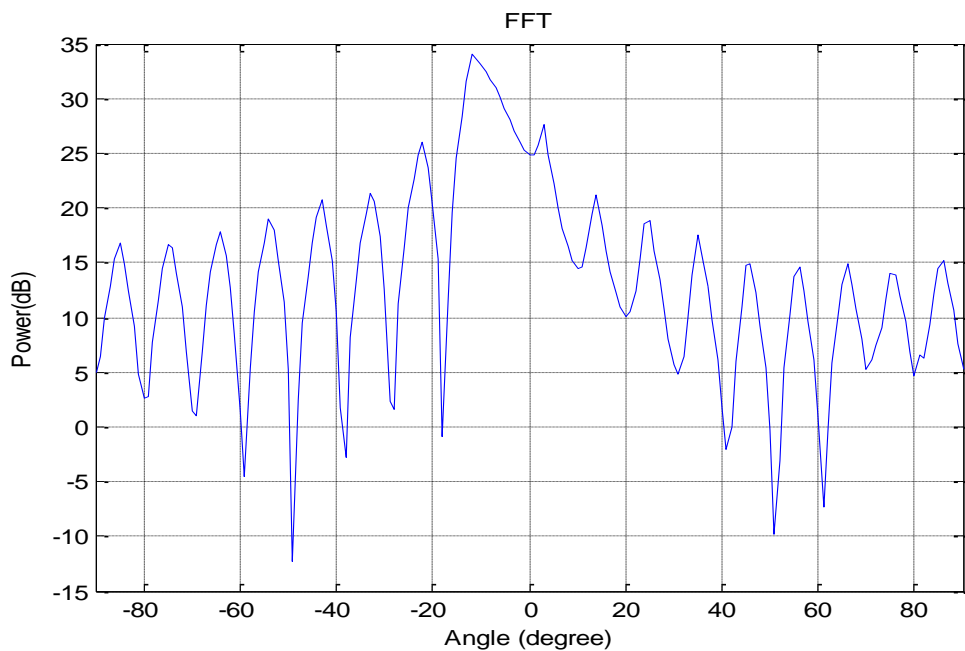


Figure (4.5) Magnitude (power (dB)) versus angle (degree) for a single-source ( $\theta = -11^\circ$ ) using the FFT approach ( $N=18$ ).

Using the same  $N=18$  samples, the Root-MUSIC method is the alternate way of data analysis... For practical purposes, the apparent

angle is  $-11.6066^\circ$  degrees. As a result, the error percentage is 6.005 percent. Also, the Root-MUSIC approach has a lower percentage error than the FFT approach does. This ensures that Root-approach MUSIC is superior to the FFT's approach. Furthermore, the Root-MUSIC technique produces a sidelobe with an amplitude greater than 10 decibels. Figure (4.6) shows the relationship between percentage error and N (number of samples) of both FFT and Root-MUSIC algorithm methods for a single source with  $\theta = -11^\circ$ . It is noticed that the percentage error for the FFT approach is much greater than that of the Root-MUSIC approach. The error for the FFT approach exceeds 9.0909% and reaches up to 70% while for Root-MUSIC is less than 40% and decreases down to less than 10%.

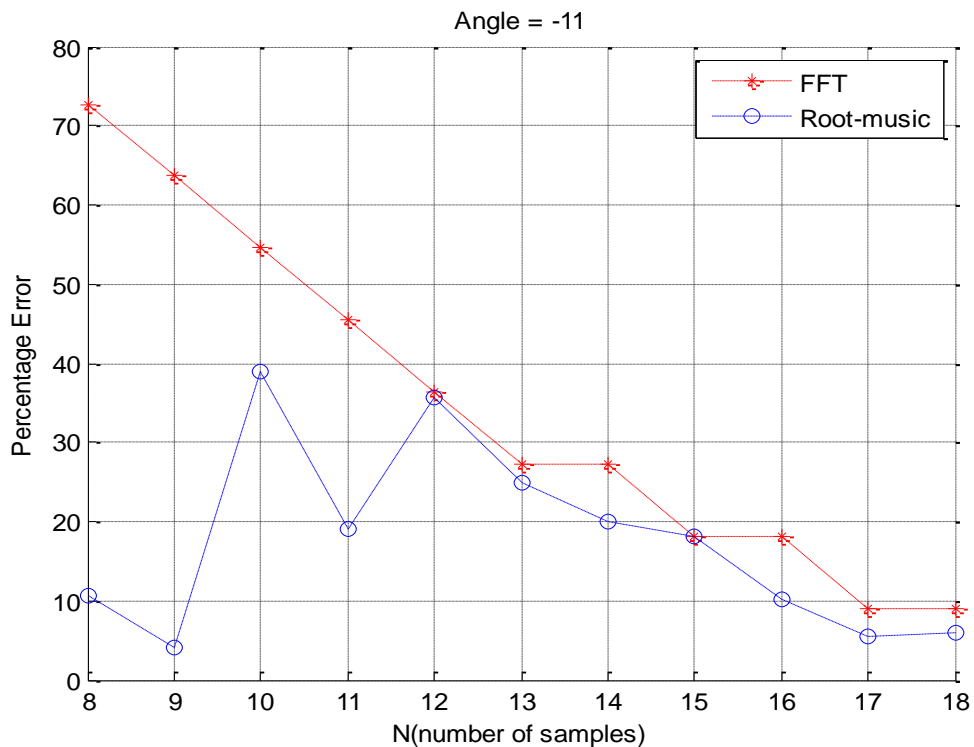


Figure (4.6) Percentage error of angle versus N for single source with  $\theta=-11^\circ$  for DOA Estimation.

### 4.5.2 Single-Source with Positive Angle :

The experiment uses a single source with a positive angle. The actual angle is positive and equals  $\theta=6^\circ$ . The following parameters are used :  $N=13$ ,  $d=0.2$  cm,  $f=40$  KHz,  $\Psi=0.8$  cm. As may be seen in Fig. (4.7), Good results were obtained with the FFT approach.. The angle that appears to be practical is  $1^\circ$  degrees. The percentage inaccuracy is 83.333 percent, which is quite high. It is less than 10 dB from the peak that corresponds to the practical (appeared) angle. The sidelobe is high, ie this is a shortcoming of the FFT method. It has been also discovered that the FFT method's result curve shows that the peak corresponding to the apparent (measured) angle is not sharp enough.

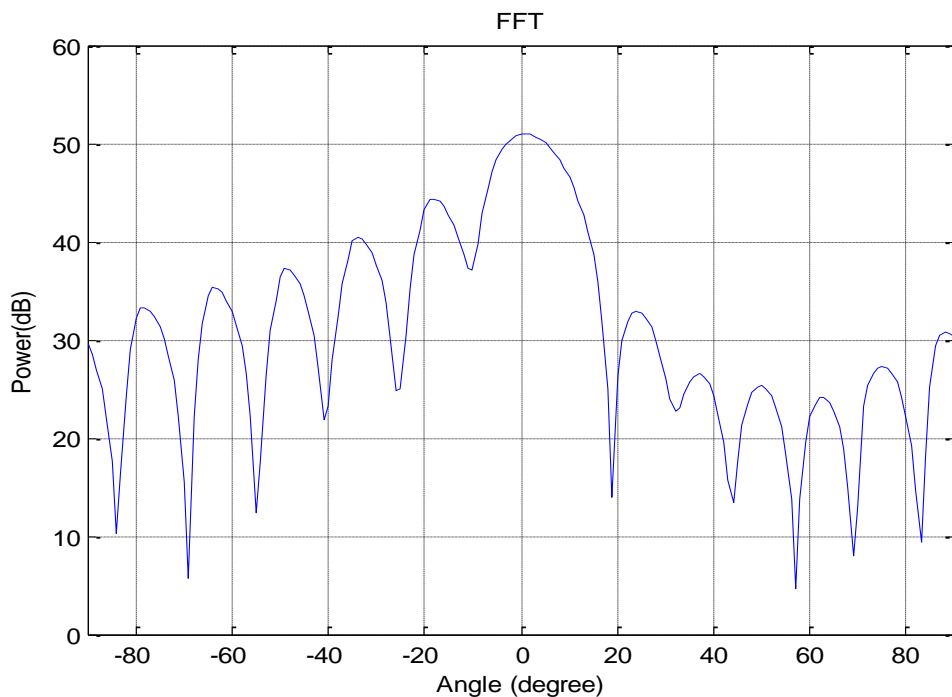


Figure (4.7) Magnitude (power (dB)) versus angle (degree) for a single-source ( $\theta = 6^\circ$ ) using the FFT approach ( $N=13$ ).

Using the same  $N=13$  samples, the Root-MUSIC technique is also an option. The apparent (practical) angle is  $5.3730^\circ$ . Because of this, the percentage of error is 10.45 percent. Root-error MUSIC's percentage is lower than the FFT's error percentage, as is the case with both approaches. The Root-MUSIC technique is superior to the FFT approach for this reason. Furthermore, the Root-sidelobe MUSIC is more than 10 dB. Figure (4.8) shows the relationship between percentage error and  $N$  (number of samples) of both FFT and Root-MUSIC algorithm methods for a single source with  $\theta = 6^\circ$ . It is noticed that the percentage error for the FFT is much greater than the Root-MUSIC. The error for the FFT exceeds 50% and reaches up to 100% while for Root-MUSIC is less than 20% and decreases down to less than 10%.

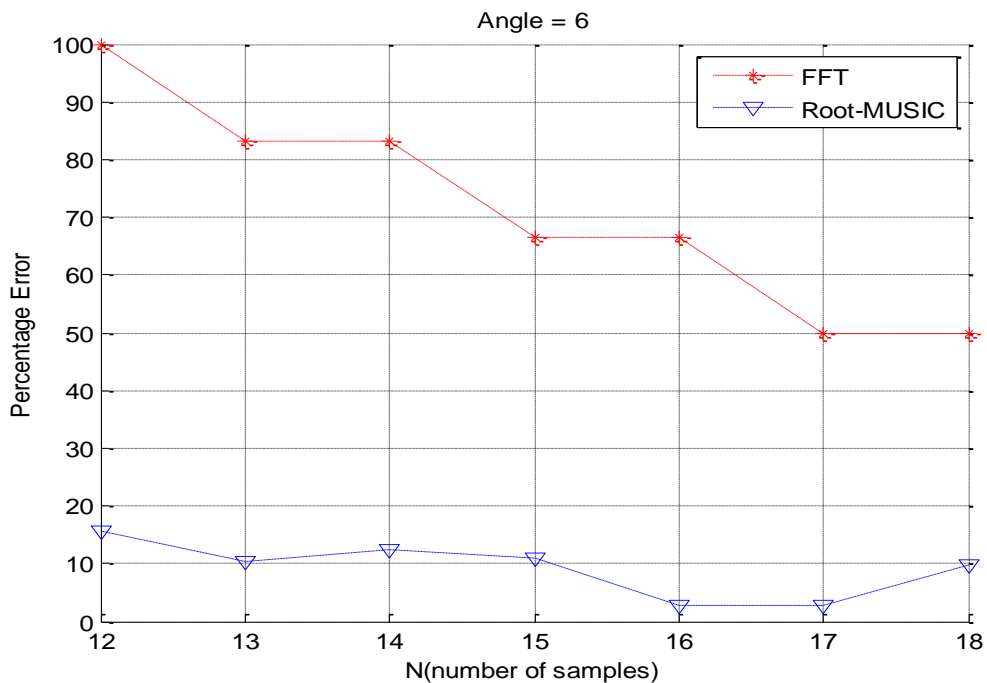


Figure (4.8) Percentage error of angle versus  $N$  for a single source with  $\theta = 6^\circ$  for DOA Estimation.

## 4.6 Experimental with Two Sources:

In this experiment, two sources are used. The first angle is negative and the second angle is positive. The first actual angle is  $\theta_1=-29^\circ$  and the second actual angle is equal to  $\theta_2=26^\circ$ . The following parameters are used:  $N=17$ ,  $d=0.2\text{cm}$ ,  $f=40\text{kHz}$ ,  $\Psi=0.8\text{cm}$ .

Figure (4.9) refers to the result of the FFT method. The first practical (apparent) angle is equal to  $-24^\circ$ . The percentage error is 17.241%. The second practical (apparent) angle is  $19^\circ$ , hence the percentage error is 26.923%. The sidelobe is high, less than 10dB from the peak that is corresponding to the highest practical (apparent) angle. This is one of the drawbacks of the FFT algorithm. Also, it is noticed, from the resulting curve using the FFT method, that the peak corresponding to the apparent (measured) angle is not sharp enough.

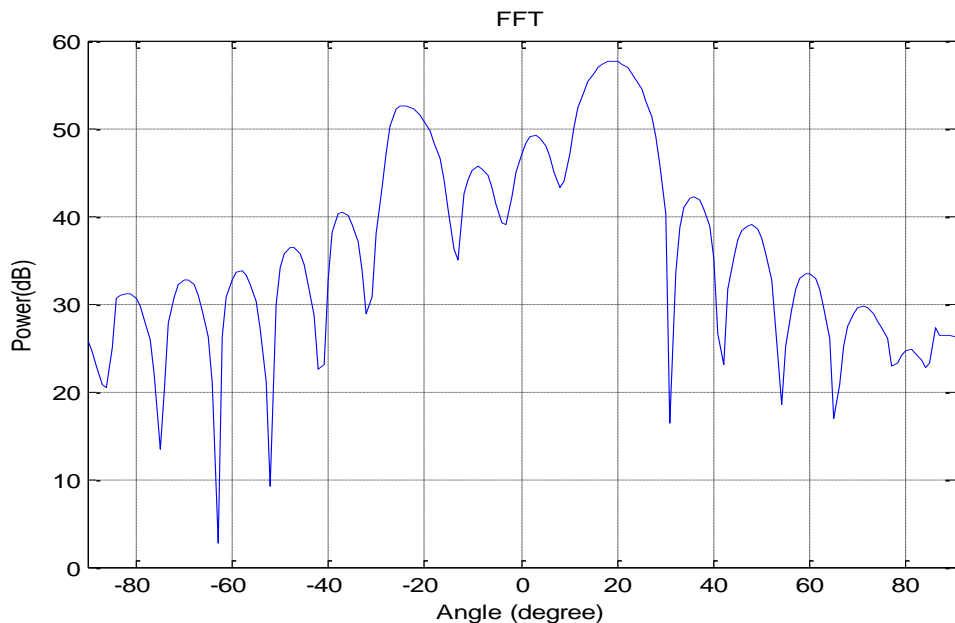


Figure (4.9) Magnitude (power (dB)) versus angle for a double (two) sources ( $\theta_1=-29^\circ$ ,  $\theta_2=26^\circ$ ) for DOA estimation using the FFT approach ( $N=17$ ).

The other method that is used is the Root-MUSIC method for the same number of samples  $N=17$ . The first practical (apparent) angle is equal to  $-30.2004^{\circ}$ . The percentage error is 4.139%, while the second practical (apparent) angle is equal to  $25.2695^{\circ}$  with a percentage error equal to 2.809%. This means that the percentage error of the Root-MUSIC method is lower than that of the FFT method. This ensures that the Root-MUSIC method is better than the FFT method. Moreover, the sidelobe that appears with the Root-MUSIC method is higher than 10 dB. Figure (4.10) shows the relationship between the percentage error and  $N$  (number of samples) for the first actual angle ( $\theta_1=-29^{\circ}$ ) of both FFT and Root-MUSIC algorithm methods. It is noticed that the percentage error for the FFT method is much greater than the Root-MUSIC method. The error for the FFT method exceeds 10% and reaches up to 27.586% while for the Root-MUSIC method is less than 10% and decreases down to less than 5%.

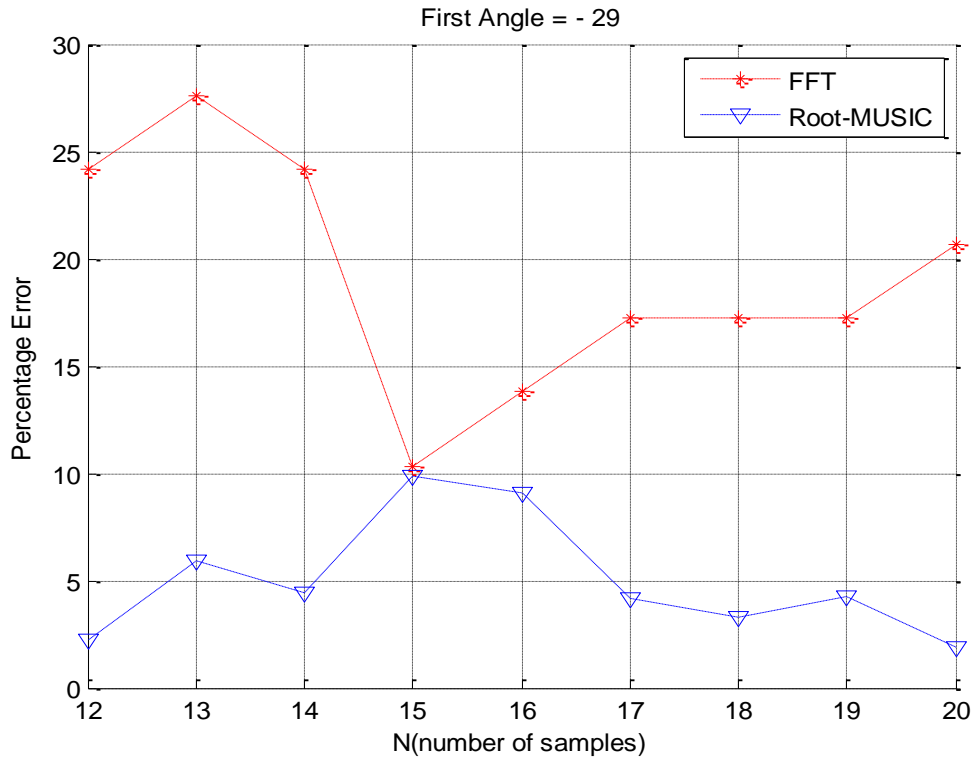


Figure (4.10) Percentage error of angle versus N for double (two) sources ( $\theta_1 = -29^\circ$ ,  $\theta_2 = 26^\circ$ ) with the first actual angle ( $\theta_1 = -29^\circ$ ) for DOA Estimation.

Figure (4.11) shows the relationship between the percentage error and N (number of samples) for the second actual angle ( $\theta_2 = 26^\circ$ ) of both FFT and Root-MUSIC algorithm methods. The percentage error for the FFT method is much greater than the Root-MUSIC method. The error for the FFT method exceeds 23% and reaches up to 34.615% while for the Root-MUSIC method is less than 7.5% and down to about 0%.

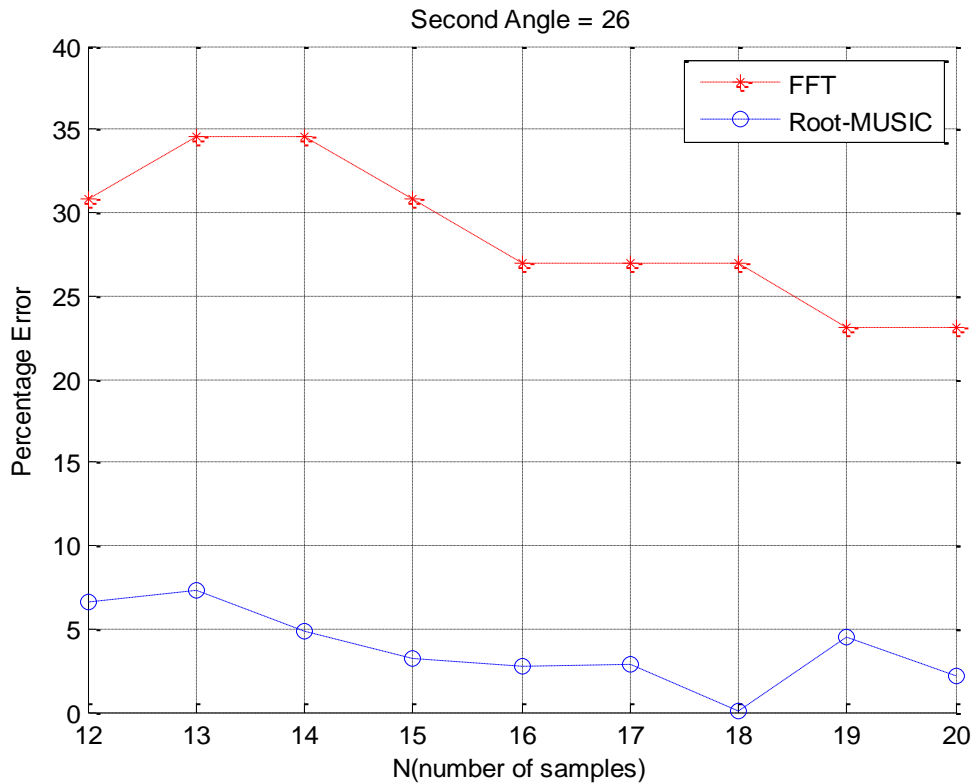


Figure (4.11) Percentage error of angle versus N for double (two) sources ( $\theta_1 = -29^\circ$ ,  $\theta_2 = 26^\circ$ ) with the second actual angle ( $\theta_2 = 26^\circ$ ) for DOA Estimation.

In the other experiments, two sources are also used. The first angle is negative and the second angle is positive. The first actual angle is  $\theta_1 = -10^\circ$  and the second actual angle is  $\theta_2 = 14^\circ$ . The following parameters are used:  $N=25$ ,  $d=0.2\text{cm}$ ,  $f=40\text{kHz}$ ,  $\Psi=0.8\text{cm}$ . Figure (4.12) illustrates the FFT algorithm's output. The first practical (appearing) angle is  $6^\circ$  degrees. The mistake rate is 40%. The second practical (apparent) angle is  $13^\circ$ , hence the error percentage is 7.142 percent. There is a high sidelobe, less than 10 dB from the peak, which corresponds to the largest practical (apparent) angle... This is a shortcoming of the FFT algorithm approach. Also,

the peak corresponding to the apparent (measured) angle is not sharp enough in the resulting curve of employing the FFT approach.

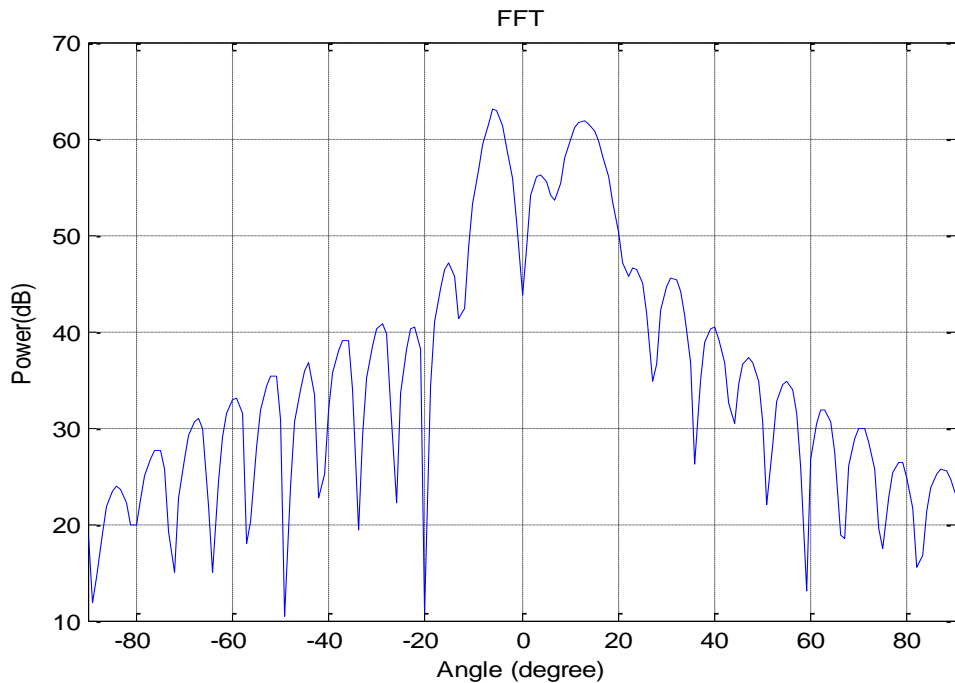


Figure (4.12) Magnitude (power (dB) versus angle for a double (two) sources ( $\theta_1 = -10^\circ$ ,  $\theta_2 = 14^\circ$ ) for DOA estimation using the FFT approach (N=25).

For the same number of samples  $N=25$ , the Root-MUSIC approach is employed. The apparent (practical) angle of  $-8.6161^\circ$  is the first to consider. The error is 13.839 percent, but the apparent (secondary) angle is  $15.9560^\circ$  degrees, with a 13.971-percent error rate. This means that the Root-MUSIC approach has a lower percentage error than the FFT method. The Root-MUSIC approach is therefore superior to the FFT method in this regard. Root-MUSIC, on the other hand, has a sidelobe that is more than 10 dB in magnitude. Figure (4.13) shows the relationship between the percentage error and  $N$  (number of samples) for the first actual angle ( $\theta_1 = -10^\circ$ ) of both FFT and Root-MUSIC algorithm methods. It is

noticed that the percentage error for the FFT method is much greater than the Root-MUSIC method. The error for the FFT method exceeds 40% and reaches 50% while for Root-MUSIC is less than 20% and decreases down to less than 1%.

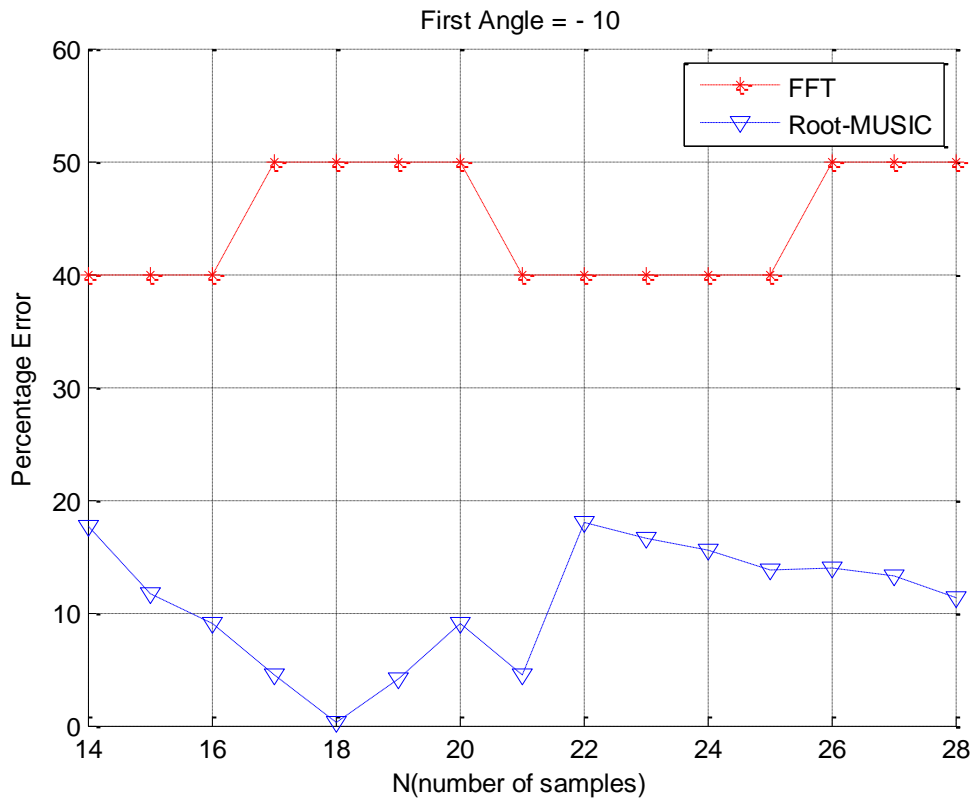


Figure (4.13) Percentage error of angle versus N for double (two) sources ( $\theta_1 = -10^\circ$ ,  $\theta_2 = 14^\circ$ ) with the first actual angle ( $\theta_1 = -10^\circ$ ) for DOA Estimation.

Figure (4.14) shows the relationship between the percentage error and N (number of samples) for the second actual angle ( $\theta_2 = 14^\circ$ ) of both FFT and Root-MUSIC algorithm methods. the percentage error for the FFT method is much greater than the Root-MUSIC method. The error for the FFT method exceeds 21% and reaches up to 28% while for Root-MUSIC is less than 14% and down to about 0.714%.

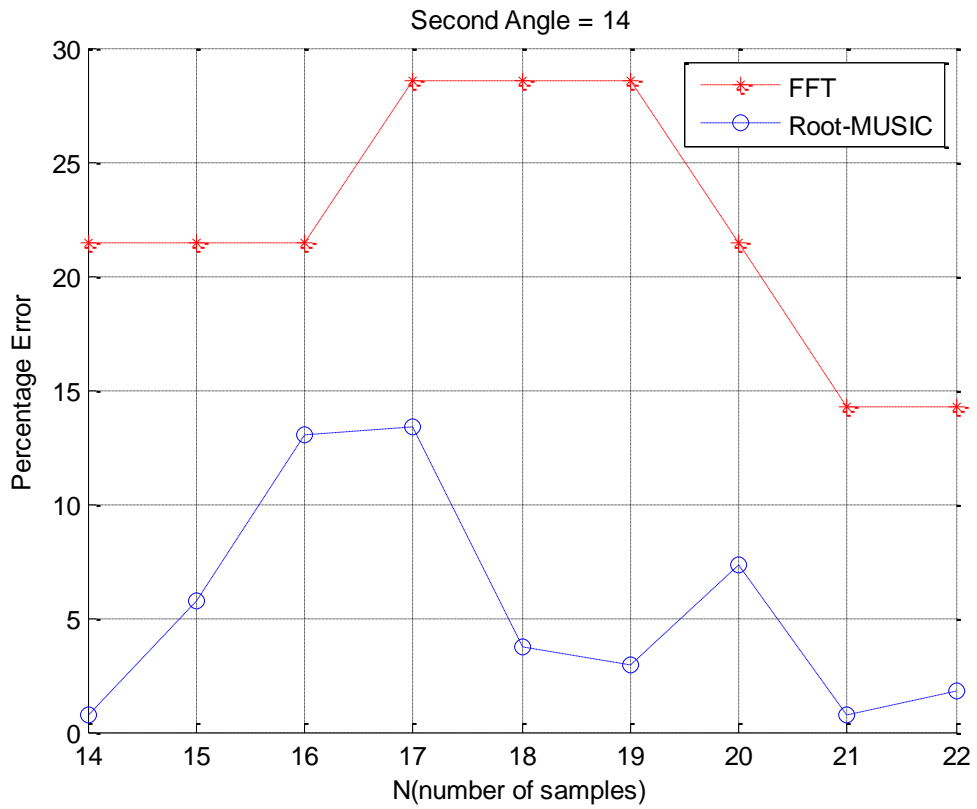


Figure (4.14) Percentage error of angle versus N for double (two) sources ( $\theta_1 = -10^\circ$ ,  $\theta_2 = 14^\circ$ ) with the second actual angle ( $\theta_2 = 14^\circ$ ) for DOA Estimation.

# CHAPTER FIVE

## Conclusions and Suggestions for Future Work

### 5.1 Conclusions

In this work we compared traditional FFT and super-resolution Root-MUSIC methods for Direction of Arrival (DOA) estimation, highlighting FFT's limitations in resolution, data requirements, and high sidelobes, which obscure signals and hinder accuracy. Despite Root-MUSIC's mathematical complexity and longer estimation times, its lower error rates and ability to discern slight angular differences demonstrate its superiority. Practical results confirm that FFT struggles with accurately detecting DOA, especially for closely spaced sources, whereas Root-MUSIC excels, benefiting from modern computing power to deliver precise and reliable DOA estimates with lower error margins and reduced sidelobe interference.

From simulation results, we can conclude that the percentage error equals zero at all points locations of the number of samples ( $N$ ) with noiseless data for single and two emitting (radiating) sources, when we use the Root-MUSIC algorithm method that is advantageous for this method but the percentage error is not equal zero of the FFT algorithm method. When we use with noisy data for single and two emitting (radiating) sources, the percentage error is minimum with high value signal to noise ratio (SNR) and with maximum  $N$  (number of samples).

From the practical results along with an investigation of the performance of both the conventional method (FFT) and super-resolution method (Root-MUSIC), we can conclude many points: The percentage errors of the FFT method is much higher, in most cases than of Root-MUSIC for both types of experiments, the two single-source experiments, and the single two sources experiment. In the FFT method the error is increased with fewer values of the number of samples  $N$  and begins decreasing, but still high, as  $N$  increases. For the Root-MUSIC method, it is noticed that the percentage error in most cases less than 15% for the two experiments of single source and less than 10% for the experiment of two sources. Also, it is noticed that high sidelobes have appeared for the FFT method in most experiments and it was less than 10 dB from the peak that corresponds to the highest practical (apparent) angle. While in the Root-MUSIC method, the sidelobes are of small values, higher than 10 dB from the peak that is corresponding to the highest practical (apparent) angle.

## **5.2 Suggestions for Future Work**

1. The application of radio frequency microwaves.
2. Applying various frequencies and wavelengths.
3. Using ULA without a scanning receiver is made possible by the use of tiny ultrasonic transducers.
4. Using of other high-resolution methods such as ESPRIT.

## References

- [1] M. H. Nguyen, J. Gruber, W. Marler, A. Hunsaker, J. Fuchs, and E. Hargittai, “Staying connected while physically apart: Digital communication when face-to-face interactions are limited,” *New Media Soc.*, vol. 24, no. 9, pp. 2046–2067, 2022.
- [2] F. J. Harris, *Multirate signal processing for communication systems*. CRC Press, 2022.
- [3] R. E. Jarvis, J. G. Metcalf, J. E. Ruyle, and J. W. McDaniel, “Measurement and signal processing techniques for extracting highly accurate and wideband RCS,” in *2021 IEEE International Instrumentation and Measurement Technology Conference (I2MTC)*, 2021, pp. 1–6.
- [4] Z. Ahmad, “Fundamentals of Narrowband Array Signal Processing,” in *Adaptive Filtering-Recent Advances and Practical Implementation*, IntechOpen, 2021.
- [5] E. Bieber, C. Campo, L. Bernard, H. Boeglen, S. Hengy, and J.-M. Paillot, “Array signal processing optimization in GNU radio for tracking and receiving applications,” in *Proceedings of the GNU Radio Conference*, 2021, vol. 2, no. 1.
- [6] Z. Leonowicz, *"Parametric methods for time-frequency analysis of electric signals"*. Citeseer, 2006.
- [7] R. Bos, S. De Waele, and P. M. T. Broersen, “Autoregressive spectral estimation by application of the Burg algorithm to

irregularly sampled data,” *IEEE Trans. Instrum. Meas.*, vol. 51, no. 6, pp. 1289–1294, 2002.

[8] V. Madisetti, *Wireless, networking, radar, sensor array processing, and nonlinear signal processing*. CRC press, 2018.

[9] S. M. Patole, M. Torlak, D. Wang, and M. Ali, “Automotive radars: A review of signal processing techniques,” *IEEE Signal Process. Mag.*, vol. 34, no. 2, pp. 22–35, 2017.

[10] S. Yan, *Broadband Array Processing*, vol. 17. Springer, 2019.

[11] S. A. Srinath, C. P. H. Prasad, and J. Valarmathi, “Direction of arrival estimation for narrowband and wideband underwater targets,” in *2017 International conference on Microelectronic Devices, Circuits and Systems (ICMDCS)*, 2017, pp. 1–7.

[12] R. Zhang, B. Shim, and W. Wu, “Direction of Arrival Estimation for Large Antenna Arrays with Hybrid Analog and Digital Architectures,” *IEEE Trans. Signal Process.*, 2021.

[13] N. Dey and A. S. Ashour, “Challenges and future perspectives in speech-sources direction of arrival estimation and localization,” in *Direction of arrival estimation and localization of multi-speech sources*, Springer, 2018, pp. 49–52.

[14] G. S. Moghadam and A. B. Shirazi, “Direction of arrival (DOA) estimation with extended optimum co-prime sensor array (EOCSA),” *Multidimens. Syst. Signal Process.*, vol. 33, no. 1, pp. 17–37, 2022.

- [15] K. Xu, Y. Quan, B. Bie, M. Xing, W. Nie, and E. Hanyu, “Fast Direction of Arrival Estimation for Uniform Circular Arrays with a Virtual Signal Subspace,” *IEEE Trans. Aerosp. Electron. Syst.*, 2021.
- [16] N. Ahmed *et al.*, “Performance analysis of efficient computing techniques for direction of arrival estimation of underwater multi targets,” *IEEE Access*, vol. 9, pp. 33284–33298, 2021.
- [17] V. F. Pisarenko, “The retrieval of harmonics from a covariance function,” *Geophys. J. Int.*, vol. 33, no. 3, pp. 347–366, 1973.
- [18] R. Schmidt, “Multiple emitter location and signal parameter estimation,” *IEEE Trans. Antennas Propag.*, vol. 34, no. 3, pp. 276–280, 1986.
- [19] A. Barabell, “Improving the resolution performance of eigenstructure-based direction-finding algorithms,” in *ICASSP’83. IEEE International Conference on Acoustics, Speech, and Signal Processing*, 1983, vol. 8, pp. 336–339.
- [20] P. R. Mahapatra, “Emitter location independent of systematic errors in direction finders,” *IEEE Trans. Aerosp. Electron. Syst.*, no. 6, pp. 851–855, 1980.
- [21] D. R. Klose and W. Skudera, “A SAW interferometer direction-finding and frequency identification method,” in *1981 IEEE MTT-S International Microwave Symposium Digest*, 1981, pp. 392–394.

- [22] D. R. Farrier, "Direction of arrival estimation by subspace methods," in *International Conference on Acoustics, Speech, and Signal Processing*, pp. 2651–2654, vol.5, 1990.
- [23] K. M. Wong, J. P. Reilly, Q. Wu, and S. Qiao, "Estimation of the directions of arrival of signals in unknown correlated noise. I. The MAP approach and its implementation," *IEEE Trans. Signal Process.*, vol. 40, no. 8, pp. 2007–2017, 1992.
- [24] E. G. Larsson, P. Stoica, and J. Li, "Spectral analysis of gapped data," in *Conference Record of the Thirty-Fourth Asilomar Conference on Signals, Systems and Computers (Cat. No. 00CH37154)*, 2000, vol. 1, pp. 207–211.
- [25] S. Araki, H. Sawada, R. Mukai, and S. Makino, "DOA estimation for multiple sparse sources with normalized observation vector clustering," in *2006 IEEE International Conference on Acoustics Speech and Signal Processing Proceedings*, 2006, vol. 5, pp. V.
- [26] L. Bai, C.-Y. Peng, and S. Biswas, "Association of DOA estimation from two ULAs," *IEEE Trans. Instrum. Meas.*, vol. 57, no. 6, pp. 1094–1101, 2008.
- [27] L. Rejfeek, D. Buresova, O. Fiser, and V. Brazda, "Comparison of parametric methods for radar signal processing," in *2015 25th International Conference Radioelektronika (RADIOELEKTRONIKA)*, 2015, pp. 141–144.

- [28] Y. Chen, A. H. C. Ko, W. S. Tam, C. W. Kok, and H. C. So, “Non-iterative DOA estimation using discrete Fourier transform interpolation,” *IEEE Access*, vol. 7, pp. 55620–55630, 2019.
- [29] Z. Ke, M. Peng, and Z. Jian-yun, “DOA estimation algorithm based on FFT in switch antenna array,” in *Proceedings of 2011 IEEE CIE International Conference on Radar*, 2011, vol. 2, pp. 1425–1428.
- [30] M. Shaghghi and S. A. Vorobyov, “Iterative root-MUSIC algorithm for DOA estimation,” in *2013 5th IEEE International Workshop on Computational Advances in Multi-Sensor Adaptive Processing (CAMSAP)*, 2013, pp. 53–56.
- [31] V. I. Vasylyshyn, “DOA estimation using beamspace root-music based estimator bank,” in *2017 XI International Conference on Antenna Theory and Techniques (ICATT)*, 2017, pp. 367–369.
- [32] F.-G. Yan, L. Shuai, J. Wang, J. Shi, and M. Jin, “Real-valued root-MUSIC for DOA estimation with reduced-dimension EVD/SVD computation,” *Signal Processing*, vol. 152, pp. 1–12, 2018.
- [33] A. A. Kamil, M. M. Ismail, and B. S. Bashar, “Comparative and analysis of evaluation of several direction of arrival estimation methods,” *Telkomnika*, vol. 19, no. 5, pp. 1724–1734, 2021.

- [34] A. Fathtabar, A. A. Khazaei, and A. Ghezelbigloo, “A New Eigen-Structure Based DOA Estimation Method for Wideband Coherent Signals,” *Wirel. Pers. Commun.*, vol. 117, no. 2, pp. 577–589, 2021.
- [35] A. Vesa, “Direction of arrival estimation using MUSIC and root-MUSIC algorithm,” in *18th Telecommunications Forum, Pg*, 2010, pp. 582–585.
- [36] J. Zhao, R. Gui, and X. Dong, “A new measurement association mapping strategy for DOA tracking,” *Digit. Signal Process.*, vol. 118, p. 103228, 2021.
- [37] C. H. You and M. A. Bin, “Spectral-domain speech enhancement for speech recognition,” *Speech Commun.*, vol. 94, pp. 30–41, 2017.
- [38] W. H. F. Smith, “Spectral windows for satellite radar altimeters,” *Adv. Sp. Res.*, vol. 62, no. 6, pp. 1576–1588, 2018.
- [39] V. V Gurenko, B. I. Bychkov, and V. V Syuzev, “An Approach to Simulation of Stationary and Non-stationary Processes in the Harmonic Basis,” in *2021 IEEE Conference of Russian Young Researchers in Electrical and Electronic Engineering (ElConRus)*, 2021, pp. 2664–2667.
- [40] A. Baxevani and K. Podgórski, “Signals Featuring Harmonics With Random Frequencies—Spectral, Distributional and Ergodic Properties,” *IEEE Trans. Signal Process.*, vol. 69, pp. 2779–2794, 2021.

- [41] S. U. Pillai and T. I. Shim, *Spectrum estimation and system identification*. Springer Science & Business Media, 2012.
- [42] W. Kong and G. Valiant, “Spectrum estimation from samples,” *Ann. Stat.*, vol. 45, no. 5, pp. 2218–2247, 2017.
- [43] M. Hamid and B. Beferull-Lozano, “Non-parametric spectrum cartography using adaptive radial basis functions,” in *2017 IEEE International Conference on Acoustics, Speech and Signal Processing (ICASSP)*, 2017, pp. 3599–3603.
- [44] M.-W. Li, J. Geng, W.-C. Hong, and L.-D. Zhang, “Periodogram estimation based on LSSVR-CCPSO compensation for forecasting ship motion,” *Nonlinear Dyn.*, vol. 97, no. 4, pp. 2579–2594, 2019.
- [45] A. Springford, G. M. Eadie, and D. J. Thomson, “Improving the lomb–scargle periodogram with the thomson multitaper,” *Astron. J.*, vol. 159, no. 5, p. 205, 2020.
- [46] F. J. Martínez-Murcia *et al.*, “Periodogram connectivity of EEG signals for the detection of dyslexia,” in *International Work-Conference on the Interplay Between Natural and Artificial Computation*, 2019, pp. 350–359.
- [47] D.-J. Jwo, W.-Y. Chang, and I.-H. Wu, “Windowing Techniques, the Welch Method for Improvement of Power Spectrum Estimation,” *C. Mater. Contin.*, 2021.
- [48] D. A. Lyon, “The discrete fourier transform, part 4: spectral leakage,” *J. object Technol.*, vol. 8, no. 7, 2009.

- [49] R. Bos, S. De Waele, and P. M. T. Broersen, “Autoregressive spectral estimation by application of the Burg algorithm to irregularly sampled data,” *IEEE Trans. Instrum. Meas.*, vol. 51, no. 6, pp. 1289–1294, 2002.
- [50] A. Subasi, *Practical guide for biomedical signals analysis using machine learning techniques: A MATLAB based approach*. Academic Press, 2019.
- [51] A. D. Poularikas, *Understanding digital signal processing with MATLAB® and solutions*. CRC Press, 2017.
- [52] R. Takalo, H. Hytti, and H. Ihalainen, “Tutorial on univariate autoregressive spectral analysis,” *J. Clin. Monit. Comput.*, vol. 19, no. 6, pp. 401–410, 2005.
- [53] P. M. T. Broersen, S. De Waele, and R. Bos, “Application of autoregressive spectral analysis to missing data problems,” *IEEE Trans. Instrum. Meas.*, vol. 53, no. 4, pp. 981–986, 2004.
- [54] F. Castanié, *Digital spectral analysis: parametric, non-parametric and advanced methods*. John Wiley & Sons, 2013.
- [55] T. Marzetta, “A new interpretation of Capon’s maximum likelihood method of frequency-wavenumber spectral estimation,” *IEEE Trans. Acoust.*, vol. 31, no. 2, pp. 445–449, 1983.
- [56] G. Yeo and C. B. Burge, “Maximum entropy modeling of short sequence motifs with applications to RNA splicing signals,” *J. Comput. Biol.*, vol. 11, no. 2–3, pp. 377–394, 2004.

[57] <http://www.mathworks.com/matlabcentral/fileexchange/28650-direction-of-arrival-estimation-with-music-algorithm>.

[58] S. V. Vaseghi, "Advanced Digital Signal Processing and Noise Reduction: Fourth Edition". A John Wiley and Sons, Ltd, 2008.

[59] M. Barkat, "Signal Detection and Estimation: Second Edition". Artech house 2019.

[60] M. H. Hayes, "Statistical Digital Signal Processing and Modeling", John Wiley & Sons, Inc., Georgia Institute of Technology, 2007.

[61] C. C. MacDuffee, The theory of matrices, vol. 5. Springer Science & Business Media, 2012.

[62] Z. Chen, G. Gokeda, and Y. Yu, "Introduction to Direction of Arrival Estimation", Artech House, 2010.

[63] J. G. Proakis and D. G. Manolakis, "Digital Signal Processing, Principles, Algorithm, and Applications", Third Edition, Prentice-Hall, Inc., 1996

[64] Z. Aliyazicioglu, H. K. Hwang, M. Grice, and A. Yakovlev, "Sensitivity Analysis for Direction of Arrival Estimation using a Root-MUSIC Algorithm.," *Eng. Lett.*, vol. 16, no. 3, 2008.

[65] P. Wang, G. Zhang, J. Xiong, C. Xue, and W. Zhang, "Root-MUSIC Algorithm with Real-Valued Eigendecomposition for Acoustic Vector Sensor Array," in *2010 First International*

*Conference on Pervasive Computing, Signal Processing and Applications*, 2010, pp. 652–656.

[66] L. Osman, I. Sfar, and A. Gharsallah, “Comparative study of high-resolution direction-of-arrival estimation algorithms for array antenna system,” *Int. J. Res. Rev. Wirel. Commun. Vol*, vol. 2, 2012.

[67] Z. Chen, Z. Cao, X. He, Y. Jin, J. Li, and P. Chen, “DoA and DoD estimation and hybrid beamforming for radar-aided mmWave MIMO vehicular communication systems,” *Electronics*, vol. 7, no. 3, p. 40, 2018.

[68] Y. Zheng and Y. Yu, “Joint estimation of DOA and TDOA of multiple reflections by matrix pencil in mobile communications,” *IEEE Access*, vol. 7, pp. 15469–15477, 2019.

[69] M. H. Chowdhury, A. B. M. Eldaly, S. Agadagba, R. C. C. Cheung, and L. L. H. Chan, “Machine Learning Based Hardware Architecture for DOA Measurement from Mice EEG,” *IEEE Trans. Biomed. Eng.*, 2021.

[70] R. J. Mailloux, “Antenna array architecture,” *Proc. IEEE*, vol. 80, no. 1, pp. 163–172, 1992.

[71] M. W. T. S. Chowdhury and M. Mastora, “Performance Analysis of MUSIC Algorithm for DOA Estimation with Varying ULA Parameters,” in *2020 23rd International Conference on Computer and Information Technology (ICCIT)*, 2020, pp. 1–5.

[72] R. K. Arumugam, A. Froehly, R. Herschel, P. Wallrath, and N. Pohl, “Direction of Arrival Estimation on Sparse Arrays Using

Compressive Sensing and MUSIC,” in *2023 17th European Conference on Antennas and Propagation (EuCAP)*, IEEE, 2023, pp. 1–5.

[73] C. Liu, X. Cheng, J. Su, and Y. Yuan, “Research and Simulation of Super-resolution Root-MUSIC Algorithm,” in *2023 4th International Symposium on Computer Engineering and Intelligent Communications (ISCEIC)*, IEEE, 2023, pp. 95–99.

## الخلاصة

في هذا العمل ناقش التحدي المتمثل في التمييز بين الترددات القريبة وزوايا المصادر في التحليل الطيفي، مع التركيز على القيود المفروضة على الطرق التقليدية مثل تحويل فورييه (FT) ، الذي يتطلب كمية كبيرة من البيانات وغالباً ما يؤدي إلى ضعف الدقة بسبب الفصوص الجانبية. يقدم تقدير اتجاه الوصول (DOA) كمجال حاسم للتحسين ويقدم طريقة تصنيف إشارات الجذر المتعددة (Root-MUSIC) كبديل عالي الدقة للنهج التقليدية مثل تحويل فورييه السريع (FFT). تقارن الدراسة Root-MUSIC و FFT باستخدام معلمات مختلفة، بما في ذلك عدد العينات، والفواصل الزمني لأخذ العينات المكانية، والطول الموجي، مع مصادر انبعاث فردية ومزدوجة. تسلط النتائج الضوء على دقة وكفاءة Root-MUSIC الفائقة مع متطلبات أقل للبيانات. يتم دعم فعالية الطرق عالية الدقة عبر تقنية فورييه FT في فصل زوايا المصدر بدقة من خلال التجارب التي أجريت باستخدام محولات الطاقة بالموجات فوق الصوتية في زوايا مصدر مختلفة، مما يدل على ميزة الأساليب عالية الدقة على الطرق التقليدية. تم تنفيذ تجارب تقدير DOA من خلال محولات الطاقة بالموجات فوق الصوتية. تتضمن كل تجربة زوايا مختلفة من المصادر. وقد أظهرت النتائج التجريبية أن الأساليب عالية الدقة تفوقت على الأساليب التقليدية.

ومن النتائج المحاكاة والعملية نستنتج أن الحد الأقصى للخطأ هو أعلى ما يمكن في النتائج العملية وأقل منه في بيانات نتائج المحاكاة بضوضاء وأقلها بيانات نتائج المحاكاة بدون ضوضاء لطريقة FFT و طريقة Root-MUSIC. وهذا يعني أن أفضل النتائج تكون في نتائج البيانات بدون ضوضاء، ثم في نتائج البيانات بضوضاء، وأسوأ النتائج هي النتائج العملية في نتائج مصدر واحد ومصدري انبعاث لكل النتائج.

## إقرار لجنة المناقشة

نشهد بأننا أعضاء لجنة التقويم والمناقشة قد اطلعنا على هذه الرسالة الموسومة ( تقنية جذر - تصنيف الإشارات المتعددة (Root-MUSIC) لتخمين اتجاه الوصول في تطبيقات الأمواج فوق الصوتية) وناقشنا الطالب (محمد رافع شكري) في محتوياتها وفيما له علاقة بها بتاريخ 18 / 2 / 2024 وقد وجدناها جديرة بنيل شهادة الماجستير/علوم في اختصاص هندسة الالكترونيات.

التوقيع:	التوقيع:
رئيس اللجنة:	رئيس اللجنة:
التاريخ: 2024/ 3 /	التاريخ: 2024/ 3 /
التوقيع:	التوقيع:
عضو اللجنة (المشرف):	عضو اللجنة:
التاريخ: 2024/ 3 /	التاريخ: 2024/ 3 /

## قرار مجلس الكلية

اجتمع مجلس كلية هندسة الالكترونيات بجلسته المنعقدة بتاريخ : / / 2024 وقرر المجلس منح الطالب شهادة الماجستير علوم في اختصاص هندسة الالكترونيات

مقرر المجلس: أ.م.د. بلال علاء الدين جبر	رئيس مجلس الكلية: أ.د. خالد خليل محمد
التاريخ: / /	التاريخ: / /

### إقرار المشرف

نشهد بأن هذه الرسالة الموسومة ( تقنية جذر - تصنيف الإشارات المتعددة (Root-MUSIC) لتخمين اتجاه الوصول في تطبيقات الأمواج فوق الصوتية) تم اعدادها من قبل الطالب (محمد رافع شكري) تحت اشرافي في قسم هندسة الالكترونيك / كلية هندسة الالكترونيات / جامعة نينوى، وهي جزء من متطلبات نيل شهادة الماجستير/علوم في اختصاص هندسة الالكترونيك.

التوقيع:

الاسم:

التاريخ: 2024/ 3 /

### إقرار المقوم اللغوي

اشهد بأنه قد تمت مراجعة هذه الرسالة من الناحية اللغوية وتصحيح ما ورد فيها من أخطاء لغوية وتعبيرية وبذلك أصبحت الرسالة مؤهلة للمناقشة بقدر تعلق الأمر بسلامة الأسلوب أو صحة التعبير.

التوقيع:

الاسم:

التاريخ: 2024/ 3 /

### إقرار رئيس لجنة الدراسات العليا

بناءً على التوصيات المقدمة من قبل المشرف والمقوم اللغوي أشرح هذه الرسالة للمناقشة.

التوقيع:

الاسم:

التاريخ: 2024/ 3 /

### إقرار رئيس القسم

بناءً على التوصيات المقدمة من قبل المشرف والمقوم اللغوي ورئيس لجنة الدراسات العليا أشرح هذه الرسالة للمناقشة.

التوقيع:

الاسم:

التاريخ: 2024/ /

تقنية جذر - تصنيف الإشارات المتعددة (Root-MUSIC)  
لتخمين اتجاه الوصول في تطبيقات الأمواج فوق الصوتية

رسالة تقدم بها

محمد رافع شكري

الى

مجلس كلية هندسة الالكترونيات - جامعة نينوى

وهي جزء من متطلبات نيل شهادة الماجستير

علوم في هندسة الالكترونيات

باشراف

الاستاذ المساعد الدكتور

مجاهد فهمي ابراهيم العزو



جامعة نينوى

كلية هندسة الالكترونيات

قسم الالكترونىك

## تقنية جذر - تصنيف الإشارات المتعددة (Root-MUSIC) لتخمين اتجاه الوصول في تطبيقات الأمواج فوق الصوتية

محمد رافع شكري

رسالة في هندسة الالكترونىك

باشراف

الأستاذ المساعد الدكتور

مجاهد فهمي ابراهيم العزو